Synthesis of $NiMn_2O_4$ and its ordered structure for Supercapacitor electrode

A thesis submitted towards partial fulfilment of the requirements for the degree of

Master of Technology in Nanoscience and Technology

Submitted by

Aminul Islam

Roll no.: **002230701024**

Examination roll no.: **M4NST24021**

Registration No.: **152106 of 2019-20**

Under the guidance of

Dr. Sachindranath Das

Department of Instrumentation Science

Jadavpur University

Kolkata – 700032

Course Affiliated to**:**

Faculty of Interdisciplinary Studies, Law and Management

Jadavpur University

Kolkata, India

2024

M.Tech (Nanoscience and Technology)

Course affiliated to

Faculty of Interdisciplinary Studies, Law and Management

Jadavpur University

Kolkata, India

CERTIFICATE OF RECOMMENDATION

We hereby recommend that this forgoing thesis entitled as "***Synthesis of $NiMn_2O_4$ and its ordered structure for Supercapacitor electrode***" carried out by **Aminul Islam** (Class Roll No: 002230701024, Registration No: 152106 of 2019-20, Examination Roll No: M4NST24021) under our guidance, be approved as a credible piece of work and be accepted as a requirement for the award of the degree Master of Technology in Nanoscience and Technology from the School of Materials Science and Nanotechnology for the academic year 2022-2024.

DIRECTOR

Dr. Mahua Ghosh Chaudhuri

School of Materials Science and Nanotechnology

Jadavpur University, Kolkata - 700032

PROJECT GUIDE

Dr. Chandan Kumar Ghosh

School of Materials Science and Nanotechnology

Jadavpur University, Kolkata - 700032

PROJECT CO-GUIDE

Dr. Sachindranath Das

Department of Instrumentation Science

Jadavpur University, Kolkata - 700032

DEAN

Faculty of Interdisciplinary Studies, Law and Management

Jadavpur University, Kolkata - 700032

M.Tech (Nanoscience and Technology)

Course affiliated to

Faculty of Interdisciplinary Studies, Law and Management

Jadavpur University

Kolkata, India

CERTIFICATE OF APPROVAL

This foregoing thesis is hereby approved as a credible study of an engineering subject carried out and presented in a manner satisfactorily to warranty its acceptance as a prerequisite to the degree for which it has been submitted. It is understood that by this approval the undersigned do not endorse or approve any statement made or opinion expressed or conclusion drawn therein but approve the thesis only for purpose for which it has been submitted.

Committee of final examination

for evaluation of Thesis

_____

_____

_____

_____

****** Only in case the Thesis is approved

DECLERATION OF ORIGINALITY AND COMPLIANCE OF ACADEMIC ETHICS

I hereby certify that the undersigned candidate completed the literature review and original research for this thesis as a requirement for his Master of Technology (Nano science and Technology) studies during the academic year 2022–2024.

All information in this document has been obtained and presented in accordance with academic standards and ethical conduct.

I further declare that I have properly cited and referred to all information and findings that are not original to this work, as required by these rules and conduct.

Name: AMINUL ISLAM

Examination Roll Number: M4NST24021

Registration Number: 152106 of 2019-20

Thesis Title: Synthesis of $NiMn_2O_4$ and its ordered structure for Supercapacitor electrode.

SIGNATURE: DATE:

Dedicated to my parents

ACKNOWLEDGEMENT

I express my gratitude to **Dr. Sachindranath Das**, my academic advisor, for his unwavering support, enthusiasm, and extensive expertise over the course of my Master's studies and research. Throughout the process of working on my thesis, he provided steadfast support and guidance. I am appreciative for the insightful remarks you provided, as they served as a source of inspiration for my whole study endeavour. Furthermore, I would like to extend my appreciation to **Dr. Chandan Kumar Ghosh** and the Energy Research Lab, as well as the Nanoscience and Nanotechnology Laboratory, for fostering a congenial working atmosphere for me.

I express my sincere appreciation to **Mr. Souvik Mal and Mr. Mithun Halder**, who have served as my mentor, for his invaluable guidance and support in addressing various project-related challenges. Furthermore, I am grateful for his collaborative efforts, which have contributed significantly to the current state of the project.

I express my sincere gratitude to **Dr. Sourav Sarkar, Dr. Mahua Ghosh** for their invaluable help, unwavering support, insightful insights, and invaluable counsel. The learning atmosphere provided by the individuals was both supportive and conducive to growth, fostering a sense of enthusiasm inside me that motivated me to pursue the study issue with great passion.

I would like to express my sincere appreciation to Roshni Begum, Raushan Kabir, Mizanur Islam, Mriganka who are my seniors, for their invaluable contributions in making my project a really remarkable and unforgettable experience. I express my gratitude to Gourab Payra, Kazi Wakar, Arijit Roy and my fellow batchmates for their invaluable aid and unwavering support over the duration of this course. The completion of my project would not have been possible without their aid. Given the substantial assistance they have provided, my expressions of appreciation are inadequate.

In conclusion, I would want to sincerely acknowledge my parents and all those who have provided me with affection and assistance, expressing my deep appreciation for their unwavering love and support.

ABSTRACT

Title: Synthesis of $NiMn_2O_4$ and its ordered structure for Supercapacitor electrode.

In recent years, the search for efficient and sustainable energy storage systems has intensified, with supercapacitors emerging as a promising solution due to their high power and energy density, rapid charge/discharge capabilities, and long cycle life. Commercial supercapacitor utilizes high surface area carbon as an electrode to store charges. But, these types of devices lack the high energy density. electrode. Ideal supercapacitor electrode materials should have a higher surface area, good electrical conductivity, optimum porosity, and excellent chemical and thermal stability. On the other hand, different transition metal oxides and few conducting polymer-based (PVA, PANI conducting polymer) polymers electrodes can store charges via fast and reversible faradic reaction with suitable electrolytes and demonstrate very high energy density. Different transition metal oxides like RuO_2, MnO_2, NiO, CuO, etc. fall under the category which store charges via faradaic mechanism. However, these metal oxides demonstrate very poor conductivity in regards to electronic conduction, which results in an increase of overall internal resistance of the electrode and thus hampering the overall power delivery. In order to address the issues of conductivity, researchers have tried to form composite with two metal oxides. Binary metal oxides typically demonstrate better electrochemical performance compared to the single metal oxides due to synergistic effects between two metal components. Bimetal oxides can better withstand repeated charge-discharge cycles without significant degradation, ensuring longevity of the device. Furthermore, the morphology of electrode materials has huge influence on the above parameters thus plays a significant role in electrochemical performance. So far, $NiMn_2O_4$ nanoparticles prepared by the sol–gel method and drop cast onto Ni-foam showed a specific capacitance of 854.7 F/g at 5 mV/s in 2 M aqueous KOH electrolyte. Spinel $NiMn_2O_4$ synthesized through microwave-assisted co-precipitation method followed by calcination at 500°C showed a specific capacitance increasing from 290.56 F/g to 751.57 F/g as the KOH electrolyte concentration was increased from 1 M to 6 M at a scan rate of 5 mV/s.

We have synthesized an SDS-assisted bimetal oxide of Ni of Mn, $NiMn_2O_4$ via hydrothermal method. Which was annealed at 400^OC and then specific capacitance was measured using a 3-electrode system, which gives 3088.8 F/g in 0.5 M Na_2SO_4 as electrolyte at 2 mV/s scan rate. Electrospining techniques is a very slow yield process for mass production. We used a rather

simple device Rotary Jet Spin (RJ-Spin) which has the same mechanism as candy floss machine. We separately annealed PVA fiber obtained from RJ-spin and annealed at $800^{O}C$ within vacuum, the FTIR of this annealed fiber confirmed the rGO phase. $NiMn_2O_4$/C (using PVA) fiber fabricated using RJ-spin setup. The obtained fiber was annealed at $900^{O}C$ in vacuum chamber and XRD result compared of both confirms the presence of $NiMn_2O_4$ particle at obtained PVA fiber as matrix. The obtained fiber had high moister affinity and sublimate most weight percentage during annealing.

List of contents

Chapter 1

1. Introduction and Objective
   1.1 Background
   1.2 Problem Statement
   1.3 Objective

Chapter 2

2. Literature review
   2.1 Introduction
   2.2 Supercapacitor Fundamentals
   2.3 Supercapacitor Types
      2.3.1 Electrochemical Double Layer Capacitors (EDLC)
      2.3.2 Pseudocapacitors
      2.3.3 Hybrid Capacitors
   2.4 Mechanism of Supercapacitor
      2.4.1 Traditional electric double layer theory
      2.4.2 Pseudocapacitance
      2.4.3 Hybrid Capacitance
      2.4.4 Electrochemical Characterisations to differentiate between the storing mechanisms
   2.5 Different Electrode Materials
      2.5.1 Porous Carbon
      2.5.2 Carbon Nanotube
      2.5.3 Graphene
      2.5.4 Ruthenium Oxide and its composites
      2.5.5 Manganese Dioxide and its composites
      2.5.6 Bimetallic oxide of Ni and Mn ($NiMn_2O_4$)
   2.6 Two Electrode Supercapacitor Device
      2.6.1 Current Collector
      2.6.2 Separator
      2.6.3 Electrolyte

2.6.4 Electrode

2.6.5 Effect on performance of electrode material due to morphological differences

2.7 Summary

Chapter 3

3. Different Characterization Techniques

3.1 X-Ray Diffractometer (XRD)

3.2 Fourier Transform Infrared Spectroscopy (FTIR)

3.3 Electrochemical characterizations

Chapter 4

4. Experimental Section

4.1 Hydrothermal Synthesis

4.2 Synthesis process of $NiMn_2O_4$ metal oxide

4.3 Synthesis of PVA microfiber using RJ-Spin

4.4 Synthesis of ordered microfiber of $NiMn_2O_4$ using RJ Spin technique

Chapter 5

5. Results and Discussion

5.1 $NiMn_2O_4$ nanoparticle via Hydrothermal route

5.2 Ordered $NiMn_2O_4$ microfiber

Chapter 6

6. Conclusion

CHAPTER 1

INTRODUCTION AND OBJECTIVE

1.1 Background

From ancient times of human civilization, the energy has been the part and parcel of civilization to sustain. Energy in the form of fire was the prima facie requirement for the generation to sustain. Since the early age, the consisted demand for global energy requirement is growing in ever-growing society, so there are the concerns about the depletion and associated pollution caused by the usage of fossil fuels. Because of this crisis, several research and technological developments have been undergoing in the areas like renewable energy, energy from alternative sources, energy storage devices, and energy harvesting from waste materials. Among sustainable sources of energy, solar energy, (1,2) tidal energy, (3,4) and wind energy (5,6) are appealing alternative options for electricity generation. However, the complete unreliability and unpredictable characteristics of these sources demands the need of development of efficient and effective energy storage systems. The power derived from whatsoever sources calls for the requirement of storage and to accumulate the energy for sporadic utilization (7-11). The idea to store electrical charge in surface has been emerged from the phenomena associated with rubbing of amber. In the mid-18th century, the effect of such phenomena was understood when physics of "static electricity" was being investigated and during that period, various electrical machines, such as the Electrophorus and the Wimshurst machine were being developed. Excellent examples of these, as well as Leyden jars, can be witnessed in the Museum of Science in Florence. However, an understanding of electricity at the molecular electronic level did not evolve until 140 years later, starting indirectly with the work of Michael Faraday and later with that of J. J. Thomson and of Millikan on the electron. The development of the Leyden jar and the discovery of the principle of charge separation and charge storage on the two surfaces of the Leyden jar, separated by a layer of glass were considered as milestones in the physics of electricity and later for electrical technology, electronics, and electrochemical engineering.

The various renewable sources have the capabilities to meet the world's ever-growing demand for energy for it to work many countries have implemented rules and policies to use this energy efficiently. Studies have shown that in tandem with end-use electrification, renewable energy, and energy efficiency account for 94% of reductions in emissions [13]. India has initiated two projects for Tidal power of 3.75 megawatts and 50 megawatts in West Bengal in 2007 and Gujrat in 2011. However, both projects were failed due to increased cost in return.

The problems of the intermittent nature of energy production from renewable energy sources as well as the pollution from the transport sector can be addressed by developing suitable

energy storage systems. At present, there are different energy storage systems like electrolytic capacitors, batteries, fuel cells, etc. [14-19]. Capacitors can store a very small amount of energy and can deliver it within a very short period of time. On the other hand, batteries and fuel cells can store a huge amount of energy. The growing demand for energy storage systems with high power density, long cycle life, and rapid charge/discharge capabilities have intensified research into advanced energy storage technologies. Among the various energy storage devices, supercapacitors, also known as electrochemical capacitors or ultracapacitors, have garnered significant attention due to their unique ability to bridge the gap between conventional capacitors and batteries. Unlike batteries, which rely on slow faradaic reactions for energy storage, supercapacitors store energy through fast electrostatic interactions, allowing for much faster charge and discharge rates.

Supercapacitors are characterized by their exceptional power density, typically an order of magnitude higher than that of batteries, and their long operational lifetimes, which can exceed millions of cycles. These features make them ideal for a wide range of applications, including hybrid electric vehicles, portable electronics, renewable energy systems, and emergency power supplies. However, despite these advantages, the energy density of supercapacitors remains lower than that of batteries, limiting their widespread adoption. This limitation has driven extensive research into the development of new materials and electrode architectures to enhance the energy storage capacity of supercapacitors.

1.2 Problem Statement

Despite the significant advancements in supercapacitor technology, there are still critical challenges that need to be addressed. One of the primary challenges is increasing the energy density of supercapacitors without compromising their power density and cycle life. This requires the development of novel electrode materials with high specific surface area, good electrical conductivity, and stable electrochemical performance. Furthermore, the electrolyte selection plays a crucial role in determining the overall performance of the supercapacitor, as it influences the operating voltage window and ionic conductivity.

Another challenge lies in the scalability and cost-effectiveness of supercapacitor production. While high-performance materials like graphene and transition metal oxides offer promising results in laboratory-scale studies, their high cost and complex synthesis processes pose barriers to large-scale commercialization. Therefore, there is a need for cost-effective, environmentally

friendly, and scalable solutions to produce supercapacitors that can meet the demands of various applications.

1.3 Objective

Sustainable development of human civilization requires efficient utilization of all- natural resources. From the previous discussions, it is pretty much clear that renewable energy is the future, and it is the most important requirement for sustainability. Guided by this fact, researchers from different countries, including India, have invested efforts in the research of energy generation from renewable sources. The primary objective of this research is to develop and characterize for electrode materials for high-performance supercapacitors. This has naturally led to the extension of research in the field of energy storage. Among the different energy storage devices, the supercapacitor is a relatively new. The specific objectives of this study are:

1. To synthesize and optimize electrode materials with enhanced energy storage capabilities.
2. To investigate the electrochemical performance of these materials in different electrolytes.
3. To evaluate the scalability and practical application potential of the developed supercapacitors.

This thesis work is an attempt to find out the relationship between particle morphology and its electrochemical storage performance. Transition metal oxide- based electrodes can store huge charges, but these types of electrodes are of high resistive in nature. By tuning the electrode material morphology, it is possible to vary the internal resistance of these types of metal oxides, which can be beneficial for electrode material. Transition metal oxides, such as RuO_2, MnO_2, and NiO, as well as conductive polymers like poly vinyl chloride, polyaniline and polypyrrole, are typical materials used in pseudocapacitors. These materials offer higher capacitance than EDLCs but often suffer from lower cycle stability and conductivity. Detailed electrochemical performance testing was carried out to establish the relation to the particle morphology with the electrochemical performance. We used a rather simple Rotary Jet Spin (RJ-Spin) setup which is identical to the candy floss machine, this has increased the yield of synthesis of metal oxide fiber, a bimetal oxide of Ni and Mn ($NiMn_2O_4$) was synthesized via a hydrothermal route. By studying the detailed electrochemical performance, the effect of morphology of these

different chemically equivalent samples was studied. Finally, to improve the electrochemical performance further, a fiber-like morphology of the $NiMn_2O_4$ with PVA was prepared using the RJ-spin technique.

References

[1] Shafiqur R, Maher BA, Al-Moallem Said A. Cost of solar energy generated using PV panels. Renew Sustain Energy Rev. 2007;11:1843-1857.

[2] Timilsina GR, Kurdgelashvili L, Narbel PA. Solar energy: markets, economics and policies. Renew Sustain Energy Rev. 2012;16(1):449-465.

[3] Rourke FO, Boyle F, Reynolds A. Tidal energy update 2009. Appl Energy. 2010;87(2):398-409.

[4] Neill SP, Hashemi MR, Lewis MJ. Tidal energy leasing and tidal phasing. Renew Energy. 2016;85:580-587.

[5] Saidur R, Islam M, Rahim N, Solangi K. A review on global wind energy policy. Renew Sustain Energy Rev. 2010;14(7): 1744-1762.

[6] Islam MR, Mekhilef S, Saidur R. Progress and recent trends of wind energy technology. Renew Sustain Energy Rev. 2013;21: 456-468.

[7] Wang L, Han Y, Feng X, Zhou J, Qi P, Wang B. Metal-organic frameworks for energy storage: batteries and supercapacitors. Coord Chem Rev. 2016;307:361-381.

[8] Guan M, Liao W-H, On the energy storage devices in piezo electric energy harvesting. Paper Presented at Smart Struc tures and Materials 2006: Damping and Isolation; 2006.

[9] Guan M, Liao W. Characteristics of energy storage devices in piezoelectric energy harvesting systems. J Intell Mater Syst Struct. 2008;19(6):671-680.

[10] Vullers R, van Schaijk R, Doms I, van Hoof C, Mertens R. Micropower energy harvesting. Solid-State Electron. 2009; 53(7):684-693.

[11] Richards PD, Myers RJ, Swinton SM, Walker RT. Exchange rates, soybean supply response, and deforestation in south America. Glob Environ Change. 2012;22(2):454-462.

[12] Gielen D, Boshell F, Saygin D, Bazilian MD, Wagner N, Gorini R. The role of renewable energy in the global energy transformation. Energ Strat Rev. 2019;24:38-50.

[13] https://doi.org/10.1002/est2.339.

[14] [8] R. Elliman, C. Gould and M. Al-Tai, Review of current and future electrical energy storage devices. 50th International Universities Power Engineering Conference (UPEC), (2015) 1-5 doi: 10.1109/UPEC.2015.7339795.

[15] A. Zayed, A. L. Shaqsi, K. Sopian, A. Al-Hinai, Review of energy storage services, applications, limitations, and benefits. Energy Reports, 6 (2020) 288-306 doi: 10.1016/j.egyr.2020.07.028.

[16] J. B. Goodenough, Rechargeable batteries challenges old and new. J Solid State Electrochem 16 (2012) 2019-2029 https://doi.org/10.1007/s10008-012-1751-2

[17] J. B. Goodenough, Evolution of Strategies for Modern Rechargeable Batteries. Accounts of Chemical Research, 46 (2013) 1053-1061 doi: 10.1021/ar2002705

[18] A. Kirubakaran, S. Jain, R. K. Nema, A review on fuel cell technologies and power electronic interface, Renewable and Sustainable Energy Reviews, 13 (2009) 2430-2440 doi:10.1016/j.rser.2009.04.004

[19] A. Choudhury, H. Chandra, A. Arora, Application of solid oxide fuel cell technology for power generation-A review. Renewable and Sustainable Energy Reviews, 20 (2013) 430-442 doi: 10.1016/j.rser.2012.11.031.

CHAPTER 2

LITERATURE REVIEW

2.1 Introduction

The consisted demand for global energy requirement is growing in ever-growing society, so there are the concerns about the depletion and associated pollution caused by the usage of fossil fuels. Because of this crisis, several research and technological developments have been undergoing in the areas like renewable energy, energy from alternative sources, energy storage devices, and energy harvesting from waste materials. Among sustainable sources of energy, solar energy, (1,2) tidal energy, (3,4) and wind energy (5,6) are appealing alternative options for electricity generation. However, the complete unreliability and unpredictable characteristics of these sources demands the need of development of efficient and effective energy storage systems. The power derived from whatsoever sources calls for the requirement of storage and to accumulate the energy for sporadic utilization (7-11). Also, storage of energy is of utmost importance for meeting on-demand energy requirements and supply extensively in remote areas and so. Among the various electrochemical technologies in existence today, batteries, capacitors and supercapacitors have saliently subjugated the domain of energy storage, rendering them ubiquitous in the energy sector. In general, the electrical energy storages (EES) are classified based on how the form of energy it used, as shown in Scheme 1.1, into mechanical, thermal, chemical, electrochemical, and EES systems.

Electrochemical Storage systems according to their energy form.

Electrical Energy Storage system

Mechanical	Thermal	Chemical	Electrochemical	Electrical
Pumped hydro storage	Thermochemical	Hydrogen storage	Lithium-ion battery	Supercapacitor
Compressed air energy storage (CAES)	Sensible thermal	Synthetic natural gas (SNG)	Lead acid battery	
Liquid air energy storage (LAES	Latent thermal		NaS BATTERY	
Flywheels			Redox flow battery	

Also, they are of extreme interest in regards to both applicability and deciphering fundamental science via research and development activities. Eventually, these fields have matured a lot in terms of both design and efficiency.

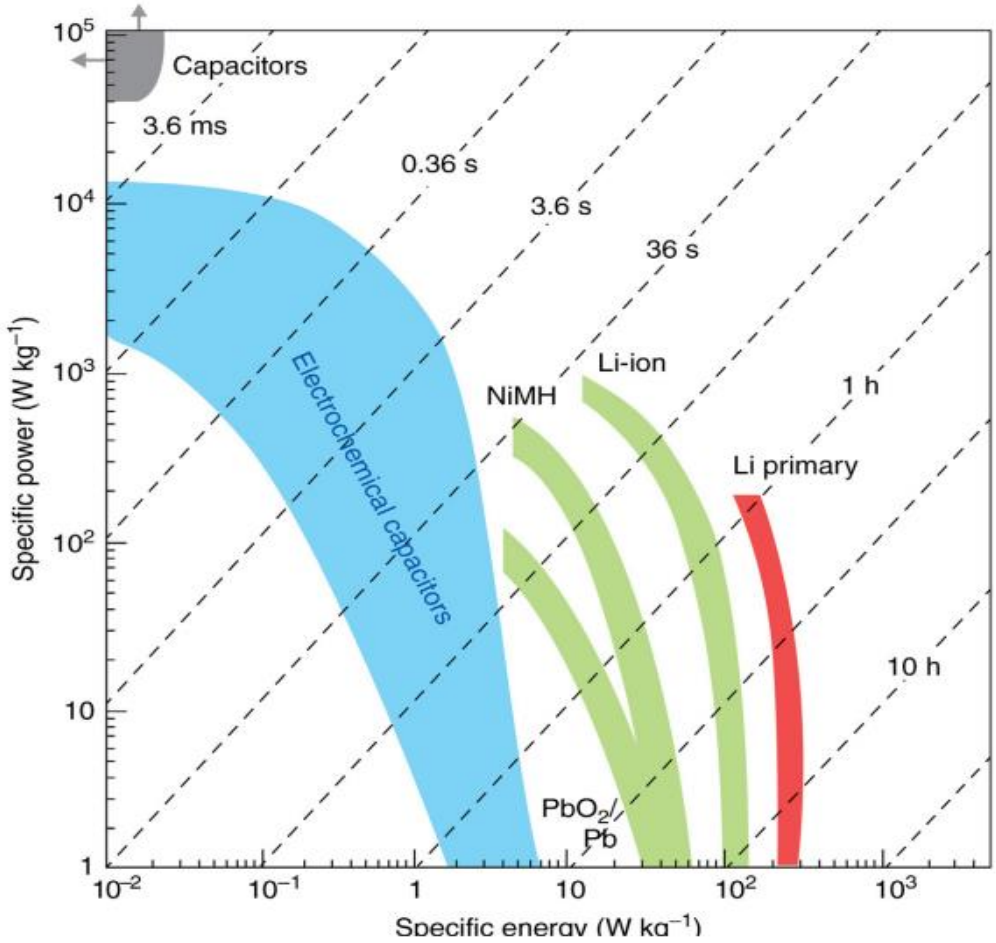


Fig 1.1 Specific power against specific energy, also called a Ragone plot for various energy storage devices. Source: Reproduced with permission from Ref. [17].

Electrochemical supercapacitors gain immense popularity as electrochemical energy storage devices due to their seamless, better characteristics, such as high power as well as reasonably high energy densities and significantly longer cycle life and stability. A plot of power density versus energy density—known as Ragone plot for the energy storage systems is shown in Fig. 1.1 [12]. As can be seen, while a supercapacitor is employed as an energy storage device, the value of specific power implies how quick it can deliver energy, and the value of specific energy indicates on how far it can deliver the energy with a single charging cycle. The time constrains of the devices mentioned in the figure are derived by dividing the energy density by the power (13). Owing to the attractive characteristics of the supercapacitors, they are presently used in a variety of applications ranging from power electronics, large-scale vehicular usage, such as EV

buses and Electric subway trains, store energy at intermittent generators in windmills to smart grid applications catering to stability, frequency smoothing and regulation, and for peak shifting. The future for energy storage devices such as batteries and the supercapacitors expected to grow exponentially. A supercapacitor in contrast from a regular capacitor owing to its very high capacitance, and is rated in Farads, which is several times of magnitude higher than the electrolytic capacitor. On application of Differential voltage on the positive and negative plates, charges the capacitor, which is just like the building up of electrical charge (static charge) while walking on a carpet and the release of energy through fingers while touching an object.



Fig 1.2 Commercial Supercapacitors

Supercapacitors are considered to be an ideal energy storage device due to its ability to undergo frequent charge–discharge cycles at high current in very short intervals. The charging time of a supercapacitor is nearly 10 s and the self-discharge of a supercapacitor is substantially higher than that of an electrostatic capacitor and little higher than a battery, the main contributor to this phenomenon is organic electrolyte. In general, the energy stored in a supercapacitor falls to nearly about 50% in duration of nearly 30 days; while a nickel-based battery self-discharges 10%–15% in a month but Li-ion battery discharges only to an extent of 5% per month (14).

Lately, the transport industry has grown in need for a compromise between energy and power density requirements in energy storage systems by introducing hybrid electric vehicles (HEVs), plug-in hybrid electric vehicles (PHEVs), and fully-electric vehicles (EVs). Batteries and supercapacitors are two separate devices, conjoined as a single device serving as pioneers in the domain of energy storage (15,16) in applications ranging from simple portable electronics

to complex electricity grid networks. However, neither of these two technologies can satisfy all requirements. A Ragone plot in Fig 1.1 is a crucial tool in determining the suitable energy technology for a specific application based on a comparison of the energy and power densities of different energy harvesting devices. As seen in Figure 1.1, batteries are acclaimed for their high energy densities, while supercapacitors possess higher power densities (18).

Consequently, there are few fields of application (19) where single storage device either batteries or supercapacitors may still be inadequate for these applications. Therefore, hybrid systems with two or more energy storage units are of immense attention worldwide. Which ensure better flexibility, longevity, and higher efficiency of the system by equitably distributing the load among the units (20-26) For instance, fuel cells have even higher energy densities as compared to batteries (27) (Figure 1.1). Yet, they fail to compensate for the recurrent variations of the required power in the system owing to their slow dynamics (28) As a result, the incorporation of devices with faster dynamics and higher power densities such as batteries and supercapacitors lead to the better overall performance of the system.

2.2 Supercapacitor Fundamentals

In a **capacitor**, energy is stored in an electric field between two conducting plates. A conventional capacitor consists of electrically conducting plates separated by an electrically insulating material. In a configuration like this the capacitance can be calculated from

$$C = \epsilon_0 \epsilon_r \frac{A}{d} \qquad 2.1$$

Where ϵ_0 is the dielectric constant of vacuum, ϵ_r is the relative dielectric constant of the dielectric material, A is the area of the conducting plates and d is the distance between the plates.

The main characteristics of a capacitor are its energy density and power density. In order to measure either of these, here density calculated as a quantity per unit mass or per unit volume. The energy E stored in a capacitor is directly proportional to its capacitance:

$$E = \frac{1}{2} CV^2 \qquad 2.2$$

In an electrochemical capacitor, also known electric double layer capacitor (EDLC), supercapacitor or ultracapacitor, the energy is also stored in the electric field at the interface between the electrode and electrolyte as shown in figure 2.2. This mechanism facilitates comparably much higher energy density for supercapacitors than achieved in conventional capacitors.

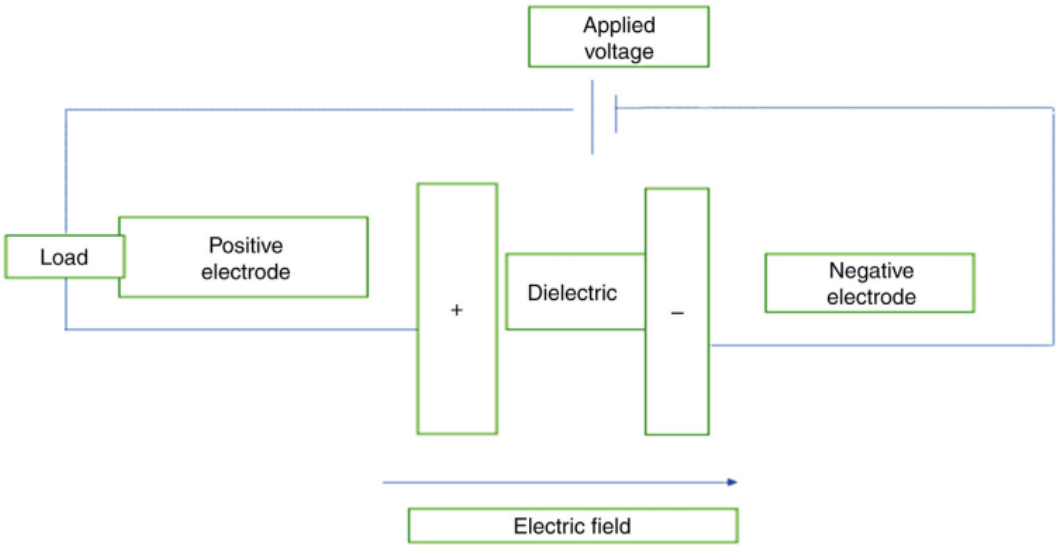


Fig 2.1 Diagrammatic representation of a conventional capacitor

It is known that the power ***P*** is the energy per unit time. To determine power ***P*** of capacitor. In the circuit shown in Fig. 2.1 the capacitor is in series with an external load ***R***. The internal components of the capacitor, such as electrodes, current collectors, and dielectric material also contribute to the resistance (in short internal resistance) which is measured cumulatively which is termed as the Equivalent Series Resistance (***ESR***). During discharge the voltage is determined by these resistances. When measured in terms of impedance (***R = ESR***), the maximum power P_{max} for a capacitor [29-31] is given by Eq. (2.3), showing that how ESR can limit the maximum power of a capacitor.

$$P_{max} = \frac{V^2}{4 \times ESR} \qquad 2.3$$

Conventional capacitors have relatively low energy densities but high-power densities compared to electrochemical batteries and fuel cells (separate energy conversion devices).

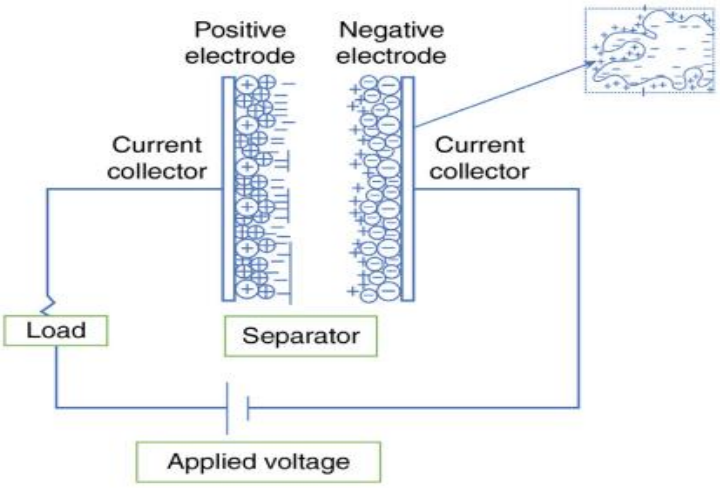


Fig 2.2 Schematics of an electrochemical double layer capacitor

Therefore, a battery can store more total energy than a capacitor can, but its power density is low so it cannot deliver the same amount of this energy as fast as the capacitor does. On the contrary, capacitors can be discharged quickly and give off a lot of power in short time intervals resulting high power output even though they do not contain much energy/mass or volume, hence they often have high power densities. Supercapacitors are similar to conventional capacitors except that they have electrodes with much greater surface area (***A***) and thinner dielectrics which decreases distance ***d*** between the electrodes. Accordingly, from Eqns (2.1) and (2.2), it can be seen that this leads to an increase in both capacitance and energy. By engineering the low ESR of characteristic of conventional capacitors, supercapacitors also are capable of attaining comparable power densities. This difference has also been noted through equation 2.3 as given by M Hessami et al (2013). Nevertheless, supercapacitors maintain the low ESR character of typical capacitors hence ensuring approximately equal power density is

achieved. Supercapacitors have better advantages than batteries and fuel cells due to their higher power density, shorter charging times as well as longer cycle life and shelf life. A schematic diagram showing some of such characteristics is illustrated in Fig 2.2. The potential distribution and equivalent circuit model of a supercapacitor is shown in figure 2.3. When voltage is applied, the potential difference is distributed at the interfaces between electrolyte and electrodes as well as inside the electrolyte (due to ionic resistance) and inside the electrodes and current collectors (due to electrical resistance). In principle, when the supercapacitor is

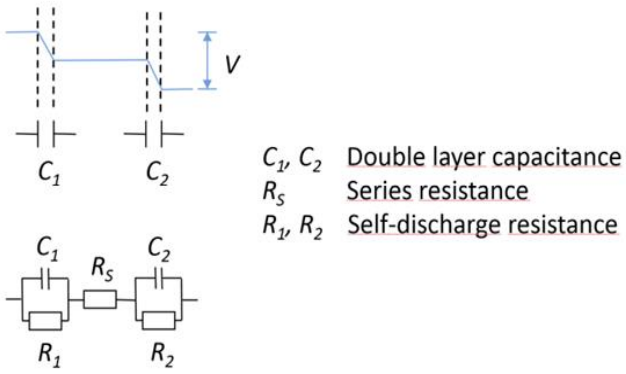


Fig2.3 Potential distribution inside a supercapacitor and its equivalent circuit model. (Zhang and Zhao 2009)

disconnected i.e. it is neither charged nor discharged the potential differences are located only at the electrode-electrolyte interfaces.

Self-discharge:

It is the phenomenon which causes the voltage of a charged supercapacitor to decrease even when it is not electrically connected to a load. The reasons can be related to chemical reactions or physical processes. (Andreas 2015, Conway 1999, Conway et al. 1997, Niu et al. 2004) To keep supercapacitor voltage constant, a small current is needed to maintain the voltage. This current is called leakage current. There are several mechanisms to cause self-discharge:

1.Ohmic leakage between the electrodes

2. Overcharging beyond electrolyte solution decomposition potential

3. Parasitic Faradaic reactions

4. Charge redistribution

The Ohmic leakage is caused by a resistive pathway between the positive and negative electrode. This is due to a problem e.g. in constructing the supercapacitor or because of a mechanical failure. Overcharging beyond the electrolyte decomposition can be obviously avoided by keeping the voltage low enough, e.g. in case of aqueous electrolytes below the

decomposition potential of water. The parasitic Faradaic reactions are reduction and oxidation (redox) reactions on the electrode surface discharging the electrode. For instance, on the positive electrode the potential may be higher than the oxidation potential of impurity ions such as e.g. iron in solution on the electrode surface. (Andreas 2015) The oxidation of the impurities causes electrons to move across the double layer into the electrode surface, which further releases the anions from the double layer, decreasing the potential of the electrode. The reactions on the negative electrode are analogous and, for instance, the reduction of oxygen can discharge the negative electrode. Charge redistribution causes a phenomenon which is similar to self-discharge but mainly relevant only for relatively short time periods. It is due to the time difference between charging different parts in the porous electrode structure. The outer part of the electrode charges more quickly than the surfaces located deep in the pores. When the charging is ended before it is completed, charges continue moving deeper into the material, which causes the voltage to decrease and is thus visible as self-discharge.

Temperature range:

As already mentioned with respect to application potential, the temperature range of supercapacitors is typically wider than that of batteries. The range is mainly limited by the properties of the electrolyte. (Zhong et al. 2015) To enable ionic conductivity, the electrolyte may not prevent the ions to move, thus the solidification of an electrolyte sets the low temperature limit. At high temperature the electrolyte starts to boil or decompose, which increases the pressure inside the supercapacitor with destructive consequences. An approximate temperature range for supercapacitors with aqueous electrolytes is from -10^{o} to near + 100^{o} C, with organic electrolytes from -40 to $+70^{o}$ C and with ionic liquid electrolytes from room temperature to over 100^{o} C. (Xiong et al. 2015)

Cycle life, calendar lifetime:

The basic reason for the longevity of supercapacitors is that their operation does not require chemical or electrochemical reactions. When charging or discharging, ions and electrons move inside electrolyte and electrodes. Thus, compared to batteries, dimensional changes due to electrochemical reactions do not take place and the materials are not exposed to mechanical deterioration in the same way. Supercapacitor's function also deteriorates with time, though slow, especially at higher temperature and when high voltage is applied. (Bohlen et al.2007A, Bohlen et al. 2007B, Kötz et al. 2006). Although energy storage in supercapacitors is not based on Faradaic reactions, parasitic electrochemical reactions occur and can reduce the lifetime.

Increasing temperature and voltage accelerate the ageing reactions exponentially. Typically, the capacitance decreases and ESR increases with time. (Azaïs et al. 2007). The main cause leading to ageing are mainly side-reactions that lead to electrolyte loss, blocking of the pores in electrodes surface and generation of volatile by-products, which may form gas bubble and thus pressure increase inside the supercapacitor. (He et al. 2016, Ratajczak et al. 2014) Surface functional groups and impurities (water in organic electrolyte, metals and e.g. oxygen) contained in the activated carbon electrodes are possible reasons for the deterioration of electrical properties. (Azaïs et al. 2007) The encapsulation of a supercapacitor may be an essential factor in determining the lifetime. Poor barrier properties against electrolyte evaporation or against oxygen penetration from air can result in fast degradation.

Main difference between Capacitor and Supercapacitor

Characteristics	**Capacitor**	**Supercapacitor**
Construction	Capacitor is a two metallic terminals (Electrodes) device with dielectric medium in between. Electric energy is stored in the electrostatic field in it.	Supercapacitor is a type of polar capacitor and electrolytic solution is used instead of dielectric. The activated carbon is used on electrodes to enlarge the area.
Definition	A Capacitor stores potential energy in the form of electric field (electrostatically) and release to the circuit as electrical energy.	A Supercapacitor lays in between Capacitor and battery. Also known as Super Cap, Double Layer Capacitor or Ultra-capacitor. Supercapacitor has very high capacitance and low voltage rating as compared to a normal Capacitor
Working	Capacitor store energy in the form of electric field.	Supercapacitor stores energy between the ions of the electrolyte & electrode in a double layer of charge.
Types	• Electrolytic • Capacitors, • Film Capacitors, • Tantalum,	• Electrostatic Double-Layer Capacitors (EDLC's) • Electrochemical Pseudocapacitors • Hybrid Supercapacitors.

	• Integrated Capacitor	
Dielectric Material	Aluminium oxide, polymer films or ceramic are used in capacitor as dielectric medium in between the electrodes.	In Supercapacitor, activated carbon is used as medium. When voltage applied, a double electric field is generated which acts like a dielectric medium.
Charge / Discharge Time	Charging and discharging of conventional capacitor is normal as compared to supercapacitor i.e. 10-3-10-6 seconds.	Supercapacitors can deliver charge much faster than a battery and store charge more than an electrolytic capacitor per volume unit. That is why it is considered between a battery and an electrolytic capacitor.
Charge / Discharge Efficiency	> 0.95	0.85 – 0.98
Operating Temperature	-20 to 65 °C (-4 to 149°F)	-40 to 65 °C (-40 – 149°F)
Energy	<0.1 Wh/kg	1-10 Wh/kg [https://doi.org/10.1016/j.enconman.2006.12.015]
Energy Density	Low	Very High
Specific Power	Up to 100,000 Wh/kg	Up to 10,000 Wh/kg
Cost	Low	High
Advantages	• It avoids excessive drawing of power • Less Battery drain due to a capacitor • High Integration Density • Real and Reactive Power Control	• Long Life Cycle • High Energy Storage • Fast Charging and Discharging Time • High Load Currents

Applications	• Smoothing power supply's output. • Power factor correction • Frequency filters, high pass, low pass filters. • Coupling & Decoupling of signals. • Motor Starter • Snubber (Surge absorber & Noise filter) • Oscillators	• Cordless electric screwdriver, which can be charged in a few minutes. • LED flashlights in digital cameras. • For stabilizing power supply in laptops and handheld devices etc. • Uninterrupted power supply (UPS) where it replaces electrolytic capacitor banks. • Supercapacitors are used in ICs, RAM, CMOS, Clocks and micro-computers etc.

2.3 Supercapacitor Types

The operational principle of a supercapacitor is based on energy storage and the distribution of the ions coming from the electrolyte with respect to surface area of the electrodes. Based on the energy storage mechanism, supercapacitors are classified into three classes: Electrochemical double-layer capacitors, pseudo-capacitors, and hybrid supercapacitors as shown in Scheme 2.1 [6b], and depicted in Fig. 3.

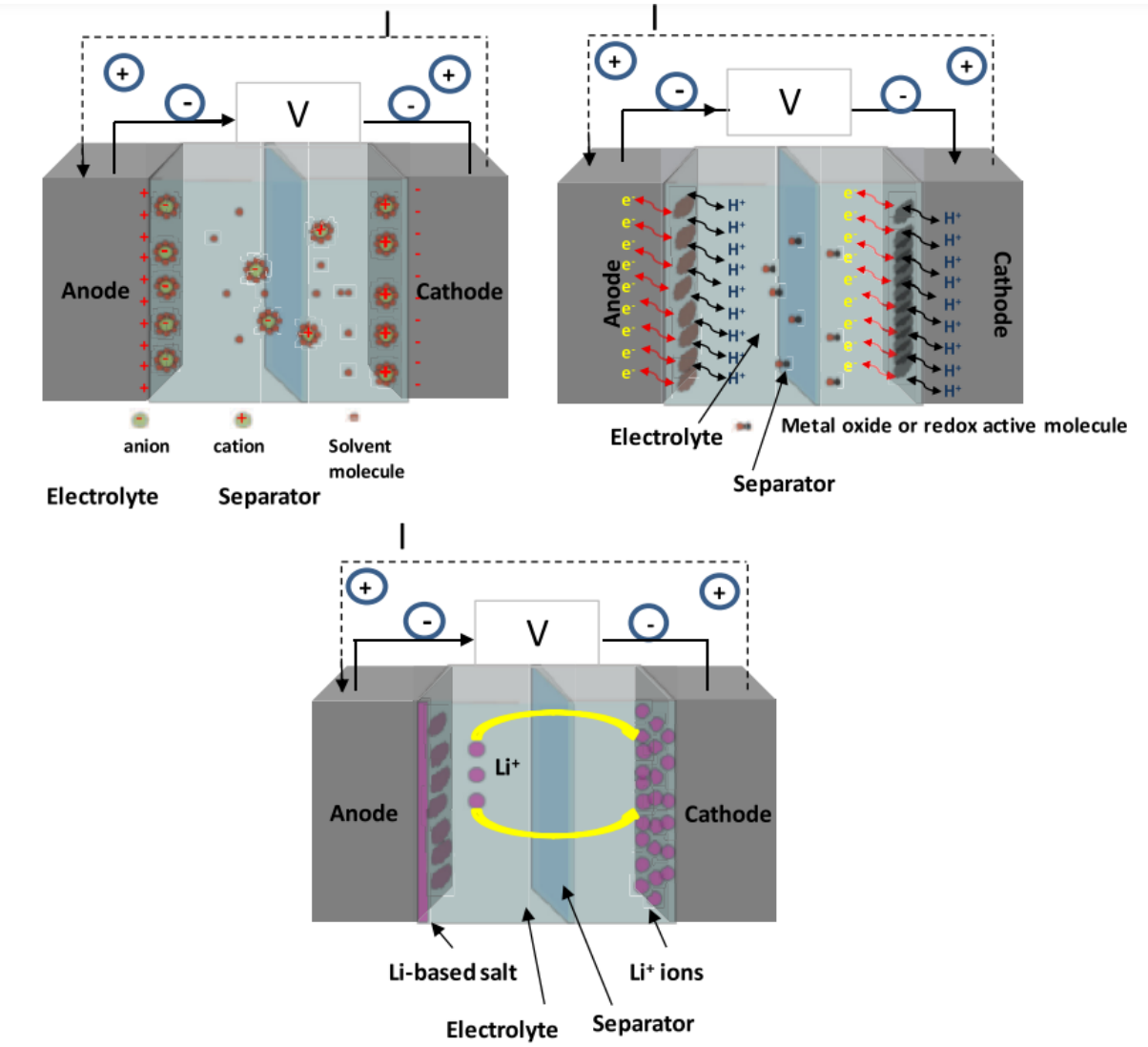
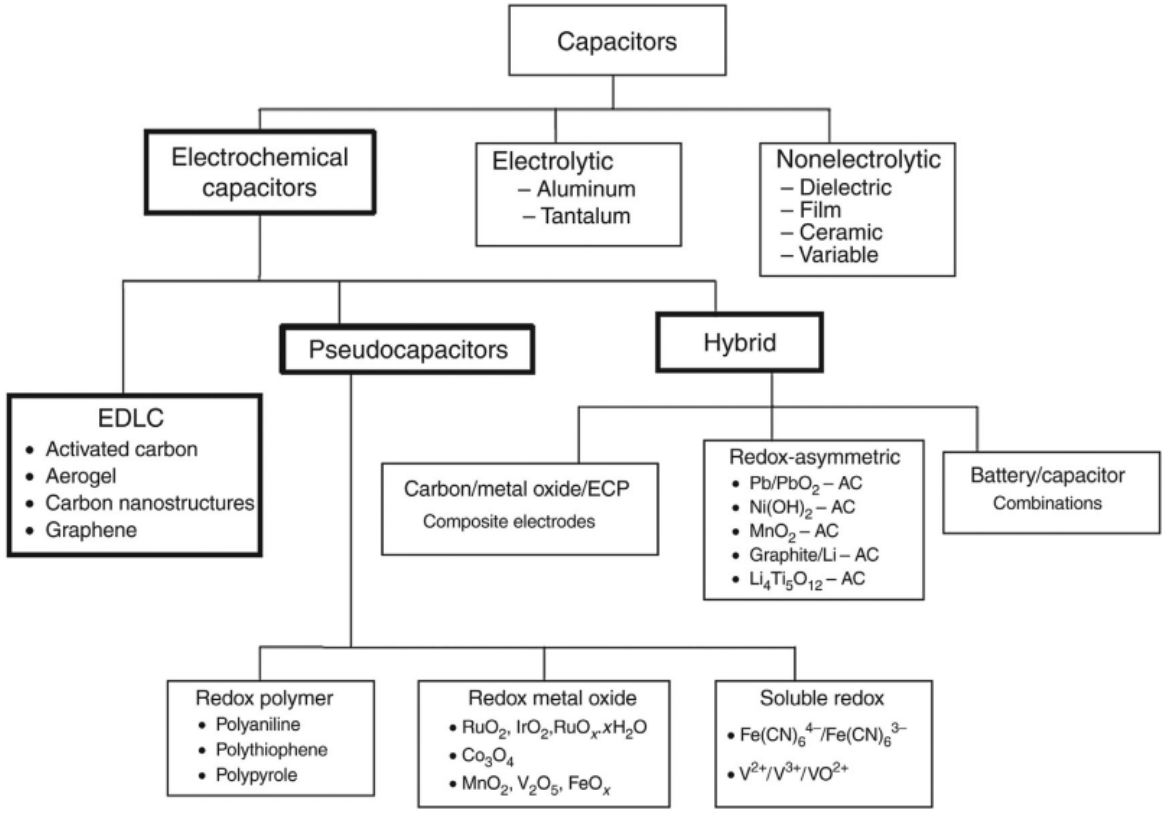


Fig 3 Schematic representation of (A) an electrical double-layer capacitor (EDLC), (B) a pseudocapacitor, and (C) a hybrid supercapacitor (HSC).

2.3.1 Electrochemical Double Layer Capacitors (EDLCs)

EDLCs comprises of two carbon-based materials as electrodes, an electrolyte, and a separator. It stores charge either electrostatically or through non-Faradic process, which involved no

transfer of charge between the electrode and the electrolyte [32,33]. The mechanism of energy storage involved by forming of Electric Double Layer (EDLCs). On the application of voltage on the electrodes, resulting the accumulation of charge on electrode surfaces, due to potential difference the ions within the electrolyte diffusing through the separator and onto pores of the oppositely charged electrode. A double layer of charge is formed to avoid recombination of ions at electrode interface. The electric double layer with the electrode surface increase in specific surface area ***A*** and decreased the separation distance ***d*** between electrodes allow EDLCs to attain higher energy density [34]. The charge storage mechanism in EDLCs allows highly fast energy intake, delivery, and higher power performance.



Scheme 2.1 Different classes and subclasses of supercapacitors. Source: Ref. [33].

This is non-Faradaic process so chemical reaction takes place, thereby there is no change in appearance of active material (no swelling observed) which is common in batteries during charging and discharging processes. The main differences between EDLCs and batteries are:

1. EDLCs can perform millions of cycles unlike batteries that can withstand only a few thousands at best.

2. Charge storage mechanism does not involve solvent of the electrolyte; but in Li-ion batteries it contributes to solid electrolyte inter phase when high-potential cathodes are employed or with graphite anodes [35,36].

However, EDLC store charge electrostatically on the surface of electrode, for that EDLC devices have a limited energy density, and for this reason the present focus of research is to increase energy performance and to enhance the range of temperature for the battery function. Performance of EDLC can be tuned depending on the choice of the electrolyte.

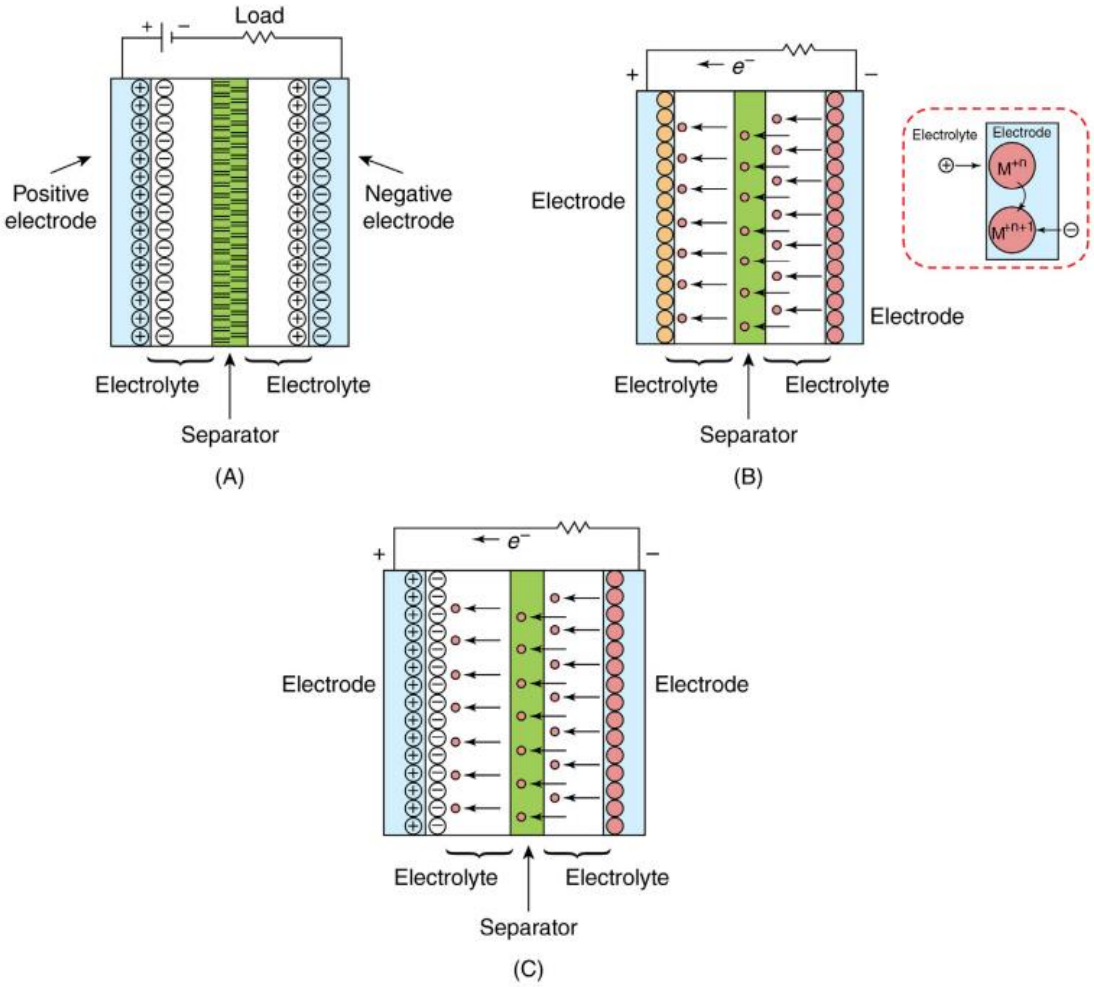


Fig 3.1 Supercapacitor types. (A) EDLC, (B) Pseudocapacitor, and (C) hybrid capacitor. *Source: Ref. [41].*

2.3.2 Pseudocapacitors

Contrary to EDLCs which stores charges Electrostatically by non-Faradaic process Pseudocapacitors stores charges in Faradaic process which involves actual transfer of charge between electrodes and electrolyte [37]. When a voltage applied onto a Pseudocapacitor redox reaction occurs on the electrode material which involves the passing of charge across the double

layers, which resulting in Faradaic current passing through the supercapacitor cell. This Faradaic process results Pseudocapacitors to attain greater specific capacitance and energy densities than EDLCs. Few Metal Oxides, Bimetal oxides, conducting Polymers shows pseudocapacitance due to Faradaic nature, results in redox reactions just similar to batteries, but lack in power density and stability during cycles [38-40].

2.3.3 Hybrid Capacitor

The purpose of Hybrid capacitors is to harness the maximum benefits to obtain better output by reducing the relative drawbacks of EDLCs and Pseudocapacitors. Hybrid capacitor is a type of supercapacitors use of both processes Faradaic and non-Faradaic for storing energy, resulting in both higher energy and power densities than those of EDLCs and better cyclic stability and high-power output and affordability as compared to Pseudocapacitor. There are three types of hybrid capacitors, characterized by their electrode configurations such as, composite type, asymmetric type, and battery type. Composite type electrodes assimilate both physical and chemical processes of energy storage onto a single electrode by integrating carbon materials to it, either with conducting polymers or metal oxides. The carbon materials allow the formation of a capacitive double-layer of charge and thus improving the interaction between the electrolyte and the deposited pseudocapacitive materials by providing a reasonably higher surface area. The capacitance of the electrodes is further enhanced via Faradaic reactions on the pseudocapacitive materials [41]. Composite electrodes developed through the hybridization of CNTs and Polypyrrole have been observed to show capacitance values higher than either of the parent materials [42,44]. The presence of the matted structure, allows a uniform overlay of Polypyrrole and 3D charge distribution that makes it possible. Furthermore, the mechanical stress induced to inject and extract ions from the polypyrrole was seen to be reduced by the structural coherence of the intertwined mat. As a result, composite electrodes are able to deliver cycling stabilities as high as that of EDLCs [45]. Asymmetric electrodes combine the both mechanisms Faradaic and non-Faradaic by pairing an EDLC electrode with a pseudocapacitor. These devices provide the benefit of utilizing abundant cost-effective materials (eg, carbon) in lieu of scarce and costly materials (eg, RO) as the negative electrode. This can be making more cost effective by using organic or polymer coated electrodes. Although incorporating a conducting polymer as positive electrode may circumvent the problems of having lower capacitance and higher resistance of the negative carbon electrodes, however, they tend to have poor potential delivery and cycling stabilities. However, this combination mitigates the complications of this trade-off to a great extent as compared to a scenario wherein the two

materials are exploited separately [45]. These Asymmetric capacitors (Hybrid Capacitors) deliver higher energy and power densities than those of EDLCs and better cycling stability as compared to pseudocapacitors [46,47]. Battery-type capacitors, on the other hand, utilize the combination of a battery type electrode and a supercapacitor type electrode. This results in a unique device with energy density comparable to batteries and power density, cycle life, and fast charge-discharge time of that of a supercapacitor. Materials, such as $Ni(OH)_2$, PbO_2, LTO ($Li_4Ti_5O_{12}$), or other alkali metals, coupled with some activated carbon have enables promising results when tested as electrodes for these devices [48-51]. It is believed that battery-type capacitors tame the potential to closes the gap between batteries and supercapacitors. Nevertheless, further intensive research on this type of device is imperative to bring out their full underlying potential [49].

2.4 Mechanism of Supercapacitor

2.4.1. Traditional Electric Double Layer Theory:

Supercapacitors bridge the gap between traditional capacitors and rechargeable type batteries, which store energy reversibly by adsorbing the ions present in the electrolyte on the electrode surface under an applied potential. The close look into the charge storing mechanism of supercapacitors electrodes is important for engineering a high-performance supercapacitor. Initially, supercapacitors were assumed to be function like parallel plate capacitors. There are several theories or models explaining for this interface between a solid and a liquid. It is interesting to witness the historical evolution of the models, incorporating successively more factors, which reflect the interfacial structure. The Figs. 2.4.1.1, pictorially illustrate the early double layer models namely Helmholtz model, Gouy-Chapman model, Stern model, and Grahame model, while Fig. 4 represent the later model by Bockris-Devanathan-Müller (known as BDM Model).

2.4.1.1 Helmholtz model: Hermann von Helmholtz was the first one to report that charged electrodes immersed in electrolyte solutions repel the ions of the same charge while attracting ions of the opposite charge to their surfaces. Two layers of opposite charge polarity form at the interface between electrode and electrolyte. He has demonstrated that that an electrical double layer (DL) is essentially a molecular dielectric and statically stores electric charge, in 1853. This theory is the original model was proposed when Helmholtz studied colloidal suspensions for the first time in the 1850s [52]. This theory is the simplest approximation for representation of the spatial charge distribution at double layer interfaces. The charge of the solid electronic

conductor is neutralized by opposite sign ions at a distance from the solid. This is the distance from the surface of the electrodes to the centre of the ions. As shown in the Fig. 2.4.1, the decomposition voltage of the electrolyte in the stored state is linearly dependent on the voltage applied to it. Here, X_H would be the distance of closest approach of the charges, that is, ionic radius, which, for the purpose of calculation, were treated as point charges. By analogy with a capacitor the capacity would be

$$C_{d,H} = \frac{\varepsilon_0 \varepsilon_r}{X_H} \qquad 2.4.1.1$$

Here ε_r is the relative permittivity, which is assumed constant with distance and ε_0 the permittivity of vacuum space. The decay of the electrostatic potential from φ_M to φ_S is linear (Fig. 2.4.1B) and $C_{d,H}$ does not vary with the potential applied to the electrode (Fig. 2.4.1C). This early model predicted a constant differential capacitance independent from the charge density depending on the dielectric constant of the electrolyte solvent and the thickness of the double-layer, and provides a good foundation for the description of the interface,

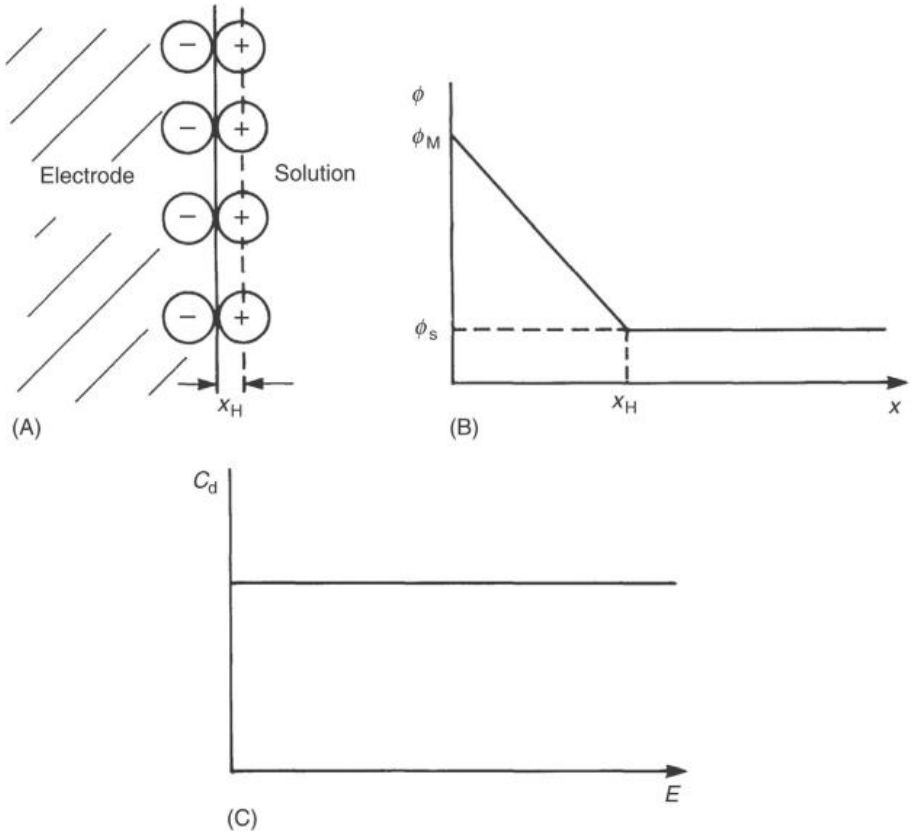
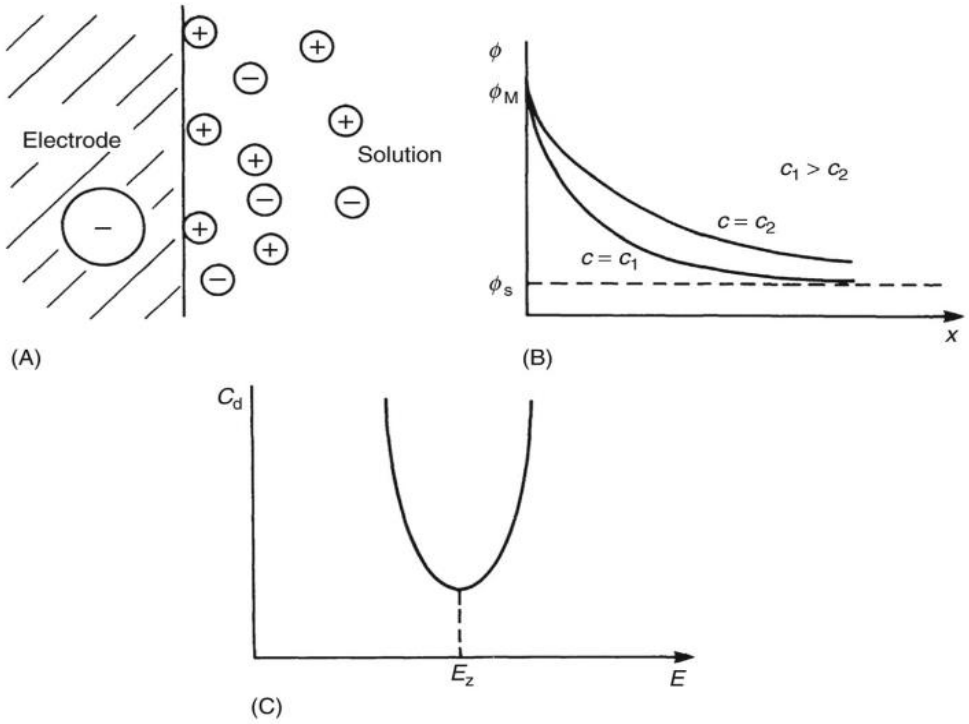


Fig 4.1.1: The Helmholtz model of the double layer. (A) Rigid arrangement of ions; (B) variation of the electrostatic potential, ϕ, with distance X, from the electrode; and (C) variation of C_d with applied potential. Source: Ref. [53]

but does not consider several major factors that includes diffusion/mixing of ions in solution, the possibility of adsorption onto the surface and the interaction between solvent dipole moments and the electrode. As of today, this is taken as the simplest theory, which does not adequately explain what occurs in nature [54,55].

2.4.1.2 Gouy-Chapman or Diffuse model: In 1910, Louis Georges Gouy and David Leonard Chapman in 1913 both observed that capacitance was not a constant and that it depended on the applied potential and ionic concentration. Gouy showed that in a liquid surrounding a charged solid the equal amount of opposite ionic charge appears, but the ions are not rigidly attached to the surface [54]. These ions in solution tend to diffuse into the liquid phase until the counter potential set up by their departure restricts this tendency. The kinetic energy of ions in solution partially determines the thickness of the diffused layer. Gouy and Chapman theorize with significant improvements by introducing a diffuse model of the double layer as can be seen from Fig. 2.4.1.2. In this model, the charge distribution of ions as a function of distance from the metal surface allows Maxwell-Boltzmann statistics to be applied. Thus, away from



2.4.1.2 The Gouy-Chapman model of the double layer. (A) Arrangement of the ions in a diffuse way; (B) variation of the electrostatic potential, ϕ, with distance, X from the electrode, showing effect of ion concentration, c; and (C) variation of Cd with potential, showing the minimum at the point of zero charge Ez. Source: Ref. [56].

the surface of the fluid bulk the electric potential decreases exponentially. This model fails to

explain for highly charged double layers [57]. Experimentally, the measured thickness of double layers is greater than the calculated.

2.4.1.3 Stern model: Although the Gouy-Chapman model makes a better approach than the Helmholtz model, but still has limited quantitative applications. The Gouy-Chapman model fails for highly charged Double layers. It presumes that the ions are like point charges and that they can approach close the surface with no limits, which is untrue. In 1924, Otto Stern proposed the combining of the Helmholtz model with the Gouy-Chapman model. In Stern's model, some of the ions adhere to the electrode as suggested by the Helmholtz model, giving an internal Stern layer, while some ions form a Gouy-Chapman diffuse layer.

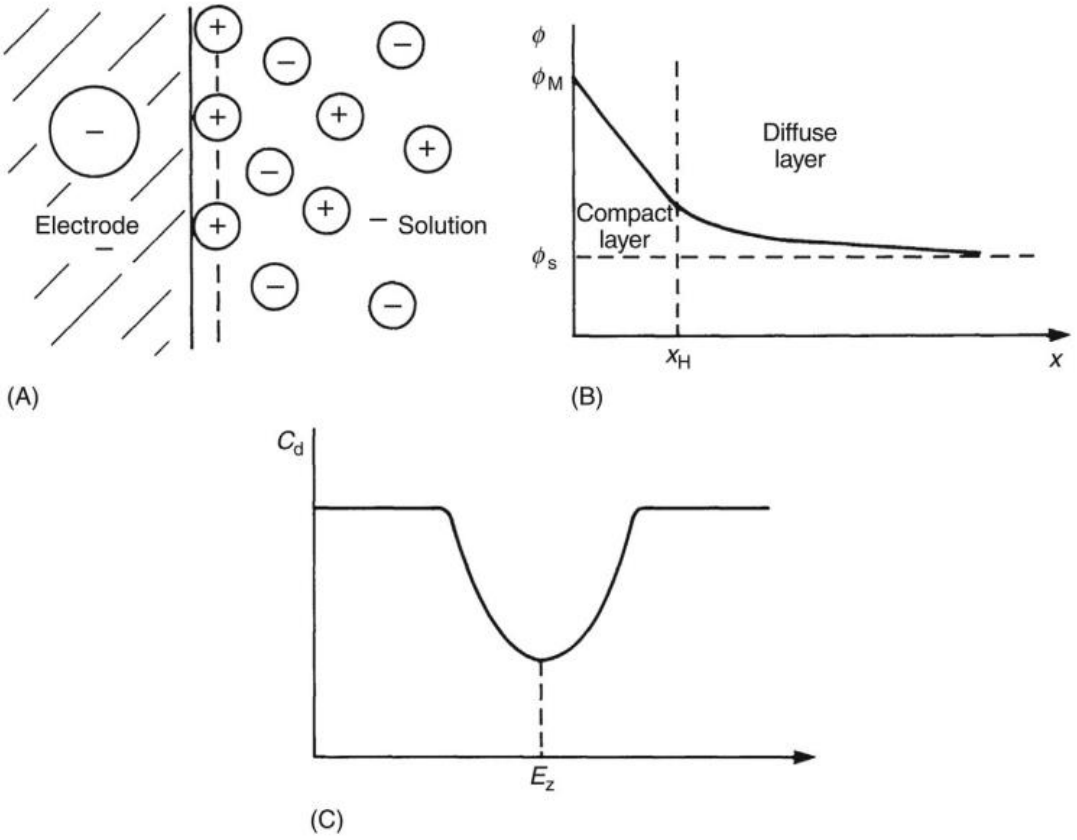


Fig 2.4.1.3 The Stern model of the double layer. (A) Arrangement of the ions in a compact and a diffuse layer; (B) variation of the electrostatic potential, ϕ, with distance, X, from the electrode; and (C) variation of C_d with potential. Source: Ref. [58].

Stern modified the Gouy-Chapman model stating that the ions have a finite size, so limiting their approach to the surface and hence the Stern layer accounts for ions' finite size and consequently an ion's closest approach to the electrode is on the order of the ionic radius. In the Gouy-Champman model. The first ions are at the δ distance away from the surface, but the

Stern model presumes that there can be specifically surface-adsorbed ions in plane δ, which is known as the Stern-layer. Ions are strongly adsorbed by the electrode surface within this so-called compact layer. In the compact layer, there are specifically adsorbed ions (forming the inner Helmholtz plane), and non-specifically adsorbed counter-ions (forming the outer Helmholtz plane) (Fig. 2.4.1.3) [58].

In mathematical terms, this is equivalent to two capacitors in series, with capacities C_H representing the rigid compact layer and C_{GC} representing the diffuse layer. The smaller of the two capacities determines the observed behaviour:

$$\frac{1}{C_d} = \frac{1}{C_H} + \frac{1}{C_{GC}} \qquad 2.4.1.3$$

Fig 2.4.1.3C shows the variation of the total capacity with potential. There are two extreme cases: The first one is where, close to E_z, $C_H \gg C_{GC}$ and so $C_d \sim C_{GC}$ and the other situation far from E_z, $C_H \ll C_{GC}$ and $C_d \sim C_H$, which satisfies the assumptions of the model. As in the Gouy-Chapman model, the more concentrated the electrolyte the less the importance of the thickness of the diffuse layer and the more rapid the potential drop. At distance X_H, there is the transition from the compact to the diffuse layer. The separation plane between the two zones is called the outer Helmholtz plane (OHP): the origin of the inner Helmholtz plane will be discussed later. Comparison between Figs. 2.4.1.2 and 2.4.1.3 reveals that this model is the best of the three so far, but does not yet explain all the facets of the curves shown.

2.4.1.4 Grahame model: In 1947, D.C. Grahame modified Stern proposed that some ionic or uncharged neutral species can penetrate the Stern layer, although the closest approach to the electrode is normally occupied by solvent molecules. This could happen if ions lose their solvation shell as they approach the electrode surface area. He called ions in direct contact with the electrode as “specifically adsorbed ions.” This model proposed the existence of three regions. The inner Helmholtz plane (IHP) passes through the centers of the specifically adsorbed ions. The OHP passes through the centers of solvated ions at the distance of their closest approach to the electrode surface. Finally, the diffuse layer is the region beyond the OHP (Fig. 2.4.1.4). The difference between this model and the Stern model is the presence of specific adsorption, in this phenomenon a specifically adsorbed ion loses its solvation, approaching closer to the electrode surface—besides this it can have the same charge as the electrode or the opposite charge, but the bonding is strong. In both the Stern and Grahame models, the potential varies linearly with distance up to the OHP (Outer Helmholtz Layer) and then varies exponentially at the diffuse layer.

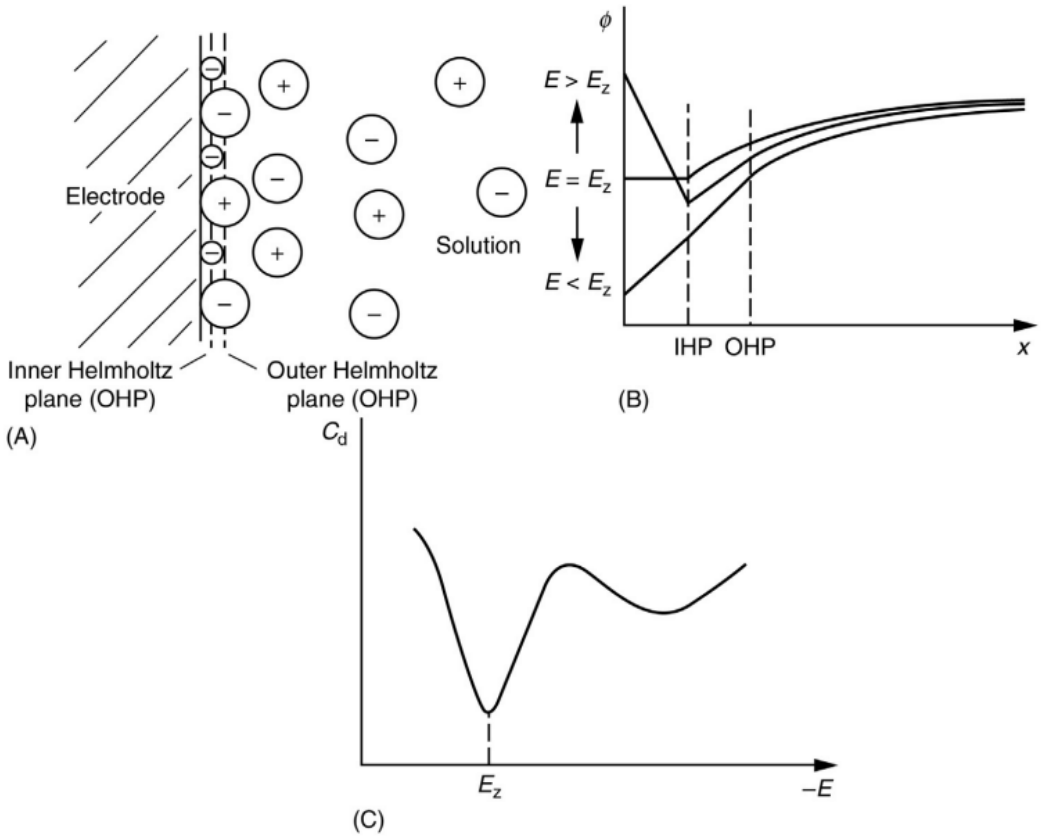


Fig 2.4.1.4 Schematic representation of Grahame model. (A) Arrangement of ions; (B) variation of the electrostatic potential, ϕ, with distance, X, from the electrode, according to the applied potential; and (C) variation of Cd with potential. Source: Ref. [58].

2.4.1.5 Electric double layer in supercapacitors

Although the models discussed above gave a satisfactory explanation of the electrical double layer on plane surfaces, they are inadequate in describing the actual charge distribution in nanoporous electrodes employed in supercapacitors. The peculiarities of ion electrosorption in porous media make the process of charge storage extremely difficult, and there is still a lack of complete understanding of the behaviour of ions in nanopores. When a supercapacitor is charged (potential applied), electrons are forced to go from the positive electrode to the negative electrode through an external circuit. As a result, cations within the electrolyte concentrate in the negative electrode and anions in the positive electrode forming an Electric Double Layer (EDL) that compensates the external charge unbalance. During the discharge, electrons travel from the negative electrode to the positive electrode through an external circuit, and both cations and anions in the pores mixed again until the cell is discharged completely. Ions do not travel in the bulk electrolyte the same way as they can within the

pores of an electrode material. The mobility of ions into the pores are greatly depends on the pore size, which if too small makes the pores inaccessible, not contributing to double layer capacitance [59]. Though not all the pores are accessible to the ions (because of the pore size) there is no linear relation between the capacitance exhibited by a material and its specific surface area [60-63] measured with a small gas molecule probe, such as N_2 or Ar. Various studies suggest that pore size below 0.5 nm is not accessible to hydrated ions [63, 64], and pores smaller than 1 nm of size can be too small for organic electrolytes [65]. Generally, there is a conundrum regarding the effect of pore size variation on capacitance. Chmiola et al. claimed that pores with sizes below 1 nm greatly contribute to the capacitance [66]. This increase was explained with the distortion of the salvation shell, thus reducing the distance between charges and enhancing the capacitance [67,68]. However, in organic electrolyte constant capacitance in the micropores was measured on the basis of a detailed study of pore size using complementary adsorption techniques. The decrease in the distance between the electronic and ionic charges is counter balanced by the corresponding decrease in the effective dielectric permittivity inside the pores, which occurs due to gradual ion desolvation [69-71]. Leaving the controversy of capacitance versus pore size behind, it is worth mentioning that industrially important values are also calculated on a volumetric basis. It then becomes clear that too wide pores contain free space, which is not used for capacitive charge storage, but decreases the density of electrodes. This effect is detrimental to volume-based capacitance as well as the existence of narrow electrolyte-inaccessible pores. Thus, tuning pore size is anyway needed to have carbon materials with narrow, short, and electrolyte accessible pores [66]. Aside from this, there is a general agreement that the power delivery of a supercapacitor can be improved by the presence of a small amount of mesopores (pores wider than 2 nm) for a rapid supply of electrolyte to the micropore surface where main charge storage takes place [72]. There have been numerous attempts to properly describe the capacitance of carbon materials depending on the pore shape and size and the specific character of their interaction with electrolytes. For mesoporous carbons with cylindrical pores, the traditional model is used [73]:

$$\frac{C}{A} = \frac{\varepsilon_0 \varepsilon_r}{b ln(\frac{b}{b-d})} \qquad \text{2.4.1.5 A}$$

where ***b*** is the pore radius and d the distance between the ion and the carbon surface. For micropores, it is assumed that the ions line up in the center of a cylindrical pore, so the capacitance is calculated from [73]:

$$\frac{C}{A} = \frac{\varepsilon_0 \varepsilon_r}{b ln(\frac{b}{a_0})} \qquad \text{2.4.1.5 B}$$

where a_0 is the effective size of the ion. This ionic radius was found to be close to the bare ion size, which means that the ions could be completely de-solvated. However, more realistic approximation to the pore shape in carbon is a slit, not a cylinder, a sandwich capacitance model was later proposed [74].

$$\frac{C_{tot}}{2A} = \frac{C_s}{A} = \frac{\varepsilon_0 \varepsilon_r}{b - a_0} \qquad \text{4.1.5 C}$$

2.4.2 Pseudocapacitance

The Pseudocapacitor stores charge in Faradaic charge storage mechanism based on fast and highly reversible surface or near-surface reduction-oxidation reactions. Notice, in case of pseudocapacitive material the electrical response is ideally the same as the one of a double-layer capacitor. That is, the state of charge varies continuously with the potential, where the proportionality constant that can be formally considered as capacitance. Some materials can also store significant charge in a double layer, such as functionalized porous carbon, combining thus both capacitive and pseudocapacitive storage mechanisms. The significance of the term and phenomenon referred to as “pseudocapacitance” has not been well realized in the fields of electrochemical capacitor and batteries. Let us therefore first evaluate on its origin and significance. Regular double-layer capacitance arises from the potential-dependence of the surface density of charges stored electrostatically (i.e., non-Faradaically) at the interfaces of the capacitor electrodes. On the capacitor electrodes (metals or carbon surfaces), the accumulated charge is a combination of excess or a deficit of conduction band electrons at or in the near-surface region of the interface, together with counterbalancing charge densities of accumulated cations or anions of the electrolyte on the solution side of the double layers at the electrode interfaces. However, a double-layer capacitor device must employ two such double layers, one at each electrode interface, working one against the other on charge or discharge. Pseudocapacitance mainly develop at electrode surfaces where a completely different charge storage mechanism applies. It is Faradaic in origin, involving the passage of charge across the double layer, as in battery charging or discharging, but capacitance arises on account of the

special relation that can originate for thermodynamic reasons between the extent of charge acceptance (Δq) and the change of potential (ΔV), so that a derivative d(Δq)/d(ΔV) or dq/dV, which is equivalent to a capacitance, can be formulated and experimentally measured by dc, ac, or transient techniques.

Different transition oxides like RuO_2, MnO_2, V_2O_5, etc., along with a few conducting polymers like PANI, PEDOT:PSS, Polypyrrole, etc. are currently under consideration to be used as electrode materials [75-79]. These electrode materials can perform a fast redox reaction with a suitable electrolyte. The storage mechanism is slow in the case of pseudocapacitor because of chemical reaction involved. For this reason, the pseudocapacitor usually shows less power density compared to EDLC.

2.4.2.1 Detailed Storage Mechanism: Different faradaic mechanisms can lead to pseudocapacitive charge storage phenomena. This mainly depends on the type of active material. These mechanisms are [80,81];

A) Underpotential Deposition: Underpotential deposition or adsorption pseudocapacitance arises when metal ions from the electrolyte are adsorbed on the current collector forming a monolayer [82,83]. This occurs when a potential is less negative than the equilibrium or Nerst potential for the reduction of the metal. Deposition of lead on gold surface is an example of such deposition as shown via the reversible chemical reaction (i);

$$2e + xPb^{2+} + Au \leftrightarrow Au \cdot xPb \qquad 2.4.2.1(i)$$

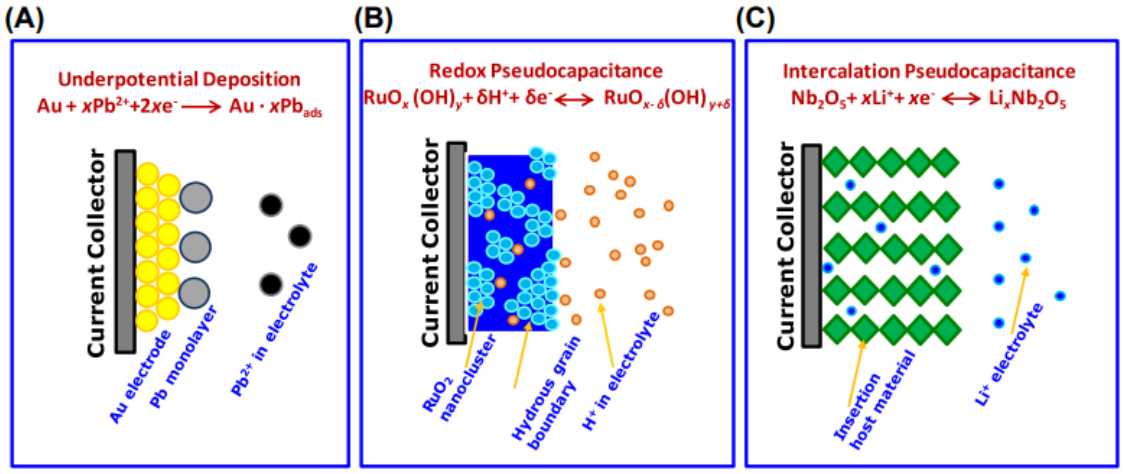


Fig 2.4.2.1 Different mechanism of pseudocapacitive charge storage, (a) Underpotential deposition (b) redox pseudocapacitance (c) intercalation pseudocapacitance.

During the charging, Pb^{2+}ions from the electrolyte solution get deposited on the surface by accepting or storing two electrons. As the process is reversible, the opposite phenomenon occurs during the discharging, resulting in two electrons release. Fig 2.4.2.1(a) shows such mechanism of charge storing.

B) Redox pseudocapacitance: Redox pseudocapacitance occurs when the ions from the electrolyte are adsorbed near the surface of the active material via fast and reversible faradaic charge transfer. Hydrous RuO_2 shows this type of pseudocapacitance. When charging, the RuO_2 accepts protons from the electrolyte and releases them back during discharge process. Protons from the electrolyte solution interact with the surface (within 10 nm of the surface) of the active material, and this faradaic process does not involve phase change of the active material [84]. Fig 2.4.2.1 (b) shows the redox pseudocapacitance mechanism.

C) Intercalation pseudocapacitance: Pseudocapacitive charge storage via intercalation of ions in the bulk of the active materials occurs when the ions from the electrolyte solution penetrate deep into the active material and perform reversible redox reactions. Intercalation pseudocapacitance is possible only when the active material has a tunnel or layer-like structure. For this reason, only a few materials show this type of charge storage like t-Nb_2O_5, 8-MnO_2, etc. [85,86]. Battery-type materials also show this type of storage mechanism. However, in the battery, the electrode suffers phase change, whereas in intercalation pseudocapacitance, no phase change occurs for the active material [87]. Figure 2.4.2.1 (c) shows the charge storage mechanism due to intercalation pseudocapacitance.

2.4.3 Hybrid Supercapacitor

Electrode materials for hybrid supercapacitor store charges via both the physical and pseudocapacitive charge storage mechanisms [88]. Because of the contribution from both these two mechanisms, energy density and power density become very high for these types of materials. Composites of different carbonaceous materials with different redox-active materials constitute this class of hybrid electrode material. In these composites, carbon-based materials store charges via double layer formation, whereas the redox-active material stores charges via reversible faradic reactions with the electrolyte. Carbon-based elements also stabilize the redox-active material against the large volumetric strain suffered during the redox reaction by providing a backbone. Alongside, carbon-based elements provide a high way to the electrons, and thus conductivity of the sample increases. Usually, the carbon-based material is responsible for enhancing the power density, and redox-active material is responsible for enhancing the

energy density of the composite. Composite of NiO-CNT, MnO_2- Graphene, PANI-CNT, etc., are examples of hybrid supercapacitor electrode materials [89-91].

2.4.4 Electrochemical characterizations to differentiate between the storing mechanisms

After synthesizing an electrode material, generally, three main characterizations are performed to test the charge storage performance of the material. These characterizations are performed in a three-electrode setup, as shown in figure 4.4.1 (a). Here 'CE' and 'WE' are the counter and working electrodes, respectively. The material under investigation is coated in a thin film form on the working electrode, which undergoes the redox reaction. The resulting current is measured between these two electrodes. The third one is the reference electrode which generates a constant reference potential with respect to which the potential of the working electrode can be measured. A few popular reference electrodes are the Calomel electrode (Hg/HgCI/KCl) or the silver-silver chloride electrode (Ag/AgCl/4M KCI).

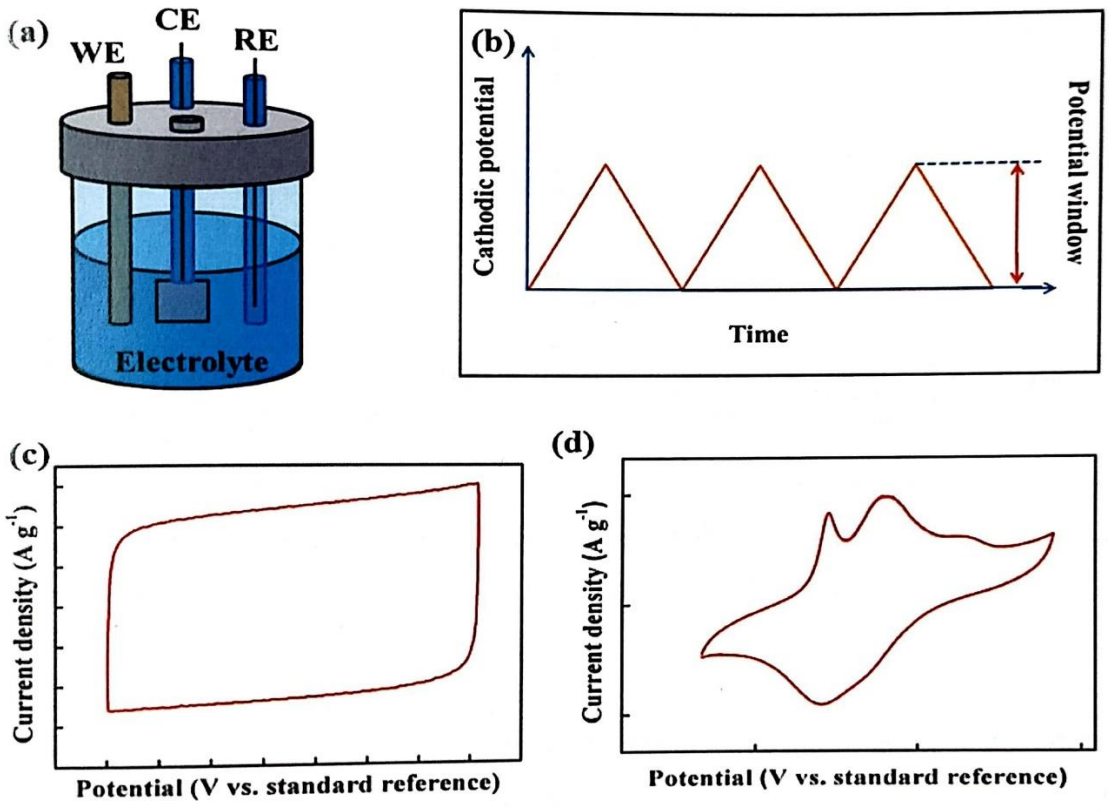


Fig 2.4.4 (a) Three Electrode set-up for Electrochemical Characterization, (b) Potential Waveform for the CV measurement. CV diagram for, (c) EDLC and (d) Pseudocapacitor

These three electrodes are kept submerged in a suitable electrolyte. Cyclic voltammetry (CV) is one of the three characterization techniques which is performed in this similar three-electrode setup [92,93]. CV study provides information on the oxidation and reduction processes of molecular species coated on the working electrode. A triangular potential (figure (2.4.4.1 (b)) is applied between the RE and WE and the resulting current is measured between CE and WE. To investigate the material property for supercapacitive application, a suitable potential window is chosen. CV scan is performed at different scan rates. Scan rate controls the rate of change of the potential, or more generally, it controls the slope of the applied triangular potential waveform. A high scan rate decreases the width of the diffusion layer formed at the working electrode, which results in a higher current. Figure 2.4.4.1 (c) shows the typical CV diagram for an EDLC, which offers a rectangular CV diagram. On the other hand, CV diagram for a pseudocapacitor (figure 2.4.4.1 (d)) deviates significantly from the rectangular shape, which sometimes contains prominent oxidation or reduction peaks.

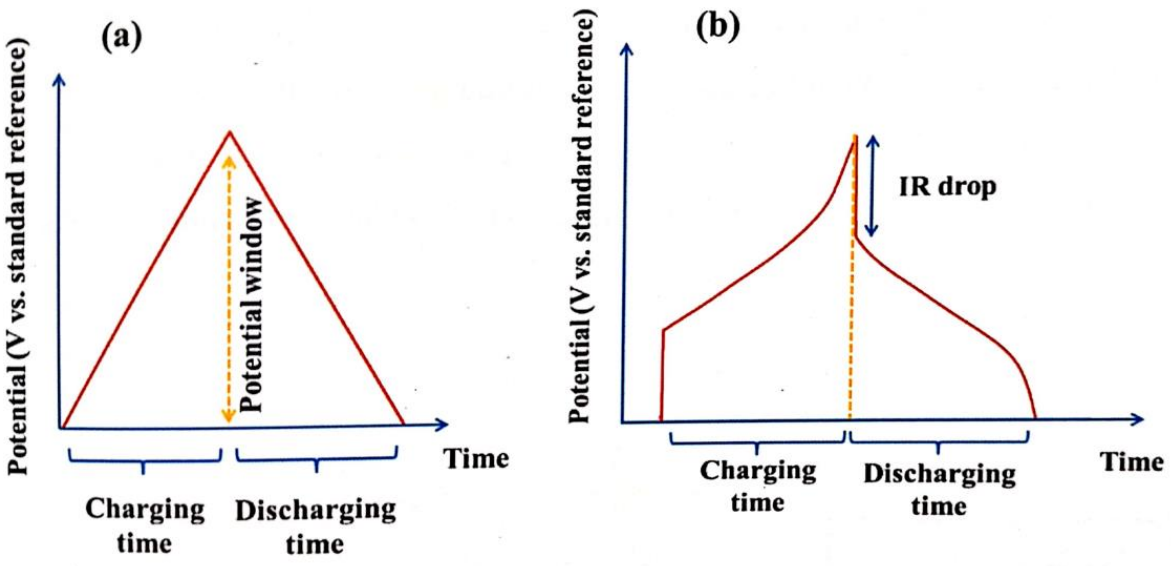


Fig 2.4.4.2 GCD profile for (a) EDLC and (b) Pseudocapacitor

The specific capacitance for the material under investigation at a particular scan rate can be obtained from the area under the CV curve using the equation 2.4.4.1

$$C_m = \frac{i}{2mv} \qquad 2.4.4.1$$

Where, v and m are the potential sweeping rate and mass of the active material, respectively. Here, i is the area under the CV curve which can be calculated from the equation 2.4.4.2 [94];

$$i = \frac{\int_{v_a}^{v_c} i(v)dv}{(v_c - v_a)} \qquad 2.4.4.2$$

Where v_c and v_a are the highest and lowest points of the potential range, respectively. Galvanostatic charge discharge (GCD) is another electrochemical characterization technique that is performed to observe the charging and discharging behavior of WE. A constant current is applied between the CE and WE, and the potential of the WE is measured over time with respect to the RE. Figure 2.4.4.2 (a) shows the typical GCD pattern for an EDLC. The triangular shape of the GCD pattern resembles the EDLC nature; on the other hand, pseudocapacitor electrode material displays non-triangular GCD curves, as evident from figure 2.4.4.2 (b). One more interesting point that can be observed from the GCD plot of figure 2.4.4.2 (b) is that during the beginning of the discharge, a sharp fall is noticed. This sharp fall is mainly due to the internal resistance as well as the contact resistance of the electrode material with the current collector [95]. Usually, the GCD performed within the same potential window as the CV. The rising half of the GCD curve the charging curve. Once the higher potential reached, the charging current is reversed to the negative value, and the discharging curve is obtained. Equation 2.4.4.3 can be used to calculate the specific capacitance from the GCD measurement for a particular current density,

$$C_m = \frac{i}{(-\frac{dV}{dt})} \qquad 2.4.4.3$$

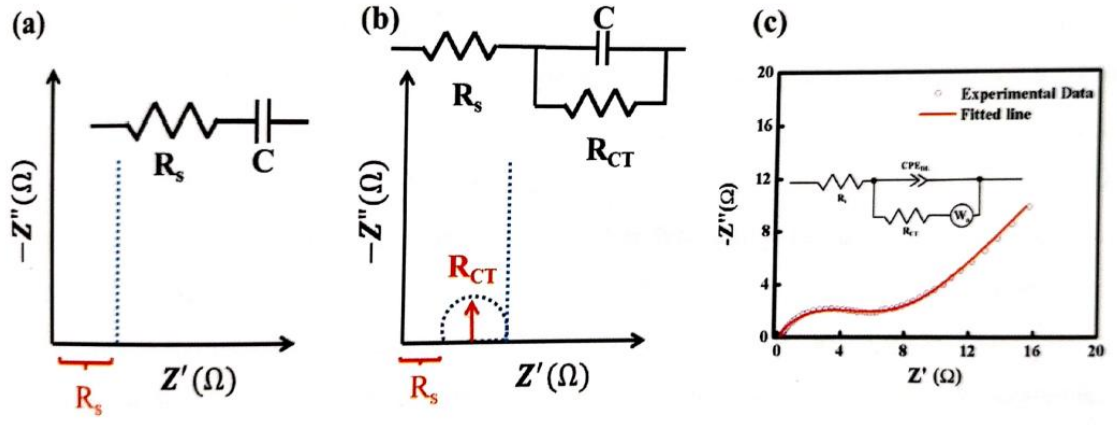


Fig 2.4.4.3 Nyquist plot (a) ideal capacitor series resistance (b) capacitor with a leakage resistance in parallel (c) actual supercapacitor electrode

Here, *i* is the current density applied externally, and *dV/dt* is the average slop the discharging part of the GCD curve.

The third characterization is the electrochemical impedance spectroscopy (EIS) which provides different dynamical processes occurring at the WE and the electrolyte. EIS can be used to determine the resistive and capacitive properties of an electrode material by applying a perturbation to the electrode in the form of a sinusoidal AC signal of magnitude 2-10 mV. The frequency of the perturbation signal is varied, and thus an impedance spectrum is obtained. We consider a circuit where an ideal capacitor C and a resistor R are connected in series. For this circuit, the complex impedance Z is given by equation (2.4.4.4)

$$Z(\omega) = R - \frac{i}{\omega C} \qquad 2.4.4.4$$

Here, ω is the frequency of the applied perturbation and i is the usual imaginary unit. The real part Z_r, and the imaginary part Z_{im} of the complex impedance are given by: (2.4.4.5)

$$Z_r = R \qquad 2.4.4.5$$

$$Z_{im} = -\frac{1}{\omega C} \qquad 2.4.4.6$$

When the frequency of the applied perturbation is varied, the Z_r, remains fixed; as for the present circuit, it is independent of frequency. Hence, the plot of $-Z_{im}$ vs Z_r becomes a straight line parallel to the $-Z_{im}$ axis, as shown in Figure 2.4.4.3 (a). From this plot value of the series resistance (R_s) can be calculated as shown in the same figure. This method of demonstrating the EIS spectra is called the Nyquist plot. Another method of demonstrating the EIS data is the Bode plot, where the logarithm of modulus of impedance (log Z) is plotted against the logarithm of applied frequency (log f). However, in reality, an ideal capacitor cannot be realized in practice. A more realistic approach to model a capacitor is to consider a high resistance parallel to that capacitor, which takes into account the leakage of charge over time. In such a case, the Nyquist plot becomes circular in the higher frequency region along with a spike parallel to the $-Z_{im}$ axis, as shown in figure 2.4.4.3 (b). From the same plot value of the leakage, resistance can be calculated from the radius of the semicircle. However, in reality, a much more complex Nyquist plot is obtained for a practical capacitor, especially for a supercapacitor, owing to much more complex charge dynamics at the electrode-electrolyte interface. In such a case, the Nyquist plot has to be fitted with different circuit elements to obtain different information like contact resistance, charge transfer resistance, Warburg impedance, etc. For example, the Nyquist plot of figure 2.4.4.3 (c) shows such a typical complex nature. This is a plot for a supercapacitor electrode material. This Nyquist plot has been fitted using the model circuit shown in figure 2.4.4.3 (c) (inset). Here, CPE_{DL} is the constant phase element that takes

into account the double layer effect at the interface of the electrode, and W_0 is the Warburg element which is due to the frequency-dependent diffusion [96].

Thus, different parameters determine the overall charge storage performance of electrode material. Table 2.4.4.1 summarizes these different parameters and their meaning.

Table 2.4.4.1: Different parameters related to the charge storage performance of the electrode material.

Parameters	**Significance**
Specific capacitance	Charge storing capability per unit mass of the electrode material.
Areal specific capacitance	Charge storing capability per unit area of the electrode material.
Volumetric specific capacitance	Charge storing capability per unit volume of the electrode material.
Specific energy	Electrical energy stored per unit mass of the active material.
Specific power	Stored electrical power unit mass of the electrode material.
Electrochemical reversibility	Determines the reversibility of the redox reaction.
Potential window	Signifies the operating voltage window within which the active material can perform the reversible redox reaction with the electrolyte.
Rate capability	Determines the capacitance response at various potential scan rates or current densities. It is related to the power generating efficiency at a high current with a minimum loss of voltage.
Long cycle life	Charge storage capability for the electrode usually degrades over repeated charging and discharging cycles. This parameter determines the long-life performance of the electrode material.
Columbic efficiency	Signifies the efficiency of the charge transfer through the electrochemical reaction. It is the ratio of charging time and the discharging time for an active material in

	GCD measurement, the charging and discharging current are the same.
Equivalent series resistance (ESR)	It determines the resistance of different components in the whole electrochemical cell. This resistance includes material resistance, electrolyte resistance etc. it can be determined from the EIS studies

2.5 Different electrode materials

At present different research groups around the world are investigating different types of materials for supercapacitor electrodes. Different EDLC based materials offer extraordinary power density as well as excellent long-life, whereas different pseudocapacitive materials offer high storage capacity with excellent energy density. Hence efforts have been made to prepare composites of these two types of materials to enhance the overall storage performance. Here we discuss a few such materials and their charge storage performances.

2.5.1 Porous Carbon

Carbons derived from different sources have been used to fabricate supercapacitor electrodes. These electrodes store charges via the formation of double layer, and no redox process is involved in the storage mechanism. Hence this type of material can extend the lifetime of the electrode owing to the physical charge storage mechanism. Porous carbon is low cost, environmentally friendly, and offers the agility to tune its surface area. Activated carbon (AC), a type of porous carbon, has been successfully commercialized because of its large surface area, micro-porosity, and relatively low cost. Different waste products like rice husks, waste of tea, waste of coffee beans, etc., have been used to synthesize AC to fabricate EDLC type supercapacitor electrodes [97]. The charge storage properties of these electrodes depend on the carbonization and activation steps during the synthesis. Inal et al. prepared AC from the waste of tea using carbonization and chemical activation using zine chloride ($ZnCl_2$). The heat-treated sample showed a good specific surface area of 923 m^2 g^1. They measured the electrochemical charge storage performance in a two- electrode configuration which exhibited the highest specific capacitance of 140 F g^1 at a current density of 1 A g^1. The device retained 98% of its initial value of specific capacitance after 10000 GCD cycles [98].

2.5.2 Carbon nanotube (CNT)

Carbon nanotubes (CNTs) have remained in the center of material science research since their discovery because of their attractive structural, mechanical, and electrical properties [99]. CNTs are fabricated when a graphite sheet is rolled to form a cylindrical shape, as shown in figure 2.2.4.1. Thus, we have a carbon nanotube with only one layer of rolled up layer of

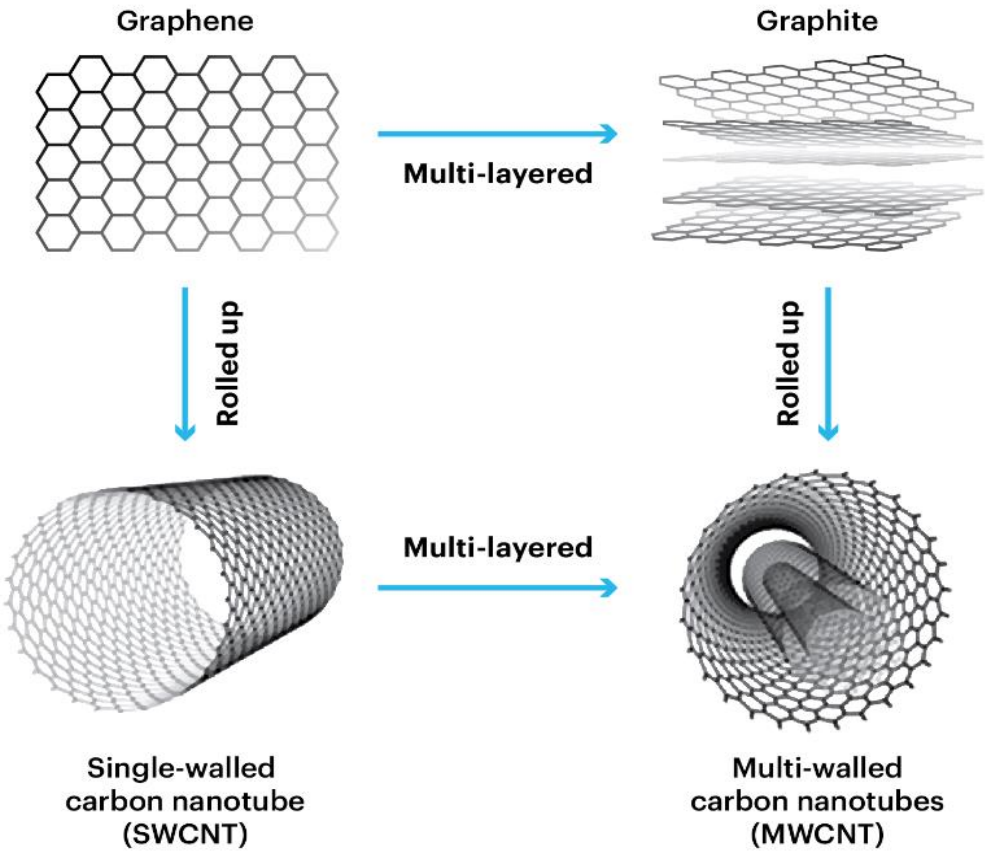


Fig 2.5.1 Different types of CNTs

graphite sheet known as single walled carbon nanotube (SWCNT) On the other hand, multiwalled carbon nanotube (MWCNT) contains more than one layer of graphite layer. CNTs can have a diameter of the order of 1 nm while their length can be of the order of a few microns, offering very high surface area and low resistivity, which is beneficial for electrochemical charge storage applications. Niu et al., in 1997, first demonstrated the supercapacitive properties of CNTs [100]. Catalytically grown carbon nanotubes having an average diameter of 80 A were used for fabricating the electrodes. Initially, the CNTs were treated with nitric acid to disassemble the CNT cluster and functionalize the surface with oxygenated groups. These acid-treated CNTs were dispersed in water and filtered, which resulted in a carbon

nanotube sheet after drying. A test device was assembled using two such sheets as electrodes separated by polymer separator. 38 wt% H_2SO_4 was used as electrolyte. A maximum specific capacitance of 104 F g was attained from the test cell. Yu et al. reported a stretchable supercapacitor based on SWCNT microfilm. To fabricate the stretchable substrate, surface treated poly(dimethylsiloxane) (PDMS) was used. SWCNT was deposited on this elastic substrate. The device demonstrated a specific capacitance of 54 F g^{-1} when no strain was applied and 52 F g^{-1} when a 30% strain was applied [101].

2.5.3 Graphene

Graphene was attracted tremendous research interest soon after its first synthesis in 2004 [102]. It is the two-dimensional single layered carbon atoms in of sp^2 hybridized state (fig 2.4.5.2). Very low electrical resistivity and high thermal and electrical conductivity, utra-high surface area (~2700 m^2g^{-1}), chemical stability, and excellent mechanical strength (~1 Tpa) make it suitable for application in Supercapacitor electrodes. Liu et al. in 2010 reported a supercapacitor device with graphene-based electrode [103].

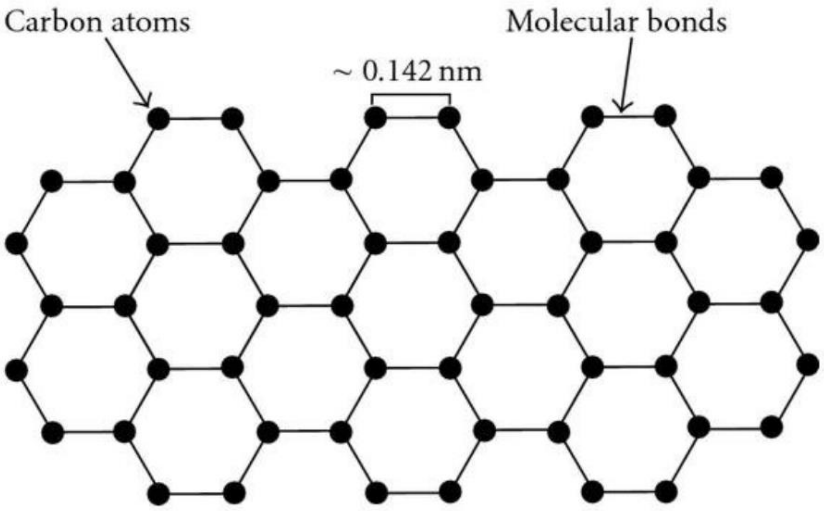


Fig 2.5.2 Structure of graphene

Graphene oxide (GO) was produced via the modified hummers method. In this process, natural graphite is oxidized using a mixture of sulphuric acid, sodium nitrate, and potassium permanganate. The obtained GO was treated with hydrazine to remove the oxygen-containing groups. Finally, the obtained graphene powder was coated on the aluminum foil to fabricate coin sized supercapacitor cell. A rectangular CV profile was obtained within a wide potential window of 4 V. This suggests excellent double layer charge storage mechanism. The coin cell displayed a specific energy density of 85.6 Wh kg at 25 °C. Zhang et al. used a novel vacuum

filtration deposition method to deposit graphene in the pore of nickel foam [104]. In this process, commercially available graphene nanoplatelets were refluxed using an acidic solution of concentrated nitric acid. This refluxed graphene, along with PVDF binder, was dissolved in absolute ethanol. The mixture was then forced through the nickel foam using a vacuum filtration deposition process. After the deposition, the deposited nickel foams were dried at 100 °C in a vacuum. A specific capacitance of 152 F g^{-1} was acquired at 10 mV s^{-1} scan rate using an aqueous 6M KOH electrolyte medium in a two-electrode setup using as-deposited nickel foams as the positive and negative electrode. The electrodes retained 95% of their initial capacitance after 2000 cycles. However, graphene nanosheets tend to aggregate during the electrode fabrication, which hampers the electrochemical performance by reducing the practical surface area [105].

2.5.4 Ruthenium oxide and its composites

Among different transitional metal oxides, RuO_2 is the most promising pseudocapacitive electrode material because of its fast charge dynamics, high theoretical specific capacitance, high electrical conductivity (~ 105 S cm^{-1}) chemical and thermal stability in the electrolyte.

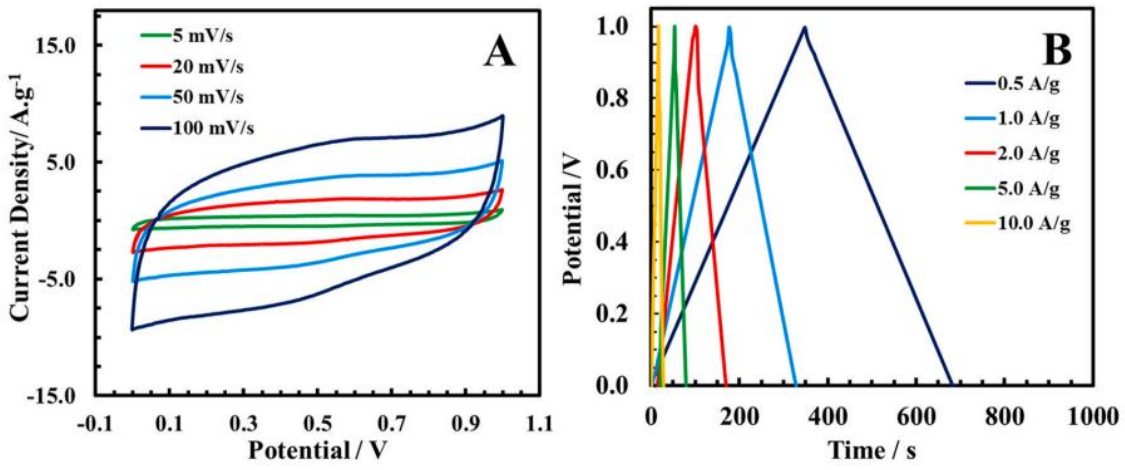


Fig 2.5.3 (A) CV and (B) GCD for the rGO/RuO_2 aerogel

The charge storage mechanism of RuO_2, was first proposed by Trasattı et al. [106], which is due to the electronic protonic "double insertion" mechanism as shown in equation (2.5.4):

$$RuO_x(OH)_y + \delta H^+ + \delta e^- \leftrightarrow RuO_{x-\delta}(OH)_{y+\delta} \qquad 2.5.4$$

The oxidation state ofruthenium varies among Ru^{4+} Ru^{3+} amd Ru^{2+}. These redox reactos mainly at the surface or nearer to the surafce of the RuO_2 coated electrode. Hence the surface area of the electrode material composing the electrode, in this case is a vital parameter to obtain higher specific capacitance. The anhydrous crystalline form of RuO_2 shows a very low specific capacitance (~30 F g^{-1}) value whereas the the hydrous form of RuO_2 offers higher specific capacitance [107]. Patil et al.synthesized hydrous RuO_2 thin film on different substrate like glass and stainless steel using chemical bath deposition.Being hydrous in nature the thin film of RuO_2 showed a higher specific capacitance opf 73 F g^{-1} at 2 mV s^{-1} scan rate in 0.5 M H_2SO_4 electrolyte [108]. Korkmaz et al synthesized a composite of rGO and RuO, in the form of an acrogel mixture. The electrochemical study revealed that this composite did not show any redox peak at the higher side of the scan rate. The CV curves thus resembled almost ideal reversible capacitive behavior, and the GCD curves showed triangular type nature as shown in figure 2.5.3 (a) and (b), respectively. The highest specific capacitance of 328.6 F g^{-1} was obtained for this sample at 5mVs^{-1} scan rate [109]. Table 2.5.4 summarises the different results concerning the charge storage capability of RuO_2, and its composites.

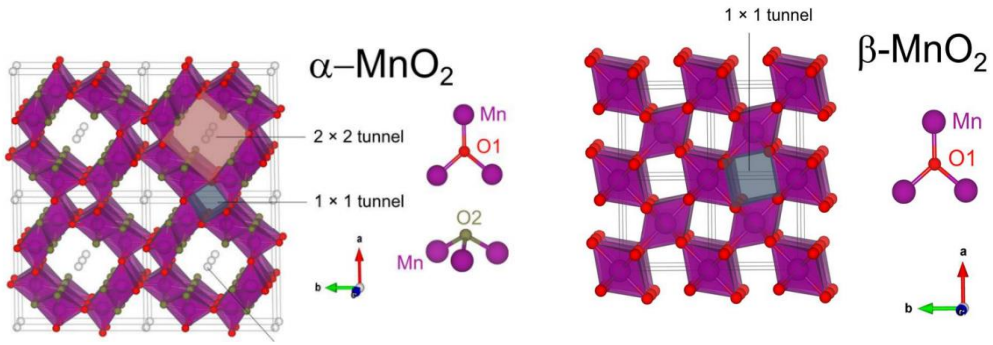
Table 2.5.4: Results from different reports on RuO_2 and its different composites;

Sample name	Measurement configuration	Specific capacitance value	Ref.
Anhydrous RuO_2	3-elctrode, electrolyte: aqueous 0.5M H_2SO_4	58 F g^{-1} @ 2 mV s^{-1}	[75]
Hydrous nanotubular array of RuO_2	3-electrode, electrolyte: aqueous 1M H2SO4	1300 F g^{-1} @ 10 mV s^{-1}	[110]
Spray deposited RuO_2 film	3-elctrode, electrolyte: aqueous 0.5M H_2SO_4	551 F g^{-1} @ mV s^{-1}	[111]
Pulse electrodeposited RuO_2	3-elctrode, electrolyte: aqueous 0.5M H_2SO_4	1724 F g^{-1} @ 5 A g^{-1}	[112]
RuO_2/Carbon nanofiber	3-elctrode, electrolyte: aqueous 2M H_2SO_4	220 F g^{-1} @ 5 mV s^{-1}	[113]

Flexible RuO_2/Graphene thin film	3-elctrode, electrolyte: aqueous 0.5M H_2SO_4	1561 F g^{-1} @ 5 mV s^{-1}	[114]
SnO_2- RuO_2 composite film	3-elctrode, electrolyte: aqueous 0.5M H_2SO_4	150 F g^{-1}	[115]
RuO_2/CNT	3-elctrode, electrolyte: aqueous 0.5M L^{-1} H_2SO_4	900 F g^{-1}	[116]
RuO_2/electrosopun carbon fiber	3-elctrode, electrolyte: aqueous 2M H_2SO_4	544 F g^{-1}	[117]
RuO_2-Fe2O3 embedded mesoporous carbon	3-elctrode, electrolyte: aqueous 0.5M H_2SO_4	1668 F g^{-1} @ 1 A g^{-1}	[118]

2.5.5 Manganese dioxide and its composites

Although RuO_2 is popular in lab-grade devices and different military-based applications because of its high cost and toxicity, it is not commercially popular. As an alternative to RuO_2, Manganese dioxide (MnO_2) has gained popularity because of its ultrahigh theoretical value of specific capacitance (~1370 F g^{-1}), environment friendliness, and abundance [119]. In 1999, Lee and Nobel Laureate Goodenough first reported the supercapacitor behaviour of



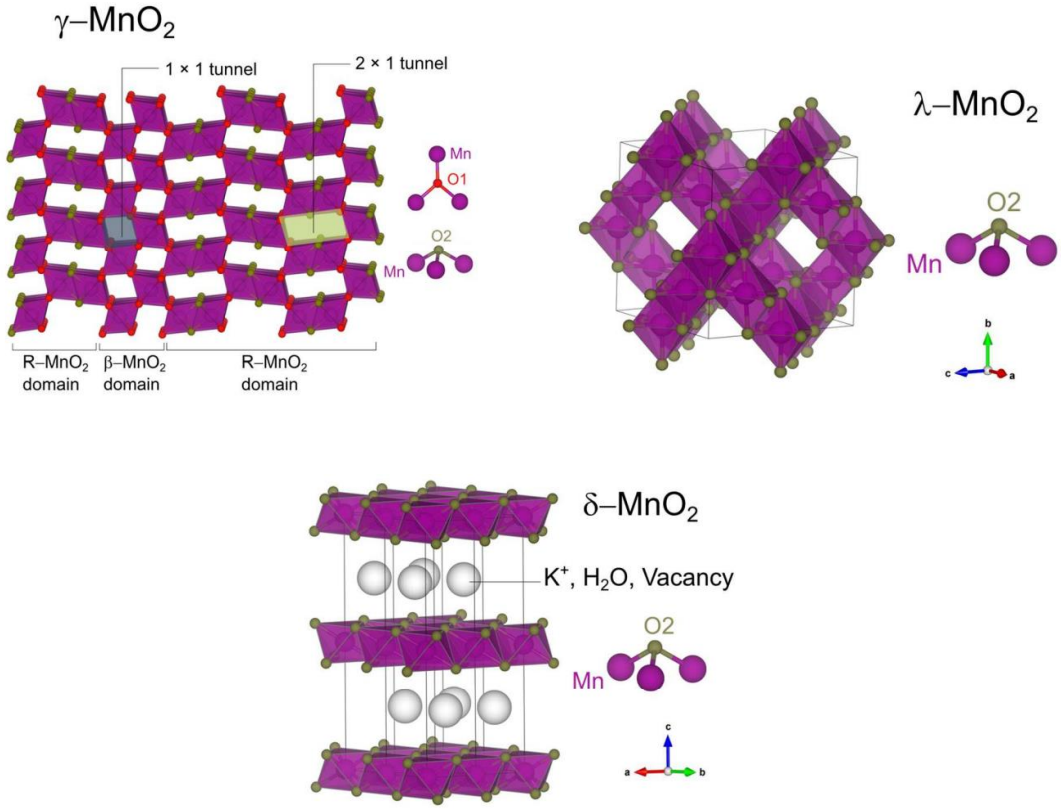


Fig 2.5.5 Different polymorphs of MnO_2 Mn atoms are shown in magenta and oxygen atoms are shown in purple

Amorphous $MnO_2.nH_2O$ in an aqueous KCl electrolyte medium. A specific capacitance value of 200 F g^{-1} was reported [120]. MnO_2 generally shows six different types of polymorphic forms, as shown in figure 2.4.5.5 [121]. Different atomic positions in these different polymorphs result in the variation of surface characteristics, pore size, and channel or tunnel size. These variations lead to significant variations in the charge storage performance of these different polymorphs. For example, Zhang et al. studied the electrochemical charge storage performance of these different polymorph phases. It was found that the specific capacitance values varied in the order: β-MnO_2< γ-MnO_2 < δ-MnO_2 < α-MnO_2 [122]. The charge storage by MnO_2 electrode in the aqueous electrolyte is due to the pseudocapacitive mechanism. Two different mechanisms are usually proposed to explain the charge storage phenomena [123]. The first one is based on the intercalation of protons (H) or metal cations (C) in the bulk of the material during the reduction process. On the other hand, during the oxidation process, the deintercalation of H^+ or C^+ occurs. Equation 2.5.5(a) and 2.5.5(b) shows the charge storage phenomena by MnO_2, through the first mechanism.

$$MnO_2 + H^+ + e^- \leftrightarrow MnOOH \qquad 2.5.5(a)$$

$$MnO_2 + C^+ + e^- \leftrightarrow MnOOC \qquad 2.5.5(b)$$

In the second mechanism, the surface adsorptions of the electrolyte ions on MnO_2 electrode surface are taken into consideration and are shown via the equation (2.5.5c).

$$(MnO_2)_{surface} + C^+ + e^- \leftrightarrow (MnO_2{}^- C^+)_{surface} \qquad 2.5.5(c)$$

This adsorption and desorption of ions occur very near the electrode's surface, and bulk of the sample remains inactive in this case. Although having many advantages, pristine MnO_2, possesses few serious drawbacks as an electrode material for supercapacitors. MnO_2 demonstrates low electrical conductivity in pristine form, which hampers the charge transport rate. It also tends to dissolve in different aqueous electrolytes, reducing the material's stability Further, through the repeated charge/ discharge cycles, the crystal structure of MnO_2, suffers irreversible volume expansion, which causes swelling in the electrode. To address these problems, different researchers across the world developed a composite of MnO_2, with different materials like CNTs, graphenes, activated carbon, carbon fiber, other metal oxides, sulfides, etc. For example, Vangapally et al. synthesized carbon/MnO_2, composite using table sugar as a source for carbon. The hydrothermal reaction was used to prepare the composite, which showed a nanorod-like morphology. This composite showed a specific capacitance of 416 F g^{-1} at 1 A g^{-1}. Because of the presence of carbon in the composite, its conductivity and electrochemical stability increase, which causes the electrode to retain a specific capacitance of 90% of the primary value after being charged and discharged for 5000 cycles [124]. A lot of work has been performed using MnO_2 and its composites to be used as electrode material for supercapacitors. Table 2.4.5.5 shows a summary of a few of the published results.

Table 2.5.5: Results from different reports on MnO_2 and its different composites.

Sample name	Measurement configuration	Specific Capacitance value	Ref.
Porous MnO_2	3-electrode.elctrolyte: aqueous 0.5M Na_2SO_4	222 F g^{-1} @ 2 mV s^{-1}	[125]
MnO_2 nanofillers	3-electrode.elctrolyte: aqueous 1M Na_2SO_4	603 F g^{-1} @ 5 mV s^{-1}	[126]
MnO_2 Nanorod	3-electrode.elctrolyte: aqueous 0.1M Na_2SO_4	166.2 F g^{-1}	[127]

Hollow MnO_2 nanofiber	3-electrode.elctrolyte: aqueous 1M Na_2SO_4	291 F g^{-1} @ 1 A g^{-1}	[128]
GO- MnO_2	3-electrode.elctrolyte: aqueous 1M Na_2SO_4	216 F g^{-1} @ 150 mA g^{-1}	[129]
MnO_2-CNT	3-electrode.elctrolyte: aqueous 1M Na_2SO_4	201 F g^{-1} @ 1 A g^{-1}	[130]
MnO_2 on Ni foam	3-electrode.elctrolyte: aqueous 1M Na_2SO_4	241 F g^{-1} @ 1 A g^{-1}	[131]
Polypyrrole covered MnO_2	3-electrode.elctrolyte: aqueous 1M L^{-1} Na_2SO_4	141 F g^{-1} @ 2 mA cm^{-1}	[132]
MWCNTs/ MnO_2/PPy composite	3-electrode.elctrolyte: aqueous 1M L^{-1} Na_2SO_4	806 F g^{-1} @ 1 A g^{-1}	[133]
Carbon@ MnO_2 core-shell nanospheres	3-electrode.elctrolyte: aqueous 1M L^{-1} Na_2SO_4	252 F g^{-1} @ 2 mV s^{-1}	[134]

2.5.6 Bimetallic oxide of Ni and Mn ($NiMn_2O_4$)

$NiMn_2O_4$ offers high conductivity, high theoretical specific capacitance and excellent stability among different bimetallic oxides. Hence it has been investigated by different researchers for its potential applications in supercapacitors, catalysis, electrochemical sensors etc. Dhass et al. synthesized $NiMn_2O_4$ using a simple sol gel route. They studied the effect of annealing temperature and the electrolyte concentration on the electrochemical performance of the electrode made of this powder. All the electrochemical performances were reported in a 3-electrode arrangement in aqueous KOH electrolyte with variable concentrations ranging from 1M to 6M. the sample annealed at 500 ^{O}C (NMO1) showed better electrochemical charge storage performance compared to the same sample annealed at 600 ^{O}C (NMO2) and 700 ^{O}C (NMO3). Next the of electrolyte concentration was studied using the NMO1 sample. It was seen that with the increasing the KOH concentration, the charge storage performance increases. In 1M KOH electrolyte, it offered 571 F g^{-1} and in 6 M KOH electrolyte, it offered a specific capacitance of 762 F g^{-1} (value measured from CV at 5 mV s^{-1} scan rate). It was concluded that the improvement of specific capacitance is due to the increment of electrolyte ions which increases the electrochemical activity [135]. Umar et al. synthesized $NiMn_2O_4$ nanodisc on

reduced graphene oxide (rGO) using a low-temperature colloidal solution method and studied it for both the electrochemical sensor and supercapacitor. The sensor was used to sense acetylacetone. The electrochemical charge storage capability was measured in a three-electrode arrangement using 1 M aqueous Na_2SO_4 electrolyte within a wide potential window of 1 V. $NiMn_2O_4$ nanodisc decorated on rGO demonstrated a highest specific capacitance of 356 F g^{-1} at 0.5 A g^{-1} current density. On the other hand, only $NiMn_2O_4$ shows a specific capacitance of 199 F g^{-1} at the same current density. This improvement of specific capacitance is mainly due to rGO, which increases the specific surface area of the sample, and thus the charge storage performance improves [136]. Choice of the current collector is an important parameter to obtain the best performance from a supercapacitor electrode. Wei et al. synthesized ultrathin $NiMn_2O_4$ arrays on Ni-foam current collector using hydrothermal reaction. Through the reaction, the coating of $NiMn_2O_4$ was formed directly on the Ni-foam. Because of this, no binder was required to fabricate the electrode. As it is well known, most of the binders are nonconductive and deteriorates the performance of the electrode. This kind of microstructure provides large number of active sites for the electrolyte ions and the conductive channel of Ni-foam effectively connects the different redox active sites electronically. The electrochemical performance measured in 6 M KOH electrolyte displayed a specific capacitance value of 662.5 F g^{-1} at current density of 1 A g^{-1} current density [137]. Table 4.5.6 summarizes the different results regarding the supercapacitive charge storage performance obtained with $NiMn_2O_4$ and its different composites.

Table 2.5.6 Results from recent reports on $NiMn_2O_4$ and its composites.

Sample name	Measurement configuration	Specific capacitance	Ref.
rGO/$NiMn_2O_4$	3-electrode. Electrolyte: aqueous 1M Na_2SO_4	693 F g^{-1} @ 1 A g^{-1}	[138]
Spherical carbon decorated with $NiMn_2O_4$	3-electrode. Electrolyte: aqueous 2M KOH	470.7 F g^{-1} @ 1 A g^{-1}	[139]
CNT/$NiMn_2O_4$ core shell nanocomposite	3-electrode. Electrolyte: aqueous 6M KOH	915.6 F g^{-1} @ 1 A g^{-1}	[140]

$NiMn_2O_4$ on Ni foam	3-electrode. Electrolyte: aqueous 6M KOH	802 F g^{-1} @ 1 A g^{-1}	[141]
$NiMn_2O_4$ supported on N_2 dopped graphene	3-electrode. Electrolyte: aqueous 6M KOH	1308.2 F g^{-1} @ 1 A g^{-1}	[142]
Co^{2+} and Zn^{2+} dopped $Ni_2Mn_2O_4$ supported on rGO	3-electrode. Electrolyte: aqueous 3.5M KOH	710 F g^{-1} @ 1 A g^{-1}	[143]

2.6 Two Electrode Supercapacitor Device

A symmetric two-electrode supercapacitor device is fabricated by utilizing the coating of the same electrode material in both electrodes. On the other hand, if two different electrode materials are used, it is termed an asymmetric supercapacitor device. Usually, in such a device the redox-active material is coated on the positive electrode, and carbonaceous material is coated on the negative electrode.

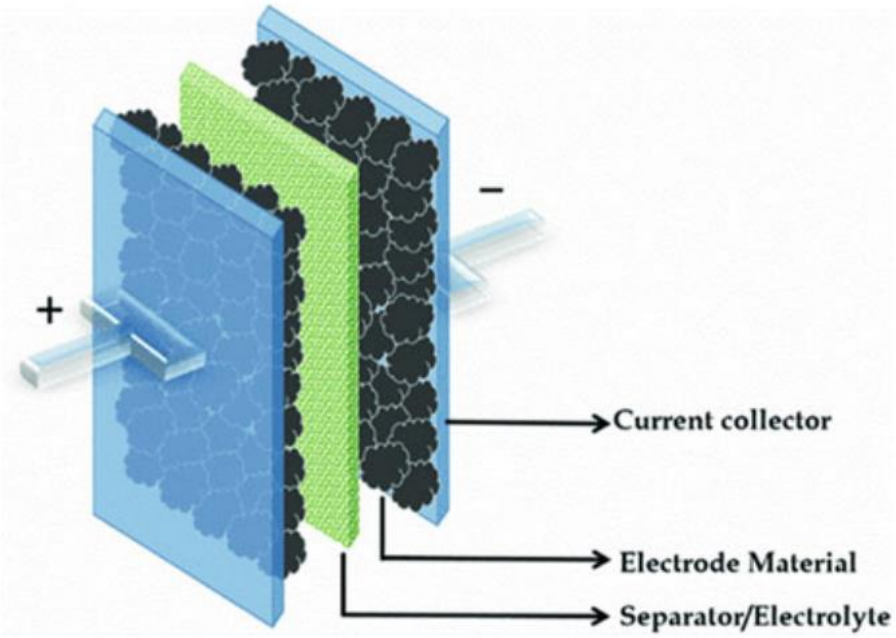


Fig 2.6a Schematic of two-electrode supercapacitor

The energy density (E, in the unit of Wh kg $^{-1}$ and the power density (P, in the unit of W kg $^{-1}$) of the device can be calculated from the equations (5 A) and (5 B) [144].

$$E = \frac{1}{2}\left[\frac{C(\Delta V)^2}{3.6}\right] \quad \text{5 A}$$

$$P = \frac{3600 \times E}{\Delta T} \quad \text{5 B}$$

Here, C is the device's specific capacitances (in the unit of F g^{-1}) at different current densities as obtained from the GCD, ΔV is the working potential window, and ΔT is the different discharge times corresponding to different current densities. For the best performance of the device, the active materials should be carefully chosen, and mass deposition of the active materials should be optimized. Apart from the active materials, we need to focus on its

important parts to obtain the optimum performance from the device. These parts are current collector, separator and electrolyte.

2.6.1 Current Collector

The current collector serves two main purposes. Firstly, it collects/sends electrons from/to electrodes during discharging/charging. Secondly, it provides the necessary mechanical support to the electrode material. A good current collector should have very less contact resistance and good bonding with the electrode material [145,146] It should also have high electric conductivity to carry or deliver power with minimum loss. To stick the electrode material more efficiently to the current collector, different surface treatments are performed. This increases the bonding capacity of the current collector. Wen et al used the atomic layer deposition (ALD) technique to fabricate platinum nanotube arrays using anodic alumina (AAO) template. They successfully fabricated a current collector of the size of 1 cm x 1 cm, free of any structural defect. Next, to deposit MnO_2, on the nanotube array electrodeposition method was used, which acted as the electrode for the supercapacitor.

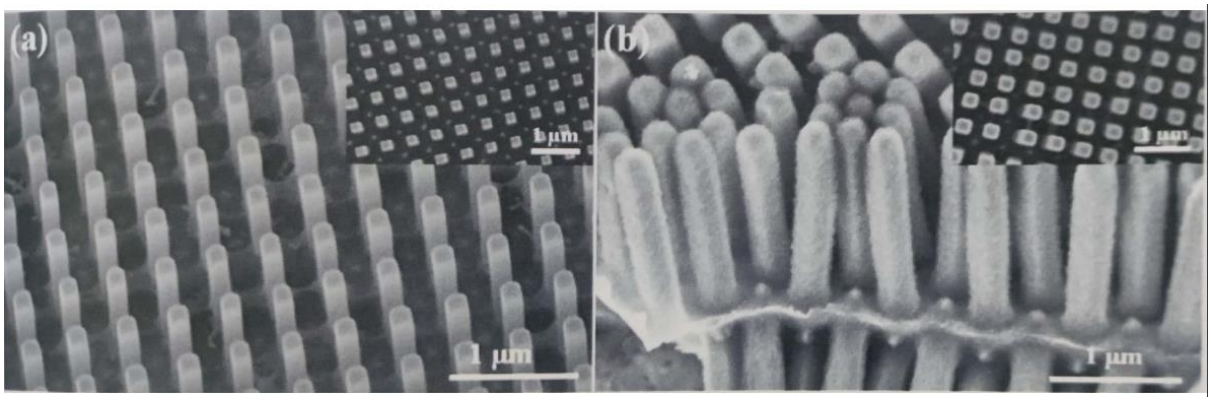


Fig 2.6.1.1 (a) Pt Nanotube array, (b) MnO_2 deposited nanotube array

Figure 5.1.1 (a) shows the SEM image of the Pt-nanotube array, and figure 2.6.1.1 (b) shows the same array after MnO_2, deposition. This structure of the current collector maximizes the surface area for MnO_2, deposition. A good charge storage capability along with excellent stability was reported for this structure [147]. Both commercially and in lab- grade devices, different materials like copper, nickel, aluminum etc, are used as current collectors. In a typical supercapacitor device, the current collector does not participate in any reaction. Hence the choice of the current collector should be such that it does not react with the electrolyte. Also, with the rise in popularity of wearable electronics, the current collector should be flexible.

Thus, a good amount of research is required to improve the material composition and architecture of the current collector to meet the global requirements.

2.6.2 Separator

The separator in a supercapacitor device is kept between two electrodes. It serves three main purposes. (1) Firstly, and most importantly, it prevents short-circuiting the device by providing electrical insulation between the two electrodes. (2) It acts as a storage reservoir for the liquid electrolyte, and thirdly during the charging- discharging process, it allows the passage of electrolyte ions [148,149]. (3) Having good mechanical strength to provide device durability. Based on these requirements, ES separators are usually made from thin and highly porous films or membranes. Commonly used separator materials are cellulose, polymer membranes and glass fibers. As generally realized, the choice of separator materials depends on the type of electrode, working temperature and ES cell voltage. In commercial devices, a cellulose-based separator is used along with organic electrolyte because of its good wettability. The choice of the separator is defined by the properties of the electrolyte. The separator material must be thermally stable at the working temperature range, and it must be chemically/electrochemically inert. Besides, its thickness must be as thin as possible to enhance the charge storage capacity. To use in the flexible supercapacitor, the separator should also be flexible enough to accommodate the change in the shape of the overall device. Among the major disadvantages of a supercapacitor, the principal one is the high self-discharge rate. Proper design strategies of the separator can suppress the self-discharge rate. Peng et al synthesized polyacrylonitrile coated sodium dodecyl benzene sulfonate (PAN@SDBS) nanofiber membrane through coaxial electrospinning method. This membrane was used as a separator for the supercapacitor. The device showed a slow self-discharge rate because of the constrained ion diffusion due to the concentration gradient through the engineered membrane [150]. Furthermore, the properties of the separators, such as chemical composition, thickness, porosity, pore size distribution, and surface morphology were found to have a noticeable influence on several EDLC performance indicators including polarizability limits, specific capacitance, ESR, characteristic time constant, specific energy, and power densities [151]. The field of separator engineering receives relatively less research interest compared to that of electrode materials and electrolytes. However, a few major drawbacks can be resolved through the proper engineering of the

separator. Hence more research is necessary to advance the general performance of the supercapacitor device.

2.6.3 Electrolyte

The electrolyte is another important part of the supercapacitor device. It is an important detrimental component that controls other important parameters like operating potential window, self-discharge, rate performance, internal resistance, cycle life, operating temperature, etc. [153]. Among the different types, electrolytes can broadly be classified into two different categories, liquid electrolytes and solid- state electrolytes.

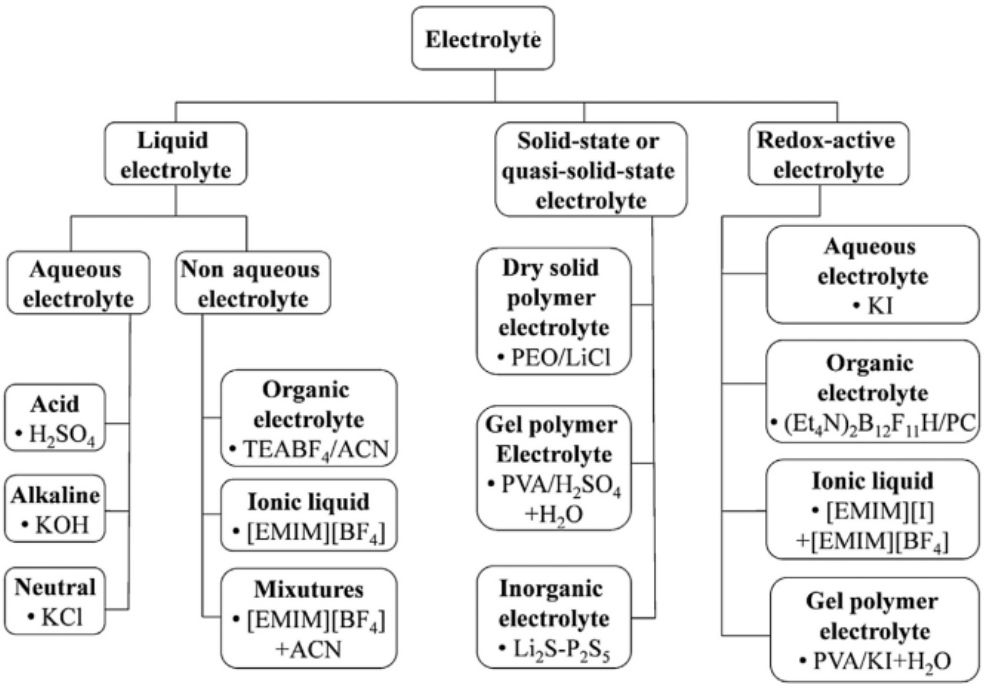


Fig 2.6.3 Classification of electrolyte for supercapacitor application. Ref: [152]

Liquid electrolytes can be further classified into two groups: aqueous electrolytes and non-aqueous electrolytes [154]. The broad classification of electrolytes has been shown in figure 2.6.3. Aqueous electrolyte-based supercapacitors usually offer high capacitance because of the high ionic conductivity of the electrolyte. But operating potential window, in this case, becomes very narrow owing to the small decomposition potential of the electrolyte. Because of this small potential window, the energy density offered by the device becomes less. On the other hand, supercapacitor with non-aqueous electrolyte can offer higher potential window and thus

a much higher energy density can be obtained. Solid electrolytes also offer high potential window, with an added benefit that in a device with solid electrolyte there is no leakage problem. Thus, there is no single electrolyte which can satisfy all the requirements for supercapacitor.

Aqueous electrolytes are extensively used in the laboratory because of their low cost and ease of handle-ability. To date, no commercial device has been fabricated with aqueous electrolytes because of low energy density. Aqueous electrolytes have higher ionic conductivity than organic and ionic liquid electrolytes [155]. H_2SO_4 is the most popular acidic type of aqueous electrolyte because of the ultrahigh ionic conductivity of 0.8 S cm^{-1} (at room temperature) [156]. Because of this high ionic conductivity, device resistance can be reduced, and power density can be increased. Different alkaline type aqueous electrolytes are also frequently used for device fabrication. Aqueous KOH electrolyte is a commonly used alkaline electrolyte that also offers high ionic conductivity of 0.6 S cm^{-1} (at 25 °C). NaOH and LiOH are also used in supercapacitor device fabrication among the other alkaline electrolytes. Alongside acidic and alkaline electrolytes, neutral electrolytes are also popular in the research field. Aqueous solutions of Na_2SO_4, KCl, NaCl, etc., have been widely used because they can provide a relatively higher potential window compared to alkaline and acidic electrolytes. Also, these types of neutral electrolytes result in less corrosion of the current collector.

Non-aqueous is another type electrolytes, organic electrolytes are mainly used in the commercial market because of their high operating potential window of 2.5 to 2.8 V. However, they are costly offer low ionic conductivity and low specific capacitance. They are also highly flammable and toxic. Tetraethyl ammonium tetrafluoroborate (TEABF4) in acetonitrile (AC) solvent or propylene carbonate (PC) are examples of organic type electrolytes [157,158].

Ionic liquids also belong to the non-aqueous type electrolyte. They are basically salts having melting points under 100 °C and comprise of inorganic or organic anions and organic cations [159]. Because of the weak interactions between the ions, they tend to have a low melting point.

By varying the combinations of cations and anions, the properties of ionic liquids can be tuned easily. lonic liquids are non-flammable, thermally, and electrochemically more stable.

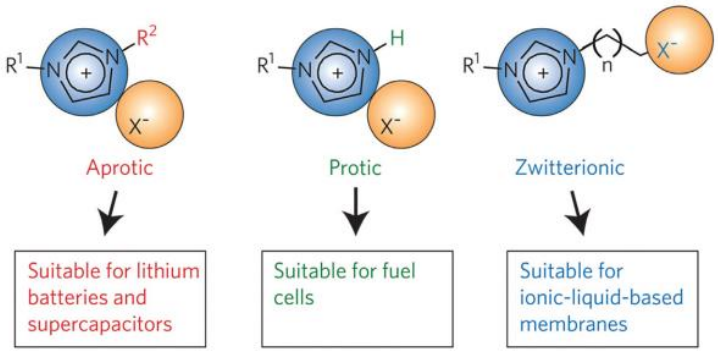


Fig 2.6.3.1 Basic types of ionic liquids: aprotic, protic and zwitterionic types. Source; Macmillan Publishers Ltd., Nature Materials [162].

A relatively high potential window (>3V) can be achieved with this type of electrolyte. Combinations of ammonium, sulfonium, pyrrolidinium, imidazolium, and phosphonium cations and hexafluorophosphate (PF), tetrafluoroborate (BF4), bis(fluorosulfonyl)imide (FSI), bis(trifluoromethanesulfonyl) imide (TFSI), and dicyanamide (DCA) anions are useally used as ionic liquid electrolytes in supercapacitor application [160, 161].

Redox-active electrolytes is a new strategy has been explored to increase the capacitance of ES by inducing the pseudocapacitive contribution from the redox-active electrolytes. The Faradaic reactions occur in the electrolyte can contribute extra capacitance to the ESs [162, 163]. In this case, the pseudocapacitance is not only emerge from the pseudocapacitive electrode materials but can also be contributed from the electrolyte (i.e., from the reduction/oxidation of the redox mediator in the electrolyte). A simple and typical example is an iodide/iodine redox pair, which is used for the redox-active aqueous electrolyte for carbon-based ESs by Lota et al. [162]. The maximum capacitance of the carbon positive electrode in a 1.0 M KI electrolyte could exhibit an extremely high value of 1840 F g^{-1}, due to the pseudocapacitive capacitance. Recently, electrochemical energy storage devices containing solid-state electrolytes have gained research attention due to the rapidly increasing demand for portable electronics, wearable electronics, etc. The solid-state electrolytes serve two different purposes. Firstly, it acts as an electrolyte to conduct the ions, and secondly, it acts as the separator for the two electrodes [163]. Among the different types of solid- state electrolytes, polymer electrolytes are most often used for supercapacitors. Polymer-based electrolytes can be classified into three different categories: solid polymer electrolyte (SPE), gel polymer electrolyte (GPE), and polyelectrolyte. Among these three types, gel polymer electrolyte is most extensively used in supercapacitor application

due to its highest ionic conductivity among the other solid- state electrolytes. A gel polymer contains a host polymer like polyethylene oxides (PEO), polyvinyl alcohol (PVA), etc., and an aqueous electrolyte like Na_2SO_4, KOH, H_2SO_4, etc [164].

2.6.4 Electrode

Properties of Ideal electrode material: Although electrolyte, separator, and current collector play a major role in determining the overall performance of the supercapacitor, the major contribution in charge storage capability and overall device stability is mainly determined by the choice of electrode material. Supercapacitor electrode material must have high surface area, good electrical conductivity, good thermal and chemical stability, corrosion resistivity and good surface wettability in the electrolyte used. Apart from these, the electrode materials should be of low cost, easy to process, and environmentally friendly with good recyclability The pseudocapacitive materials require additional criteria which are to easily transfer the faradic charge This is essential to enhance the overall performance [165] The specific capacitance value of typical electrode material is dependent on many essential parameters like its surface area, morphology, distribution of pore size, and pore shape. It is seen that the material with reduced pore sizes offers high capacitance and high energy density However, the reduced pore size increases the resistive nature of the electrode material, which reduces the power density [166].

Thus, the most important requirements for fabricating an efficient supercapacitor electrode include improving the number of available electrochemically active sites by enhancing specific surface area of the electrode material, tuning the pore size and pore shape of the electrode material and increasing the connection between individual redox active sites by tuning the morphology [167-169]. Different researchers have tried to tune the morphology of the electrode material to improve the electrochemical charge storage performance.

2.6.5 Effect on the performance of electrode material due to Morphological differences

The morphology of electrode materials significantly impacts the performance of supercapacitors, influencing factors such as specific capacitance, energy density, and cycling stability. Here are the key aspects of how morphological characteristics affect the performance of supercapacitor electrodes:

Key Morphological Factors Influencing Performance

1. Surface Area and Porosity:

Specific Capacitance: A higher specific surface area allows for more electroactive sites, which enhances the specific capacitance of the electrodes. Materials with well-defined porous structures, such as activated carbons or metal-organic frameworks, can provide increased surface area that directly correlates with improved energy storage capabilities.

Ion Accessibility: The porosity of the electrode materials facilitates the penetration of the electrolyte ions, which is crucial for charge/discharge processes. Hierarchical porous structures that combine micro, meso, and macroporosity can optimize ion transport and enhance overall performance.

2. Particle Size and Shape:

Charge Transport: The size and shape of the electrode particles can influence the rate of charge transport. Smaller particles typically enhance the rate of ion diffusion, allowing for faster charge/discharge cycles. For example, nanostructured materials often exhibit superior performance compared to their bulk counterparts due to the reduced diffusion distances for ions.

Morphological Design: Specific shapes, such as nanorods or flower-like structures, can improve the mechanical stability of the electrodes while also providing a larger surface area for electrochemical reactions. These designs can help mitigate issues like cracking and degradation during cycling.

3. Conductivity:

Electrical Conductivity: The morphology of the electrode can affect the formation of conductive networks within the material. For instance, the integration of conductive additives like carbon nanotubes or graphene can enhance the overall conductivity of the electrode, leading to better performance under high current densities.

Composite Structures: Hybrid materials that combine conductive polymers with carbon-based materials can leverage the benefits of both components. The morphology of these composites can be engineered to optimize electron and ion transport, thus enhancing the overall efficiency of the supercapacitor.

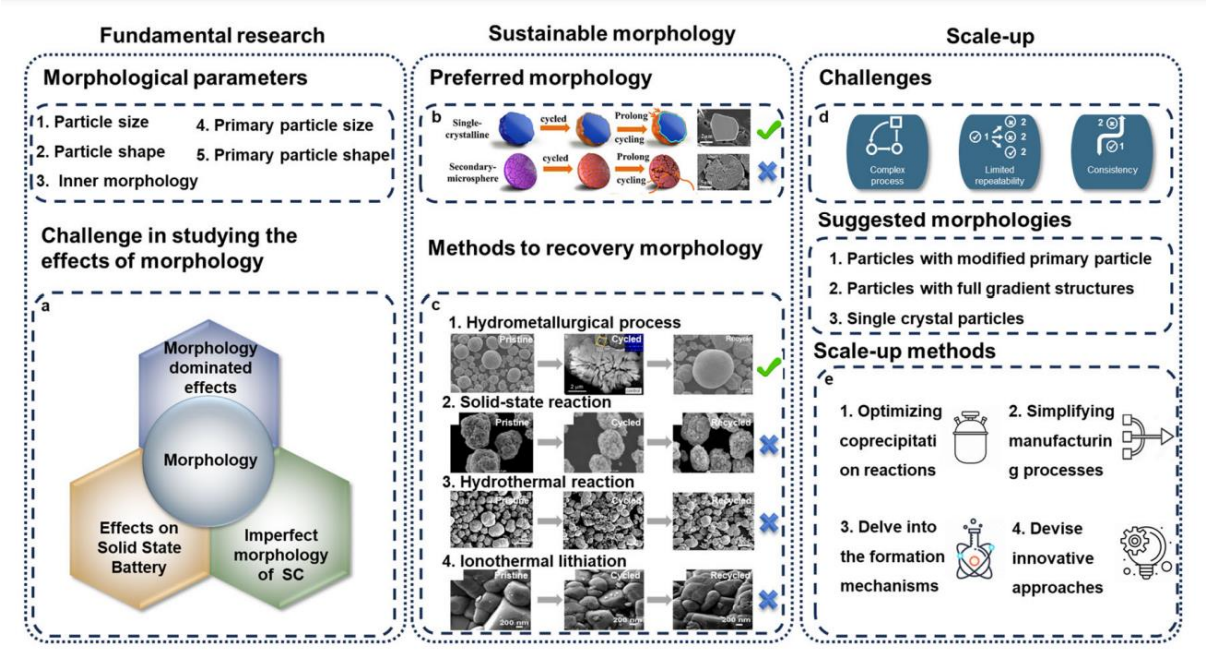


Fig 2.6.5.1 a) The schematic of challenge in studying the effects of morphology. b) The schematic of preferred single crystal morphology for sustainability (crack evolution and the internal morphological difference for PC and SC particles during prolonged cycling). c) SEM image of morphology of pristine, cycled, and recycled cathode materials from the hydrometallurgical process, solid-state reaction, hydrothermal reaction, and Ionothermal lithiation. d) The challenges for scale-up. e) The methods for scale-up. Panel b is adapted with permission from ref. [170], Elsevier, 2020. Panel c is adapted with permission from ref. [171], Copyright Elsevier, 2021, ref. [172], Copyright American Chemical Society, 2022, ref. [173], Copyright Elsevier, 2022, and ref.[174], Copyright Wiley-VCH, 2020.

Recent Advances in Morphological Engineering

Recent research has focused on innovative approaches to engineer the morphology of supercapacitor electrodes for enhanced performance:

- Hierarchical Structures: Developing electrodes with hierarchical structures can improve both ion transport and mechanical stability. For example, flower-like structures of transition metal oxides on conductive substrates have shown promising results in enhancing capacitance and cycling stability.

- 3D Architectures: Three-dimensional electrode designs, such as those formed from interconnected carbon nanotubes or graphene, can significantly improve the accessibility of the electrolyte and enhance the overall electrochemical performance.

- Electrochemical Synthesis Techniques: Techniques like electro-polymerization allow for the creation of conductive polymers with tailored morphologies. These methods can produce electrodes with high surface areas and controlled porosity, leading to improved capacitance and stability.

Kim and co-workers synthesized nickel oxide (NiO) nano structures with different morphologies through the sol-gel method [175] The morphologies of the synthesized samples were varied by changing the basicity of the precursor solution. Under weak basic conditions (using hexamethylene tetramine (HMTA)), flower-like nanostructure, as shown in figure 5.5.2 (a) was obtained. The medium basic precursor prepared by ammonium hydroxide (NH_4OH) resulted in the formation of nanoslice of NiO and is shown in figure 5.5.2 (b). On the other hand, much smaller nano particles of NiO having a diameter 50 nm were obtained under strong basic condition

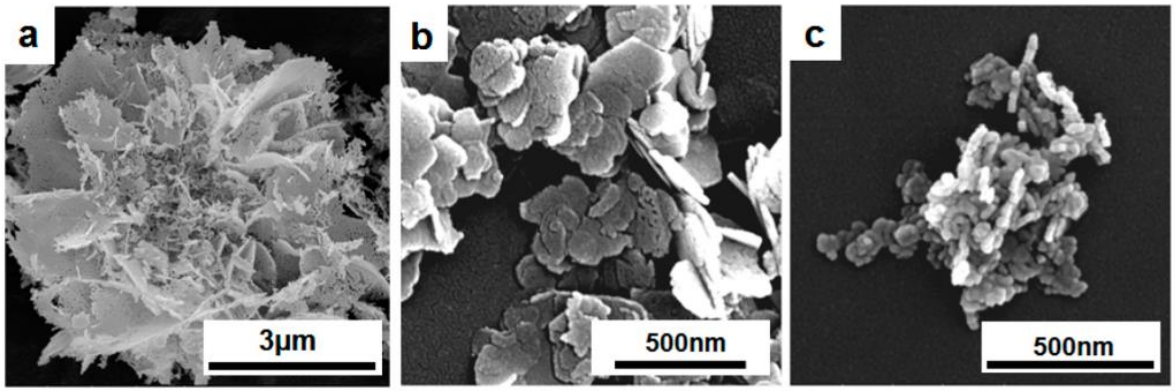


Fig 2.6.2 SEM image of (a) nanoflower, (b) nanoslice, (c) nanoparticle. Ref. [121]

obtained by adding lithium hydroxide (LiOH) in the precursor. From the BET specific surface area measurement, it was estimated that the nanoflower-like structure had a specific surface area of 159 $m^2\ g^{-1}$ with a pore volume of 0.66 cc g^{-1}. Whereas the same value for the other two samples was 193 m^2g^{-1} for nanoslice (pore volume 0.3 cc g^{-1}) and 233 m^2g^{-1} (pore volume 0.51

cc g^{-1}) for the nanoparticles of NiO. Hence, at first glance, it may seem that the sample with a larger specific surface area should offer better electrochemical storage performance. However, electrochemical characterizations revealed that the morphology with minimum surface area (nanoflower of NiO) demonstrated the highest specific capacitance of 480 F g^{-1} at a current density of 0.5 A g^{-1} in 2 M aqueous KOH solution.

Arafat et al prepared single and binary composite samples of $NiFe_2O_4$ for supercapacitor application [176]. Four different techniques were used for the preparation of Nickle ferrite ($NiFe_2O_4$) that were electrospinning, hydrothermal, sol-gel, and green method using tamarindus indica seed powder and $Fe(NO_3)_3.9H_2O$ (2:1 molar ratio) in DI water. SEM and TEM techniques were used to study the morphology shown in fig. 2.6.5.3.

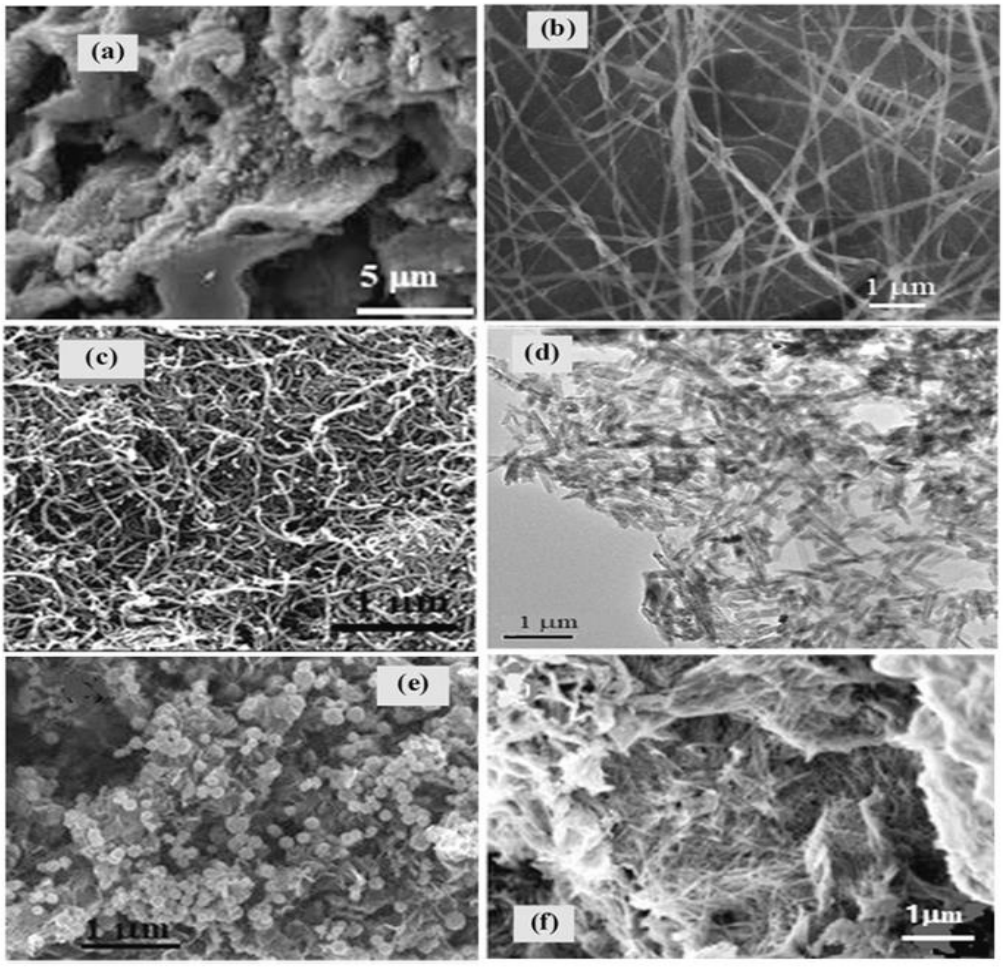


Fig 2.6.5.3 SEM micrographs for (a) AAC; (b) Nanofibers; (c) nanotube; (d) nanorod; (e) nanoparticle; (f) AAC@nanofiber. Ref. [176]

The SEM micrographs of the activated carbon sample ($NiFe_2O_4$@AAC) Fig 2.6.5.3 (a) and TEM shows fig 2.5.5.4 (a) plates with a flake-like structure containing fibres with diameters of

1nm. The SEM and TEM micrographs (fig 2.6.5.3b and 2.6.5.4b) of nanofibers with an average diameter of 55 nm with lengths to few mm., Fig 2.6.5.3c and 2.6.5.4c illustrates nanotubes

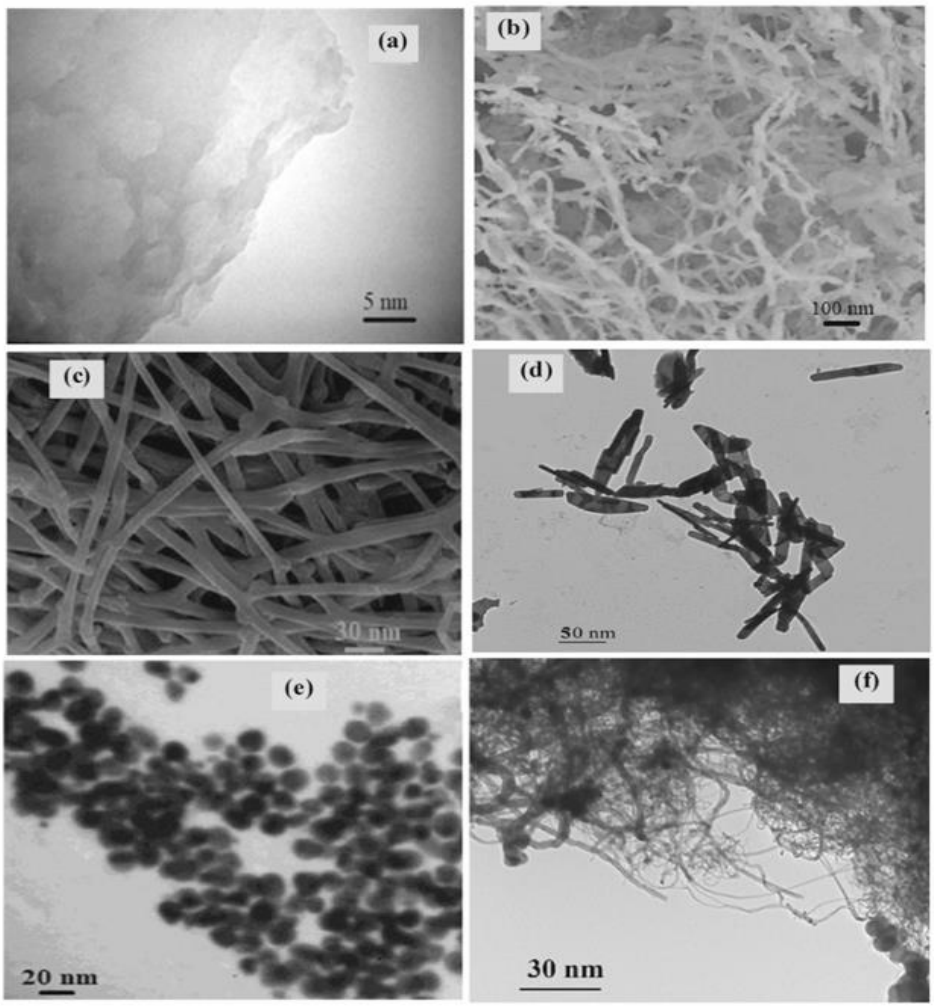


Fig 2.6.5.4 TEM micrographs for (a) AAC; (b) Nanofibers; (c) nanotube; (d) nanorod; (e) nanoparticle; (f) AAC@nanofiber. Ref. [176]

structure with an average pore diameter of 9 nm with length 230 nm. The Fig 2.6.5.3d and 2.6.5.4d shows rod like structure with an average diameter of 30 nm and length 150 nm. The fig 2.5.5.3e and 2.5.5.4e demonstrates particles with a spherical structure with average diameter of 35nm. The micrographs of AAC@$NiFe_2O_4$ fiber (fig 2.6.5.3f and 2.6.5.4f) shows the reduction in fiber lengths.

The electrochemical characterization showed at a fixed scan rate 5 mV/s the AAC; Nanofibers; nanotube; nanorod; nanoparticle; AAC@nanofiber shows specific capacitance 424, 1140, 680, 550, 385, 1283 F g^{-1} respectively [176].

2.7 Summary

In summary, the morphology of electrode materials in supercapacitors is a critical factor that affects their electrochemical performance. By optimizing surface area, porosity, particle size, and conductivity through advanced morphological designs, researchers can significantly enhance the efficiency and stability of supercapacitor technologies. Future developments will likely focus on integrating these morphological strategies with scalable production methods to facilitate commercial applications.

References

[1] Shafiqur R, Maher BA, Al-Moallem Said A. Cost of solar energy generated using PV panels. Renew Sustain Energy Rev. 2007;11:1843-1857.

[2] Timilsina GR, Kurdgelashvili L, Narbel PA. Solar energy: markets, economics and policies. Renew Sustain Energy Rev. 2012;16(1):449-465.

[3] Rourke FO, Boyle F, Reynolds A. Tidal energy update 2009. Appl Energy. 2010;87(2):398-409.

[4] Neill SP, Hashemi MR, Lewis MJ. Tidal energy leasing and tidal phasing. Renew Energy. 2016;85:580-587.

[5] Saidur R, Islam M, Rahim N, Solangi K. A review on global wind energy policy. Renew Sustain Energy Rev. 2010;14(7): 1744-1762.

[6] Islam MR, Mekhilef S, Saidur R. Progress and recent trends of wind energy technology. Renew Sustain Energy Rev. 2013;21: 456-468.

[7] Wang L, Han Y, Feng X, Zhou J, Qi P, Wang B. Metal-organic frameworks for energy storage: batteries and supercapacitors. Coord Chem Rev. 2016;307:361-381.

[8] Guan M, Liao W-H, On the energy storage devices in piezo electric energy harvesting. Paper Presented at Smart Struc tures and Materials 2006: Damping and Isolation; 2006.

[9] Guan M, Liao W. Characteristics of energy storage devices in piezoelectric energy harvesting systems. J Intell Mater Syst Struct. 2008;19(6):671-680.

[10] Vullers R, van Schaijk R, Doms I, van Hoof C, Mertens R. Micropower energy harvesting. Solid-State Electron. 2009; 53(7):684-693.

[11] Richards PD, Myers RJ, Swinton SM, Walker RT. Exchange rates, soybean supply response, and deforestation in south America. Glob Environ Change. 2012;22(2):454-462.

[12] P. Simon, Y. Gogotsi, Materials for electrochemical capacitors, Nat. Mater. 7 (2008) 845–854.

[13] Materials for Supercapacitor Applications. http://dx.doi.org/10.1016/B978-0-12-819858-2.00001-9.

[14] Materials for Supercapacitor Applications. http://dx.doi.org/10.1016/B978-0-12-819858-2.00001-9.

[15] Simon P, Gogotsi Y. Materials for electrochemical capacitors. Nanoscience and Technology: A Collection of Reviews from Nature Journals. Singapore: World Scientific; 2010:320-329.

[16] Tarascon J-M, Armand M. Issues and challenges facing rechargeable lithium batteries. Materials for Sustainable Energy: A Collection of Peer-Reviewed Research and Review Articles from Nature Publishing Group. Singapore: World Sci entific; 2011:171-179.

[17] Simon P, Gogotsi Y, Dunn B. Where do batteries end and supercapacitors begin? Science. 2014;343(6176):1210-1211.

[18] P. Simon, Y. Gogotsi, Materials for electrochemical capacitors, Nat. Mater. 7 (2008) 845–854.

[19] Wang L, Han Y, Feng X, Zhou J, Qi P, Wang B. Metal-organic frameworks for energy storage: batteries and supercapacitors. Coord Chem Rev. 2016;307:361-381.

[20] Destraz B, Barrade P, Rufer A. Power assistance for diesel electric locomotives with supercapacitive energy storage. Paper presented at 2004 IEEE 35th Annual Power Electronics Specialists Conference (IEEE Cat. No. 04CH37551); 2004.

[21] Miller JM, McCleer PJ, Everett M, Strangas EG. Ultra capacitor plus battery energy storage system sizing methodology for HEV power split electronic CVT's. Paper presented at Proceedings of the IEEE International Symposium on Industrial Electronics, ISIE 2005; 2005.

[22] Thounthong P, Raël S, Davat B. Control strategy of fuel cell/supercapacitors hybrid power sources for electric vehicle. J Power Sources. 2006;158(1):806-814.

[23] Meinert M. New mobile energy storage system for rolling stock. Paper presented at 2009 13th European Conference on Power Electronics and Applications; 2009.

[24] Butterbach S, Vulturescu B, Coquery G, et al. Design of a supercapacitor-battery storage system for a waste collection vehicle. Paper presented at 2010 IEEE Vehicle Power and Pro pulsion Conference, 2010.

[25] Jian Cao A. New battery/ultracapacitor hybrid energy storage system for electric, hybrid, and plug-in hybrid electric vehicles/Jian Cao, A. Emadi. IEEE Trans Power Electron. 2012;27(1):122-132.

[26] Zeng C, Lian H, Chen T, et al. A wavelet transform based power allocation strategy for lithium battery and ultra capaci tor hybrid vehicular power system. Paper presented at 2016 31st Youth Academic Annual Conference of Chinese Associa tion of Automation (YAC); 2016.

[27] Shin D, Lee K, Chang N. Fuel economy analysis of fuel cell and supercapacitor hybrid systems. Int J Hydrogen Energy. 2016;41(3):1381-1390.

[28] Kadri A, Marzougui H, Aouiti A, Bacha F. Energy manage ment and control strategy for a DFIG wind turbine/fuel cell hybrid system with super capacitor storage system. Energy. 2020;192:116518.

[29] B.E. Conway, Electrochemical Supercapacitors: Scientific Fundamentals and Technological Applications, Kluwer- Plenum, New York, (1999).

[30] A. Burke, Ultracapacitors: why, how, and where is the technology, J. Power Sources 91 (1) (2000) 37–50, doi: 10.1016/S0378-7753(00)00485-7.

[31] A. Chu, P. Braatz, Comparison of commercial supercapacitors and highpower lithium-ion batteries for powerassist applications in hybrid electric vehicles I. Initial characterization, J. Power Sources 112 (1) (2002) 236–246, doi: 10.1016/S0378-7753(02)00364-6.

[32] M.V. Kiamahalleh, S.H.S. Zein, G. Najafpour, S.A. Sata, S. Buniran, Multiwalled carbon nanotubes based nanocomposites for supercapacitors: a review of electrode materials, Nano 7 (2012) 1, doi: 10.1142/S1793292012300022.

[33] (a)M.S. Halper, J.C. Ellenbogen, Supercapacitors: A Brief Overview, The MITRE Corporation, McLean, Virginia, USA, 2006.(b)F. Ḅeguin, E. Frackowiak (Eds.), Supercapacitors: Materials, Systems, and Applications, WileyVCH Verlag GmbH & Co. KGaA, Weinheim, Germany, 2013 (Chapter 2).

[34] H. Choi, H. Yoon, Nanostructured electrode materials for electrochemical capacitor applications, Nanomaterials 5 (2) (2015) 906–936, doi: 10.3390/nano5020906.

[35] P. Simon, Y. Gogotsi, Materials for electrochemical capacitors, Nat. Mater. 7 (2008) 845–854, doi: 10.1038/ nmat2297.

[36] M.S. Ata, Advanced materials and fabrication methods for electrochemical supercapacitors, Master Thesis, McMaster University, 2012. Available from: https://macsphere.mcmaster.ca/bitstream/11375/12736/1/fulltext. pdf.

[37] S. Mohapatra, A. Acharya, G.S. Roy, The role of nanomaterial for the design of supercapacitor, Lat. Am. J. Phys. Educ. 6 (2012) 380–384.

[38] S.M. Chen, R. Ramachandran, V. Mani, R. Saraswathi, Recent advancements in electrode materials for the high performance electrochemical supercapacitors: a review, Int. J. Electrochem. Sci. 9 (2014) 4072–4085.

[39] M. Beidaghi, Design, Fabrication, and Evaluation of On-chip Micro-supercapacitors, PhD Thesis, Florida International University, 2012. Available from: https://digitalcommons.fiu.edu/cgi/viewcontent.cgi?referer=https:// www.google.com/&httpsredir=1&article=1766&context=etd.

[40] T. Chen, L. Dai, Carbon nanomaterials for high-performance supercapacitors, Mater. Today 16 (2013) 272–280, doi: 10.1016/j.mattod.2013.07.002.

[41] M. Vangari, T. Pryor, L. Jiang, Supercapacitors: review of materials and fabrication methods, J. Energy Eng. 139 (2013) 72–79, doi: 10.1061/(ASCE)EY. 1943-7897.0000102.

[42] Frackowiak E, Machnikowski J, Kaczmarska H, Beguin F. Boronated mesophase pitch coke for lithium insertion. J Power Sources. 2001;97:140-142.

[43] Frackowiak E, Machnikowski J, Kaczmarska H, Beguin F. Boronated mesophase pitch coke for lithium insertion. J Power Sources. 2001;97:140-142.

[44] Zhai Y, Dou Y, Zhao D, Fulvio PF, Mayes RT, Dai S. Carbon materials for chemical capacitive energy storage. J Adv Mater. 2011;23(42):4828-4850.

[45] Energy Storage. 2023;5:e339. https://doi.org/10.1002/est2.339.

[46] Laforgue A, Simon P, Fauvarque J, et al. Activated carbon/conducting polymer hybrid J Electrochem Soc. 2003;150(5):A645. supercapacitors.

[47] Burke A. R&D considerations for the performance and application of electrochemical capacitors. Electrochim Acta. 2007; 53(3):1083-1091.

[48] Pell WG, Conway BE. Peculiarities and requirements of asym metric capacitor devices based on combination of capacitor and battery-type electrodes. J Power Sources. 2004;136(2):334-345.

[49] Wang X, Zheng JP. The optimal energy density of electro chemical capacitors using two different electrodes. J Electrochem Soc. 2004;151(10):A1683.

[50] Li H, Cheng L, Xia Y. A hybrid electrochemical supercapacitor based on a 5 V Li-ion battery cathode and active car bon. Electrochem Solid State Lett. 2005;8(9):A433.

[51] Xia L, Tang B, Wei J, Zhou Z. Recent advances in alkali metal-ion hybrid Supercapacitors. Batteries Supercaps. 2021;4: 1108-1121.

[52] Helmholtz, Ueber einige gesetze der vertheilung elektrischer strome in korperlichen leitern mit anwendung auf die thierisch-elektrischen versuche, Annalen der Physik 165 (1853) 211-233.

[53] C.M.A. Brett, A.M.O. Brett, Electrochemistry: Principles, Methods, and Applications, Oxford University Press, UK, 2002.

[54] M. Endo, T. Takeda, Y. Kim, K. Koshiba, K. Ishii, High power electric double layer capacitor (EDLC's); from operating principle to pore size control in advanced activated carbons, Carbon Sci. 1 (3) (2001) 117–128.

[55] V. Bagotsky, Fundamentals of Electrochemistry, John Wiley & Sons, Inc, Hoboken, New Jersey, (2005).

[56] C.M.A. Brett, A.M.O. Brett, Electrochemistry: Principles, Methods, and Applications, Oxford University Press, UK, 2002.

[57] V. Bagotsky, Fundamentals of Electrochemistry, John Wiley & Sons, Inc, Hoboken, New Jersey, (2005).

[58] C.M.A. Brett, A.M.O. Brett, Electrochemistry: Principles, Methods, and Applications, Oxford University Press, UK, 2002.

[59] P. Sharma, T.A. Bhatti, Review on electrochemical double-layer capacitors, Energy Convers. Manag. 51 (12) (2010) 2901–2912, doi: 10.1016/j.enconman.2010.06.031.

[60] O. Barbieri, M. Hahn, A. Herzog, R. Kötz, Capacitance limits of high surface area activated carbons for double layer capacitors, Carbon 43 (6) (2005) 1303–1310, doi: 10.1016/j.carbon.2005.01.001.

[61] D. Qu, H. Shi, Studies of activated carbons used in double-layer capacitors, J. Power Sources 74 (1) (1998) 99–107, doi: 10.1016/S0378-7753(98)00038-X.

[62] J. Gamby, P. Taberna, P. Simon, J. Fauvarque, M. Chesneau, Studies and characterizations of various activated carbons used for carbon/carbon supercapacitors, J. Power Sources 101 (1) (2001) 109–116.

[63] H. Shi, Activated carbons and double layer capacitance, Electrochim. Acta 41 (10) (1996) 1633–1639, doi: 10.1016/0013-4686(95)00416-5.

[64] D. Qu, Studies of the activated carbons used in double-layer supercapacitors, J. Power Sources 109 (2) (2002) 403–411, doi: 10.1016/S0378-7753(02)00108-8.

[65] Y.J. Kim, Y. Horie, S. Ozaki, Y. Matsuzawa, H. Suezaki, C. Kim, N. Miyashita, M. Endo, Correlation between the pore and solvated ion size on capacitance uptake of PVDC-based carbons, Carbon 42 (8–9) (2004) 1491–1500, doi: 10.1016/j.carbon.2004.01.049.

[66] J. Chmiola, G. Yushin, Y. Gogotsi, C. Portet, P. Simon, P. L. Taberna, Anomalous increase in carbon capacitance at pore sizes less than 1 nanometer. Science 313(5794), (2006) 1760–1763. DOI: 10.1126/science.1132195.

[67] P. Simon, A. Burke, Nanostructured carbons: double-layer capacitance and more, Electrochem. Soc. Interface 17 (1) (2008) 38–44.

[68] C. Largeot, C. Portet, Relation between the ion size and pore size for an electric double-layer capacitor, J. Am. Chem. Soc. 130 (9) (2008) 2730–2731, doi: 10.1021/ja7106178.

[69] A. García-Gómez, G. Moreno-Fernández, B. Lobato, T. Centeno, Constant capacitance in nanopores of carbon monoliths, Phys. Chem. Chem. Phys. 17 (24) (2015) 15687–15690, doi: 10.1039/C5CP01904D.

[70] F. Stoeckli, T.A. Centeno, Pore size distribution and capacitance in microporous carbons, Phys. Chem. Chem. Phys. 14 (33) (2012) 11589–11591, doi: 10.1039/C2CP41545C.

[71] T.A. Centeno, F. Stoeckli, The volumetric capacitance of microporous carbons in organic electrolyte, Electrochem. Commun. 16 (1) (2012) 34–36, doi: 10.1016/j.elecom.2011.12.017.

[72] C. Vix-Guterl, E. Frackowiak, K. Jurewicz, M. Friebe, J. Parmentier, F. Béguin, Electrochemical energy storage in ordered porous carbon materials, Carbon 43 (6) (2005) 1293–1302, doi: 10.1016/j.carbon.2004.12.028.

[73] J. Huang, B. Sumpter, V. Meunier, Theoretical model for nanoporous carbon supercapacitors, Angew. Chem. 120 (3) (2008) 530–534, doi: 10.1002/anie.200703864.

[74] G. Feng, R. Qiao, J. Huang, B.G. Sumpter, V. Meunier, Ion distribution in electrified micropores and its role in the anomalous enhancement of capacitance, ACS Nano 4 (4) (2010) 2382–2390, doi: 10.1021/nn100126w.

[75] V. Subramanian, S. C. Hall, P. H. Smith, B. Rambabu, Mesoporous anhydrous RuO as a supercapacitor electrode material, Solid State lonics, 175 (2004) 511-515. doi:10.1016/j.ssi.2004.01.070.

[76] X. Li, X. Li, G. Wang, X. Wang, J. Ji, Flexible supercapacitor based on MnO_2, nanoparticles via electrospinning. J. Mater. Chem. A. 1 (2013) 10103-10106. doi:10.1039/c3ta11727h.

[77] A. Ray, A. Roy, P. Sadhukhan, S. R. Chowdhury, P. Maji, S. K. Bhattachrya, S. Das, Electrochemical properties of TiO_2-V_2O_5 nanocomposites as a high performance supercapacitors electrode material, Appl. Surf Sci. 443 (2018) 581-591 doi: 10.1016/j.apsusc. 2018.02.277.

[78] A. Roy, A. Ray, S. Saha, S. Das, Investigation on energy storage and conversion properties of multifunctional PANI-MWCNT composite, Int. J. Hydrogen Energy. 43 (2018) 7128-7139. doi:10.1016/j.ijhydene. 2018.02.153.

[79] J. S. Lee, D. H. Shin, J. Jang, Polypyrrole-coated manganese dioxide with multiscale architectures for ultrahigh capacity energy storage, Energy Environ. Sci. 8 (2015) 3030-3039. doi:10.1039/c5ee02076j.

[80] B. E. Conway, V. Birss, J. Wojtowicz, The role and utilization of pseudocapacitance for energy storage by supercapacitors, Journal of Power Sources 66 (1997) 1-14.

[81] V. Augustyn, P. Simon, B. Dunn, Pseudocapacitive oxide materials for high-rate electrochemical energy storage, Energy Environ. Sci. 7 (2014) 1597-1614 doi:10.1039/c3ec44164d.

[82] V. Sudha, M. V Sangaranarayanan, Underpotential Deposition of Metals: Structural and Thermodynamic Considerations, J. Phys. Chem. B. (2002) 2699-2707.

[83] E. Herrero, L. J. Buller, H. D. Abruña, Underpotential deposition at single crystal surfaces of Au, Pt, Ag and other materials, Chem. Rev. 101 (2001) 1897-1930. doi:10.1021/cr9600363.

[84] H. Xia, S. Meng, G. Yuan, C. Cum, L. Lu, A Symmetric RuD, / RuO, Supercapacitor Operating at 1.6 V by Using a Neutral Aqueous Electrolyte, Electrochem. Solid-State Lett. 15 (2012) 2012-2015. doi:10.1149/2.023204esl.

[85] S. P. Gupta, B. A. Kakade, B. R. Sathe, Q. Qiao, D. J. Late, P. S. Walke, Thermally driven high-rate intercalated pseudocapacitance of flower-like architecture of ultrathin few layered 8-MnO nanosheets on carbon nano-onions, ACS Appl. Energy Mater. 3 (2020) 11398-11409. doi:10.1021/acsaem.0c02325.

[86] A. A. Lubimtsev, P. R. C. Kent, B. G. Sumpter, P. Ganesh, Understanding the origin of high- rate intercalation pseudocapacitance in Nb,O, crystals, J. Mater. Chem. A. 1 (2013) 14951- 14956. doi: 10.1039/c3ta13316h.

[87] Y. Liu, S. P. Jiang, Z. Shao, Intercalation pseudocapacitance in electrochemical energy storage: recent advances in fundamental understanding and materials development, Mater. Today Adv. 7 (2020) 100072. doi: 10.1016/j.mtadv 2020,100072.

[88] A. Muzaffar, M. B. Ahamed, K. Deshmukh, J. Thirumalai, A review on recent advances in hybrid supercapacitors: Design, fabrication and applications, Renewable and Sustainable Energy Reviews. 101 (2019) 123-145. doi:10.1016/j.rser.2018.10.026.

[89] A. Roy. A. Ray, S. Saha, M. Ghosh, T. Das, B. Satpatı, M. Nandi, S. Das, NiO-CNT composite for high performance supercapacitor electrode and oxygen evolution reaction, Electrochim. Acta. 283 (2018) 327-337. doi:10.1016/j.electacta 2018.06.154.

[90] X. Dong, X. Wang, J Wang, H. Song, X. Li, L. Wang, M. B. Chan-park, C. Ming, P. Chen, Synthesis of a MnO graphene foam hybrid with controlled MnO, particle shape and its use as a supercapacitor electrode, Carbon 50 (2012) 4865-4870. doi: 10.1016/j carbon 2012.06.014.

[91] B. Che, H. Li, D. Zhou, Y. Zhang, Z. Zeng, C. Zhao, C. He, E. Liu, X. Lu, Porous polyaniline/carbon nanotube composite electrode for supercapacitors with outstanding rate capability and cyclic stability, Compos Part B Eng. 165 (2019) 671-678. doi: 10.1016/j.compositesb 2019.02.026.

[92] PT. Kissinger, W Lafayette, W. R. Heineman, Cyclic Voltammetry, J. Chem. Educ. 9 (1983) 702-706 doi: 10.1021/ed060p702.

[93] J. J. Van Benschoten, J. Y Lewis, W R. Heineman, D. A. Roston, P. T. Kissinger, Cyclic Voltammetry Experiment, J. Chem. Educ. 9 (1983) 772-776 doi:10.1021/ed060p772.

[94] A. Ray, A. Roy, S. Saha, Transition Metal Oxide-Based Nano-materials for Energy Storage Application, Intech Open (2018) 1-17. doi: 10.5772/intechopen 80298.

[95] M. Sufyan, S. Dai, M. Wang. D. Guo, L. Chen, X. Wang, C. Hu, Y. Xi, High performance solid state fl. exible supercapacitor based on molybdenum sulfide hierarchical nanospheres, Journal of Power Sources. 285 (2015) 63-69. doi:10.1016/j.jpowsour 2015.03.079.

[96] W. Wang, S. Guo, 1. Lee, K. Ahmed, J. Zhong, Z. Favors, F. Zaera, M. Ozkan, C.S. Ozkan, Hydrous ruthenium oxide nanoparticles anchored to graphene and carbon nanotube hybrid foam for supercapacitors, Sci. Rep. 4 (2014) 9-14. doi:10.1038/srep04452.

[97] L. Miao, Z. Song, D. Zhu, L. Li, L. Gan, M. Liu, Recent advances in carbon-based supercapacitors, Mater. Adv. 1 (2020) 945-966. doi:10.1039/d0ma00384k.

[98] 11. Gurten Inal, Z. Aktas, Enhancing the performance of activated carbon based scalable supercapacitors by heat treatment, Appl. Surf. Sci. 514 (2020) 145895. doi:10.1016/j.apsusc. 2020.145895.

[99] S. Lijima, Helical microtubules of graphitic carbon, Nature 354 (1991) 56-58. doi: 10.1038/354056a0.

[100] C. Niu, E. K. Sichel, R. Hoch, D. Moy, and H. Tennent, High power electrochemical capacitors based on carbon nanotube electrodes electrodes, Appl. Phys. Lett. 1480 (2012) 21-24. doi: 10.1063/1.118568

[101] C Yu, C. Masarapu, J. Rong, B. Wei, H. Jiang, Stretchable Supercapacitors Based on Buckled Single-Walled Carbon Nanotube Macrofilms, Adv. Mater. 21 (2009) 4793-4797 doi:10.1002/adma.200901775.

[102] X. J. Lee, B. Y. Z. Hiew, K. C. Lai, L. Y. Lee, S. Gan, S. Thangalazhy-Gopakumar, S. Rigby, Review on graphene and its derivatives: Synthesis methods and potential industrial implementation, J. Taiwan doi:10.1016/j.jtice.2018.10.028 Inst. Chem Eng 98 (2019) 163-180.

[103] C. Liu, Z. Yu, D. Neff, A. Zhamu, B. Z. Jang, Graphene-Based Supercapacitor with an Ultrahigh Energy Density, Nano Lett. 10 (2010) 4863-4868. doi:10.1021/nl102661q.

[104] S. Zhang, Y. Li, N. Pan, Graphene based supercapacitor fabricated by vacuum filtration deposition, J. Power Sources 206 (2012) 476-482. doi:10.1016/j.jpowsour 2012.01.124.

[105] M. D. Stoller, S. Park, Y. Zhu, J. An, R. S. Ruoff, Graphene-Based Ultracapacitors, Nano Lett. 8 (2008) 3498-3502. doi: 10.1021/nl802558y.

[106] S. Trasatti, Physical electrochemistry of ceramic oxides, Electrochim. Acta. 36 (1991) 225- 241. doi:10.1016/0013-4686(91)85244-2

[107] Y Liu, F. Zhou, V. Ozolins, Ab Initio Study of the Charge-Storage Mechanisms in RuO, - Based Electrochemical Ultracapacitors, J. Phys. Chem. C. 116 (2012) 1450-1457 doi:10.1021/jp207616s

[108] U. M. Patil, S. B. Kulkarni, V. S. Jamadade, C.D. Lokhande, Chemically synthesized hydrous RuO, thin films for supercapacitor application, J. Alloys Compd. 509 (2011) 1677-1682. doi:10.1016/j.jallcom.2010.09.133.

[109] S. Korkmaz, A. Kariper, O. Karaman, C. Karaman, The production of rGO/ RuO, aerogel supercapacitor and analysis of its electrochemical performances, Ceram. Int. 47 (2021) 34514-34520. doi:10.1016/j.ceramint.2021.08.366.

[110] C. C. Hu. K. 11. Chang, M. C. Lin, Y. T. Wu, Design and tailoring of the nanotubular arrayed architecture of hydrous RuG, for next generation supercapacitors, Nano Lat. 6 2000) 2000- 2695. doi:10.1021/nl061576,

[111] T. P. Gujar, V. R. Shinde, C. D. Lokhande, W.Y. Kim, K.D. Jung, 0.5, 100, Spray deposited amorphous RuO, for an effective use in slectrochemical supercapacitor, Electrochem Commun. 9 (2007) 504-510. doi:10.1016/j.elecom.2006.10.017.

[112] R. Arunachalam, R. K. V. Prataap, R. Pavul Raj, S. Mohan, J. Vijayakumar, L.. Péter, M. Al Ahmad, Pulse electrodeposited Ru), electrodes for high-performance пиротскраво applications, Surf. Eng. 35 (2019) 103-109. doi:10.1080/02/70844.2018.1426408

[113] C. M. Chuang, C. W. Huang, H. Teng, J. M. Ting, Hydrothermally synthesized RuO/Carbon nanofibers composites for use in high-rate supercapacitor electrodes, Compos. Sci. Technol. 72 (2012) 1524-1529, doi: 10.1016/j.compscitech 2012.05.024.

[114] $. Cho, J. Kim, Y. Jo, A. T. A. Ahmed, H. B. Chavan, H. Woo, A. 1. Inandar, J. L. Gunjakar, S. M. Pawar, Y. Park, H. Kim, H. Im, Bendable Ruby/graphene thin film for fully flexible supercapacitor electrodes with superior stability, J. Alloys Compd. 725 (2017) 108-114 doi:10.1016/j.jallcom.2017.07.135

[115] S. N. Pusawale, P. R. Deshmukh, J. L. Gunjakar, C. D. Lokhande, inO-RuO, composite films by chemical deposition for supercapacitor application, Mater Chem. Phys. 139 (2013) 416- 422. doi:10.1016/j.matchemphys.2012.12.059.

[116] J. H. Park, J. M. Ko, O. Ok Park, Carbon Nanotube/RaO, Nanocomposite Electrodes for Supercapacitors, J. Electrochem. Soc. 150 (2003) A864. doi:10.1149/1.1576222

[117] M. Y. Chung, C. T. Lo, High-performance binder-free RuOyelectrospun carbon fiber for supercapacitor electrodes, doi:10.1016/j.electacta 2020.137324 Electrochim Acta 364 (2020) 137324.

[118] D. Xiang, L. Yin, C. Wang, L. Zhang, High electrochemical performance of RaO-FeO nanoparticles embedded ordered mesoporous carbon as a supercapacitor electrode material, Energy. 106 (2016) 103-111. doi:10.1016/j.energy 2016.02.141.

[119] D. Majumdar, Review on Current Progress of MnO-Based Ternary Nanocomposites for Supercapacitor Applications, doi:10.1002/cele 202001371. ChemElectroChem, (2021) 291-336

[120] H. Y. Lee, J. B. Goodenough, Supercapacitor Behavior with KCI Electrolyte, J. Solid State Chem. 144 (1999) 220-223. doi: 10.1006/jssc. 1998.8128.

[121] J. Shin, J. K. Sco, R. Yaylian, A. Huang, Y. S. Meng, A review on mechanistic understanding of MnO, in aqueous electrolyte for electrical energy storage systems, Int. Mater. Rev. 65 (2020) 356-387. doi: 10.1080/09506608.2019.1653520.

[122] Y. Zhang, C. Sun, P. Lu, K. Li, S. Song, D. Xue, Crystallization design of MnO, towards better supercapacitance, CrystEng Comm. 14 (2012) 5892-5897. doi:10.1039/c20025610)

[123] M. Toupin, T. Brousse, D. Bélanger, Charge storage mechanism of MnO, electrode used in aqueous electrochemical capacitor, Chem. Mater. 16 (2004) 3184-3190. doi:10.1021/cm049649j

[124] N. Vangapally, K. K. V., A. Kumar, S. K. Martha, Charge storage behavior of sugar derived carbon/MnO, composite electrode material for high-performance supercapacitors, J. Allays Compd. 893 (2022) 162232. doi: 10.1016/jjallcom 2021.162232

[125] P. Wang, Y. Zhao, L. Wen, J. Chen, Z. Lei, Ultrasound Microwave-Assisted Synthesis of MnO, Supercapacitor Electrode Materials, Ind. Eng. Chem. Res. 53 (2014) 20116-20123. doi: 10.1021/ie5025485

[126] Z. Yu, B. Duong, D. Abbitt, J Thomas, Highly ordered MnO, nanopillars for enhanced supercapacitor performance, Adv. Mater. 25 (2013) 3302-3306. doi: 10.1002/adma 201300572.

[127] Y. Li, H. Xic, J. Wang, L. Chen, Preparation and electrochemical performances of a-MnO nanorod for supercapacitor, Mater. Lett. 65 (2011) 403-405. doi: 10.1016/j.matlet2010.10.048.

[128] K. Xu, S. Li, J. Yang, J. Hu, Hierarchical hollow MnO nanofibers with enhanced supercapacitor performance, Colloid Interface Sci. 513 (2018) 448-454. doi: 10.1016/j.jcis.2017.11.052.

[129] S. Chen, J. Zhu, X. Wu, Q. Han, X. Wang. Graphene Oxide-MnO, Nanocomposites for Supercapacitors, ACS Nano 4 (2010) 2822-2830. doi: 10.1021/mn901311t

[130] L. Li, Z. A. Hu, N. An, Y.Y. Yang, Z. M. Li, H.Y. Wu, Facile synthesis of MnO,/CNTs composite for supercapacitor electrodes with long cycle stability, J. Phys. Chem. C. 118 (2014) 22865-22872. doi: 10.1021/jp505744p.

[131] D. Yan, Z. Guo, G. Zhu, Z. Yu, H. Xu, A. Yu, MnO, film with three-dimensional structure prepared by hydrothermal process for supercapacitor, J. Power Sources. 199 (2012) 409-412 doi:10.1016/j.jpowsour.2011.10.051

[132] A. Bahloul, B. Nessark, E. Briot, H. Groult, A. Mauger, K. Zaghib, C. M. Julien, Polypyrrole- covered MnO, as electrode material for supercapacitor, J. Power Sources. 240 (2013) 267-272. doi: 10.1016/j.jpowsour 2013.04.013

[133] Y. Chen, X. Zhang, C. Xu, H. Xu, The fabrication of asymmetry supercapacitor based on MWCNTs/MoO /PPy composites, Electrochim Acta A (2010) 424-439 doi:10.1016/j.electacta 2019.04.072.

[134] Y. Zhao, Y. Meng, P. Jiang, Carbon@Mn), core-shell nanospheres for flexible hig performance supercapacitor electrode materials, J. Power Sources. 159 (2014) 219-236 doi: 10.1016/j.jpowsour 2014.02.086

[135] S. D. Dhas, P. S. Maldar, M. D. Patil, M. R. Waikar, R. G. Sonkawade, 5. K. Chakarvarti, S.K. Shinde, D.Y. Kim, A. V. Moholkar, Probing the electrochemical properties of NiMn,O nanoparticles as prominent electrode materials for supercapacitor applications, Mater, Sel. Eng B Solid-State Mater. Adv. Technol. 271 (2021) 115298. doi: 10.1016/j.msch 2021.115298.

[136] A. Umar, M. S. Akhtar, S. Ameen, M. Imran, R. Kumar, Y. Wang, A. A. Ibrahim, H. Albargi, M. Jalalah, M. A. Alsaiari, M. S. Al-Assiri, Colloidal synthesis of NiMn,O, nanodisks decorated reduced graphene oxide for electrochemical applications, Microchem. J. 160 (2021) 105630. doi: 10.1016/j.microc 2020.105630.

[137] H. Wei, J. Wang, L. Yu, Y. Zhang, D. Hou, T. Li, Facile synthesis of NiMn,O, nanosheet arrays grown on nickel foam as novel electrode materials for high-performance supercapacitors, Ceram. Int. 42 (2016) 14963-14969. doi:10.1016/j.ceramint.2016.06.140.

[138] Z. Wang, Z. Zhu, C. Zhang, C. Xu, C. Chen, Facile synthesis of reduced graphene oxide/NiMn O nanorods hybrid materials for high-performance supercapacitors. Electrochim Λετα. 230 (2017) 438-444. doi:10.1016/j.electacta 2017.02.023.

[139] M. R. Kim, M. Naidukalla, S. Kim, M. Kim, I Kim, NiMn,O, Nanosheet-Decorated Hierarchically Porous Polyaromatic Carbon Spheres for High-Performance Supercapacitors, ChemElectroChem 4 (2017) 1214-1221. doi: 10.1002/celc 201700023

[140] Y Sun, X. Du, J. Zhang, N. Huang, L. Yang, X. Sun, Microwave-assisted preparation and improvement mechanism of carbon nanotube@NiMn,O, core-shell nanocomposite for high performance asymmetric supercapacitors, J. Power Sources 473 (2020) 228609. doi: 10.1016/j. jpowsour 2020 228609

[141] X. Du, L. Yang, Y. Fu, S. Liu, N. Huang, S. Wang, Microwave-Assisted Synthesis of Ni,Mn O Grown on Nickel Foam as Electrode Material for High-Performance Supercapacitors, Chemistry Select. 6 (2021) 5567-5574. doi: 10.1002/slet 202100895

[142] M. Zhang, Z. Song, H. Liu, T. Ma, Biomass-derived highly porous nitrogen-doped graphene orderly supported NiMn,O, nanocrystals as efficient electrode materials for asymmetric supercapacitors, Appl. Surf. Sci. 507 (2020) 145065. doi: 10.1016/j.дряше 2019.145065.

[143] M. Sandhiya, K. Subramani, M. Satlush, Augmenting the electrochemical performance of NiMn O, by doping of transition metal ions and compositing with rGO, J. Calloid Interface Sel. 598 (2021) 409-418 dor: 10.1016/j.jcin 2021.04.023.

[144] A. Roy, A. Ray, S. Saha, M. Ghosh, T. Das, B. Satpati, M. Nandi, S. Das, NiO-CNT composite for high performance supercapacitor electrode and oxygen evolution reaction, Electrochim. Acta. 283 (2018) 327-337. doi:10.1016/j.electacta 2018.06.154.

[145] S. Park, Y. Lec, G. An, The rational design and interface engineering of an electrolyte and current collector for a stable and high-performance aqueous supercapacitor, Int. J. Energy Res. 45 (2021) 16027-16037. doi:10.1002/er.6830.

[146] L. Liu, H. Zhao, Y. Let, Review on Nanoarchitectured Current Collectors for Pseudocapacitors, Small Methods. 3 (2019) 1800341. doi: 10.1002/smtd 201800341

[147] L. Wen, Y. Mi, C. Wang, Y. Fang, F. Grote, H. Zhao, M. Zhou, Y Lei, Cost-effective Atomic Layer Deposition Synthesis of Pt Nanotube Arrays Application for High Performance Supercapacitor, Small. 10 (2014) 3162-3168 doi:10.1002/smll. 201400436.

[148] B. Szubzda, A. Szmaja, M. Ozimek, S. Mazurkiewicz, Polymer membranes as separators for supercapacitors, Appl. Phys. A. 117 (2014) 1801-1809. doi: 10.1007/s00339-014-8674-y.

[149] S. Xian-Zhong, Z. Xiong, H. Bo, M. Yan-Wei, Effects of Separator on the Electrochemical Performance of Electrical Double-Layer Capacitor and Hybrid Battery-Supercapacitor, Acta Physico-Chimica. 30 (2014) 485-491. doi: 10.3866/PKU WHXB201401131.

[150] H. Peng, L. Xiao, K. Sun, G. Ma, G. Wei, Z. Lei, Preparation of a cheap and environmentally friendly separator by coaxial electrospinning toward suppressing self-discharge of supercapacitors, J. Power Sources. 435 (2019) 226800. doi:10.1016/jjpowsour 2019.226800.

[151] K. Tonurist, T. Thomberg, A. Janes, I. Kink, E. Lust, Specific performance of electrical double layer capacitors based on different separator materials in room temperature ionic liquid, Electrochem. Commun. 22 (2012) 77–80, doi: 10.1016/j.elecom.2012.05.029.

[152] C. Zhong, Y. Deng, W. Hu, J. Qiao, L. Zhang, J. Zhang, A review of electrolyte materials and compositions for electrochemical supercapacitors, Chem. Soc. Rev. 44 (2015) 7484–7539, doi: 10.1039/C5CS00303B.

[153] C. Zhong, Y. Deng, W. Hu, J. Qiao, L. Zhang, J. Zhang, A review of electrolyte materials and compositions for electrochemical supercapacitors, Chem. Soc. Rev. 44 (2015). doi:10.1039/c5cs00303b.

[154] B. Pal, S. Yang, S. Ramesh, V. Thangadurai, R. Jose, Electrolyte selection for supercapacitive devices: a critical review, Nanoscale Adv. 1 (2019) 3807-3835. doi:10.1039/C9NA00374F.

[155] C. Zhao, W. Zheng, A Review for Aqueous Electrochemical Supercapacitors, Front. Energy Res. 3 (2015) 23. doi:10.3389/fenrg 2015.00023.

[156] M. Toupin, T. Brousse, D. Bélanger, Charge Storage Mechanism of MnO, Electrode Used in Aqueous Electrochemical Capacitor, Chem. Mater. 16 (2004) 3184-3190 doi: 10.1021/cm049649j.

[157] J. Krummacher, C. Schütter, LH. Hess, A. Balducci, Non-aqueous electrolytes for electrochemical capacitors, doi:10.1016/j.coelec 2018.03.036. Curr. Opin Electrochem. 9 (2018) 64-69.

[158] J. Park, Y.-E. Yoo, L. Mai, W. Kim, Rational Design of a Redox-Active Nonaqueous Electrolyte for a High-Energy-Density Supercapacitor Based on Carbon Nanotubes, ACS Sustain. Chem. Eng. 7 (2019) 7728-7735. doi: 10.1021/acssuschemeng 8606486.

[159] L. Miao, Z. Song, D. Zhu, L. Li, L. Gan, M. Liu, Ionic Liquids for Supercapacitive Energy Storage: A Mini-Review, Energy & Fuels. 35 (2021) 8443-8455. doi:10.1021/acs.energyfuels. 1000321.

[160] K. Karuppasamy, J. Theerthagiri, D. Vikraman, C.-J. Yim, S. Hussain, R. Sharma, T. Maiyalagan, J. Qin, H.-S. Kim, Ionic Liquid-Based Electrolytes for Energy Storage Devices: A Brief Review on Their Limits and Applications, Polymers 12 (2020) 918. doi: 10.3390/polym12040918.

[161] L. Yu G. 2. Chen, Ionic Liquid-Based Electrolytes for Supercapacitor and Supercapattery, Front. Chem. 7 (2019) 272. doi: 10.3389/fchem.2019.00272.

[162] M. Armand, F. Endres, D.R. MacFarlane, H. Ohno, B. Scrosati, Ionic-liquid materials for the electrochemical challenges of the future, Nat. Mater. 8 (2009) 621–629, doi: 10.1038/nmat2448.

[163] G. Lota, E. Frackowiak, Striking capacitance of carbon/iodide interface, Electrochem. Commun. 11 (2009) 87–90, doi: 10.1016/j.elecom.2008.10.026.

[164] K. Fic, E. Frackowiak, F. Beguin, Unusual energy enhancement in carbon-based electrochemical capacitors, J. Mater. Chem. 22 (2012) 24213–24223, doi: 10.1039/C2JM35711A.

[165] P. Forouzandeh, V. Kumaravel, S. C. Pillai, Electrode Materials for Supercapacitors: A Review of Recent Advances, Catalysts. 10 (2020) 969 doi: 10.3390/catal 10090969.

[166] S. Kondrat, P. Wu, R. Qiao, A. A. Kornyshev, Accelerating charging dynamics in subnanometre pores, Nat. Mater. 13 (2014) 387-393, doi: 10.1038/nmat3916.

[167] Q. Lu, J. G. Chen, J. Q. Xiao, Nanostructured Electrodes for High-Performance Pseudocapacitors, Angew. Chemie Int. Ed. 52 (2013) 1882-1889. doi: 10.1002/anie.201203201.

[168] C.-C. Hu, K.-H. Chang, M.-C. Lin, Y.-T. Wu, Design and Tailoring of the Nanotubular Arrayed Architecture of Hydrous RuO, for Next Generation Supercapacitors, Nano Lett 6 (2006) 2690-2695, doi: 10.1021/nl061576a.

[169] L. Mao, K. Zhang, H. S. On Chan, J. Wu, Nanostructured MnO_2/graphene composites for supercapacitor electrodes: The effect of morphology, crystallinity and composition, J. Mater Chem. 22 (2012) 1845-1851. doi:10.1039/C1JM14503G.

[170] Ma, X. et al. Recycled cathode materials enabled superior performance for lithium-ion batteries. Joule https://doi.org/10.1016/j.joule.2021.09.005 (2021).

[171] Montoya, A. T. et al. Direct recycling of lithium-ion battery cathodes: a multi stage annealing process to recover the pristine structure and performance. ACS Sustain. Chem. Eng. 10, 13319–13324 (2022).

[172] Fan, X. et al. Crack-free single-crystalline Ni-rich layered NCM cathode enable superior cycling performance of lithium-ion batteries. Nano Energy 70, https://doi.org/10.1016/j.nanoen.2020.104450 (2020).

[173] Yu, X. et al. Achieving low-temperature hydrothermal relithiation by redox mediation for direct recycling of spent lithium-ion battery cathodes. Energy Stor. Mater. 51,54–62 (2022).

[174] Wang, T. et al. Direct recycling of spent NCM cathodes through ionothermal lithiation. Adv. Energy Mater. 10, https://doi.org/10.1002/aenm.202001204 (2020).

[175] S.-I. Kim, J.-S. Lee, H.-J. Ahn, H.-K. Song, J.-H. Jang, Facile Route to an Efficient NiO Supercapacitor with a Three-Dimensional Nanonetwork Morphology, ACS Appl. Mater. Interfaces. 5 (2013) 1596-1603. doi: 10.1021/am3021894.

[176] https://doi.org/10.1016/j.jmrt.2022.06.095.

CHAPTER 3

DIFFERENT CHARACTERIZATION TECHNIQUES

3.1 X-Ray Diffractometer (XRD)

The thesis work comprises the analysis and discussions of the results obtained from different characterization facilities. These characterization techniques mainly include the structural, compositional, and morphological studies of the different electrode materials under consideration. Once the desired material is synthesized, and the formation of the same is confirmed by the structural, compositional, and morphological analyses, electrochemical characterization techniques are used to access its charge storage performance. This chapter



Fig 3.1 Rigaku SmartLab diffractometer

deals with all the different tools and techniques used to investigate a particular electrode material.

X-ray diffraction is an analytical technique that is used to identify the crystalline structure and the composition of the materials [1-3]. A crystalline solid has a periodic structure with a repeated arrangement of atoms. A beam of monochromatic X-ray, when incident on such periodic crystalline material, diffraction of rays occurs. These monochromatic X-rays are produced using a cathode ray tube having a wavelength comparable to the lattice constant of the material. Keeping the direction of the incident X-ray beam fixed, the sample and detector

are rotated using an arrangement known as a goniometer. The detector records the intensity of the reflected X-rays as a function of the angle between the directions of the incident beam and diffracted beam. At some certain angles, when the geometry of the goniometer satisfies Bragg's equation consistent with the sample's lattice spacing, a peak in the intensity is observed. By studying such peaks, different properties regarding the sample can be obtained. We have used the Rigaku SmartLab diffractometer in this thesis work, as shown in figure 3.1 The diffractometer has a Cuka source which generates a monochromatic ray having λ = 1.542 Å and a D/tex Ultra ID silicon detector.

3.2 Fourier Transform Infrared Spectroscopy (FTIR)

Fourier transform infrared spectroscopy (FTIR spectroscopy) is the preferred method of spectroscopy in the infrared (IR) regime of electromagnetic waves [4, 5]. When infrared



Fig. 3.2 Perkin-Elmer RX1 spectrometer

radiation is incident on a sample, a part of the intensity is absorbed by the sample, and the other part gets transmitted. An infrared spectrum contains absorptions peaks at different wavelengths (hence at different photon energies of the radiation) for a sample. The position of these absorption peaks represents the vibrational frequencies for the vibrations between the bonds of

the molecules and atoms constituting the material. As every different material is composed of different atoms and molecules, each different material produces a different IR spectrum. An IR spectrum is like a fingerprint for a particular sample, and no two samples can have the exact same infrared pattern. Thus, different organic and inorganic compounds can be positively identified using this technique. Apart from this, the amount of material present in a sample can be estimated from the size of the peaks in the spectrum.

Older IR instruments utilized different dispersive elements like (IR prisms, gratings etc.) to separate the individual wavelengths from the IR source. A detector measured the transmittance or absorbance of a sample at an individual wavelength. However, this method was very slow, and FTIR resolves this problem by incorporating an optical interferometer [6]. An interferometer produces an IR signal containing all the different wavelengths encoded in it. Thus, the transmittance or absorbance can be measured very quickly. The absorption data at individual wavelengths can be decoded by performing a Fourier transform of the signal, which is accomplished by a digital computer present in the instrument itself. Figure 3.2.1 shows the Perkin-Elmer RX1 spectrometer, which we have used in this thesis work. This spectrometer offers a working range of 250-4000 cm^{-1} and has a deuterated triglycine sulfate (DTGS) detector.

3.3 Electrochemical Characterizations

To evaluate an electrode material for its electrochemical charge storage performance, different electrochemical characterizations are. Cyclic voltammetry (CV), Galvanostatic Charge Discharge (GCD), and Electrochemical Impedance Spectroscopy (EIS) are principal among them. Here we discuss the different technical and practical aspects behind these characterization techniques. These three characterizations can be performed both in 3-electrode and 2-electrode modes. 3-electrode mode is used to evaluate the performance of electrochemical charge storage capability of particular electrode material of interest. On the other hand, the 2-electrode mode is used to characterize the performance of a two-electrode device like supercapacitor. Both 3-electrode and 2-electrode electrochemical characterizations can be done using an electrochemical workstation equipped with hardware to precisely control and measure potential and current. In addition to that, to perform EIS, the workstation must be

equipped with hardware to control the frequency of an AC signal over a wide range (0.01 Hz to 10^5 Hz).



Fig. 3.3 (a) 3-electrode electrochemical cell setup, (b) Corrtest CS-313 electrochemical workstation, (c) Saturated Colemel electrode (reference electrode), (d) Platinum electrode (counter electrode), (e) Active electrode/Working electrode

In 3-electrode mode, as the name suggests, there are three electrodes. The Working Electrode (WE) is the electrode where the potential is applied with respect to the reference electrode (RE), and the current is measured with respect to the counter electrode (CE).

Working Electrode (WE)

The working electrode is where the electrochemical reaction of interest occurs. Here are common materials and methods for preparing a working electrode:

Material Selection: Common materials mainly inert material includes glassy carbon, gold, platinum, and carbon paste which does not participate in the electrochemical reaction. The choice depends on the specific electrochemical properties required for measurements. The material whose electrochemical performance has to be tested (active material) is coated on the surface of WE.

Preparation Steps:

1. Cleaning: The electrode surface must be thoroughly cleaned. This can involve polishing with fine sandpaper, followed by rinsing with distilled water for several times and dried.
2. Coating: The dried rods are then wrapped with Teflon tape, keeping the circular flat end open. Teflon tape acts as an encapsulation for the sidewall of the rod.

The shape and size of the electrode can influence the current response. Common configurations include disc, rod, or planar electrodes here we used graphite rod obtained from battery.

The electrochemical performances of $NiMn_2O_4$ electrode material were studied in a **Corrtest CS313** (CorrTest, China) multi-channel electrochemical workstation at room temperature using Cyclic Voltammetry (CV), Galvanostatic charge–discharge (GCD), and Electrochemical Impedance Spectroscopy (EIS) methods. All the measurements were carried out in conventional three electrodes assembly, where platinum (Pt) electrode (1 cm × 1 cm) was used as the counter electrode and Calomel electrode as a reference electrode. To prepare the working electrodes, Teflon-coated graphite rod was used as a current collector.

In these cases, the coated surface of the WE serve as an active area where the electrochemical reaction takes place. Before coating the active material, the circular flat end of the rod is polished using fine emery paper and washed several times. Then the rods are dried in a vacuum. Next, the active material is dropcasted on the circular flat end. For this purpose, 2 mg of Material of interest added with 1 mL of ethanol and the slurry was prepared. Then 0.04 mg of active material dropcasted on the top and let it dry, after drying 5 microlitre of nefion dropcasted on it as a binder. The carbon black is used as a conductive additive, and Nefion is used as a binder [16], we measured with and without carbon black. Following the dropcasting, the rods are kept in a vacuum at 65° C for 3h to dry the coated slurry. This results in the formation of a thin coating of the active material on the flat end of the rod (obtained from battery). The rods were weighed before and after deposition. The difference in mass gives the mass of the deposited material. The counter electrode (CE) is an inert conductor usually made

of platinum, here we used Platinum electrode as counter electrode (Fig. 3.3 (d), 1cm×1cm). The current flows between CE and WE. The reference electrode (RE) is the third and final electrode that is used to measure the potential of the WE. RE should be able to maintain a constant potential during the electrochemical reaction and must be chemically stable. There are various REs like Saturated Calomel Electrode (SCE), Standard Hydrogen Electrode (SHE), etc. We have used saturated Calomel electrodes as our RE for all the electrochemical measurements (figure 3.2.2 (c). It maintains a constant potential of 0.197 V with respect to SHE. The high stability in the potential value is reached by a redox reaction in the RE, as given in equation (3.2)

$$Hg_2Cl_2(s) + e^- \leftrightarrow 2Hg(l) + Cl^-(aq) \quad (3.2)$$

All these three electrodes are connected to the respective terminals of the electrochemical workstation and then kept submerged under an electrolyte solution to conduct the experiments. We have used **Corrtest CS- 313** electrochemical workstation for the purpose of all the electrochemical measurements. The photo of the workstation is shown in figure 3.3 (b). While performing the 2-electrode measurement, the WE is connected to the positive terminal of the device, and CE and RE are connected together to the negative terminal of the device.

After obtaining the data, the specific capacitance of the device can be calculated both from the CV and GCD experiments using equations (2.3.1) and (2.3.3). Information concerning the different dynamic processes which occur at the electrode-electrolyte interface during the charging-discharging can be obtained from the EIS experiment.

References

[1] L. D. Whittig, & W. R. Allardice, X-ray diffraction techniques. Methods of Soil Analysis: Part 1 Physical and Mineralogical Methods, 5 (1986) 331-362. doi: 10.2136/sssabookser5.1.2ed.c12

[2] B. E. Warren, X-ray diffraction methods, Journal of applied physics, 12 (1941) 375-384, doi: 10.1063/1.1712915

[3] H. Stanjek, & W. J. H. 1. Häusler, Basics of X-ray Diffraction. Hyperfine interactions, 154 (2004) 107-119.

[4] C. Berthomieu, & R. Hienerwadel, Fourier transform infrared (FTIR) spectroscopy, Photosynthesis research, 101 (2009)157-170. doi: 10.1007/s11120-009-9439-x

[5] C. M. Parler, J. A. Ritter, & M. D. Amiridis Infrared spectroscopic study of sol-gel derived mixed- metal oxides. Journal of non-crystalline solids, 279 (2001) 119-125. doi: 10.1016/S0022- 3093(00)00401-4.

[6] W. D. Perkins, Fourier transform infrared spectroscopy. Part II. Advantages of FT-IR. Journal of Chemical Education, 64 (1987) A269. doi: 10.1021/ed064pA269

[16] M. Arunkumar and A. Paul, Importance of Electrode Preparation Methodologies in Supercapacitor Applications, ACS Omega, 2 (2017) 8039-8050 doi: 10.1021/acsomega. 7601275

[17] N. Elgrishi, K. J. Rountree, B. D. McCarthy, E. S. Rountree, T. T. Eisenhart, and J. L. Dempsey, A Practical Beginner's Guide to Cyclic Voltammetry, J. Chem. Educ. 95 (2018) 197-206. doi: 10.1021/acs.jchemed.7600361

CHAPTER 4

EXPERIMENTAL SECTION

4.1 Hydrothermal Synthesis

Hydrothermal synthesis is referred to the synthesis by chemical reactions of materials in a closed container where the substance solution heated above an ambient temperature and pressure. It is different from solid-state reactions, where the mechanism mainly involves diffusion of atoms or ions at the interface between reactants substances. This synthesis technique has been found to be an effective way for rational synthesis and crystal engineering of microporous crystals [1], ionic conductors [2], complex oxides ceramics and fluorides [3,4], inorganic-organic hybrid materials, magnetic materials [5], low dimensional aluminophosphates and unique condensed materials.

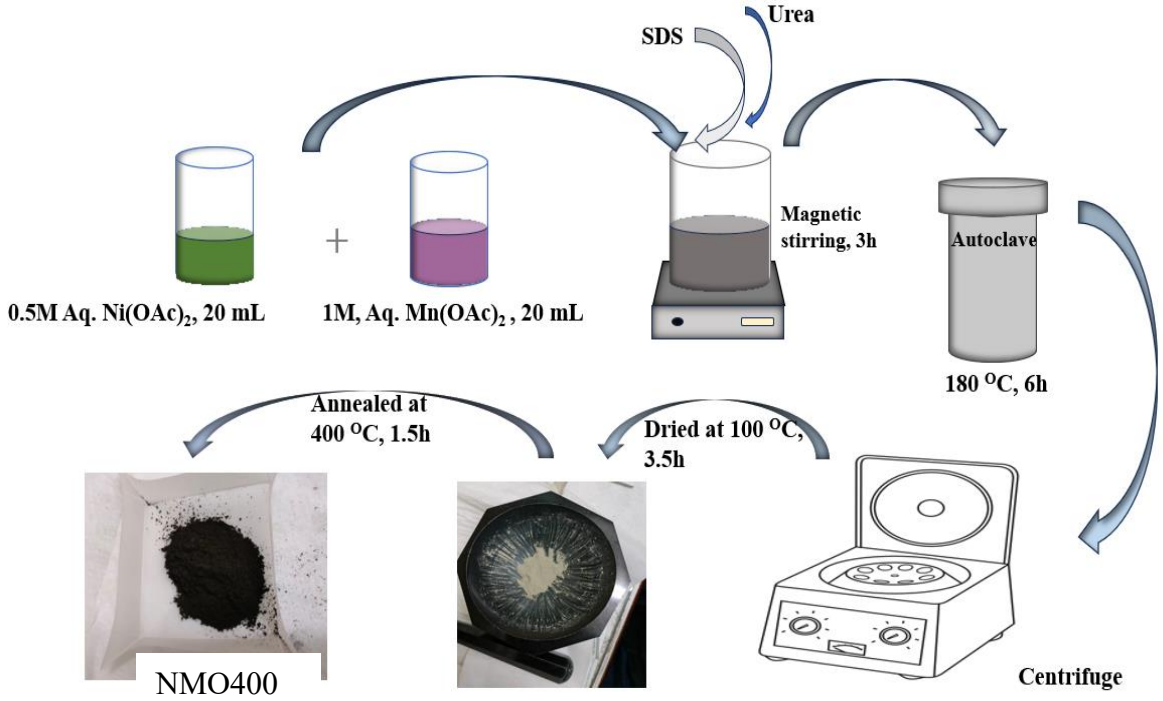
The first reported Hydrothermal synthesis of crystal was done by German geologist Karl Emil von Schafhäutl in 1845, who grew microscopic quartz in a pressure cooker. In, 1848, Robert Bunsen reported growing crystals of barium and Strontium carbonate at 200 ^{O}C and at pressure of 15 atmosphere.

4.2 Synthesis Process of $NiMn_2O_4$ metal oxide

Ingredients:

- Nickel acetate Tetrahydrate ($(CH_3COO)_2Ni.4H_2O$)
- Manganese acetate Tetrahydrate ($(CH_3COO)_2Mn.4H_2O$)
- Urea ($CO(NH_2)_2$)
- SDS (Sodium Dodecyl Sulfate)

Nickel Acetate Tetrahydrate and Manganese acetate Tetrahydrate were purchased from Loba Chemie and both Urea and SDS were purchased from Merck. Different surfactants and mineralizer are usually used to vary the morphology of the composite such as cetyle trimethylammonium bromide (CTAB), Sodium Dodecyl sulfate (SDS), and Glucose and the mineralizer ammonium fluoride (NH_4F). All the chemicals were analytical grade and used without any further purification. Initially, 0.5 M 20 mL aqueous solution (mixed with DI) of nickel acetate and 20 mL 1M of manganese acetate were mixed and stirred for using magnetic stirrer for about 10 minutes. After stirring 0.61 gm urea added as a reducing agent. Which is again stirred for 1 hour at 450 rpm. After that 1.60 gm Sodium Dodecyl sulfate (SDS) was added then stirred for 2 hours at 300 rpm. Here, urea act as a carbonate ion source. The above



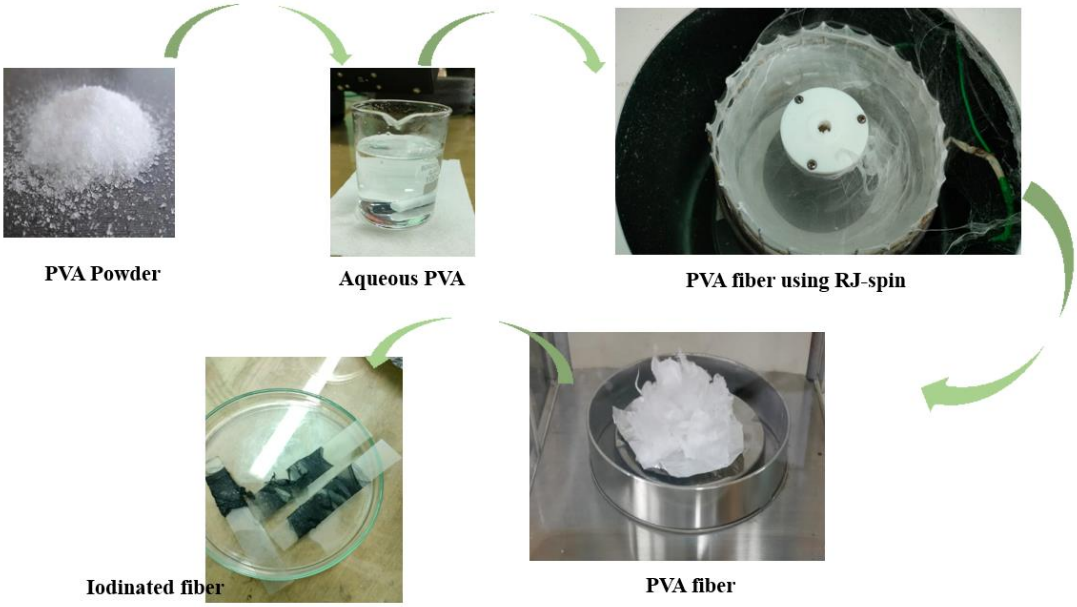
solution was then transferred to a Teflon lined stainless steel autoclave and kept at temperature 180 ^{O}C for 6 hours in a furnace. After heating the autoclave was left to cool down at room temperature naturally. The collected aqueous sample was then centrifuged and washed several times using DI and the precursor precipitate collected. And dried first at 100 ^{O}C for 3.5 h.

Once dried it was annealed at 400 ^{O}C for 1.5h to enhance the crystallinity and phase purity. Finally, the obtained powder grinded and further ball milled for 6 hours to get the final $NiMn_2O_4$ nanoparticle. The sample was labelled as NMO400.

4.3 Synthesis of PVA microfiber using RJ spin

Poly Vinyl Alcohol (PVA) is a type of polymer (Molecular weight 26,300) with a degree of hydrolysis was purchased from Merck. PVA is water-soluble, non-toxic and biocompatible. It possesses good chemical stability. First an aqueous solution (15 wt %) prepared from PVA powder dissolved in DI water and stirred using magnetic stirrer at 700 rpm, for 1.5h kept at temperature 80 ^{O}C. Then this PVA solution was then fed to the RJ-spin using a micro-syringe drop-wise. Before feeding the solution, the chamber of RJ-spin heated around 50 ^{O}C using a kettle heating coil. The RJ-spin was used at 6000 rpm with the heating on and additionally hot air blown at the fiber to prevent it from clotting. After collecting the fiber, it

was treated with Iodine vapor by keeping it in a close chamber with iodine vapor in it at 82 ^{O}C for 24h to improve stability and prevent it from breakage during annealing. After iodine



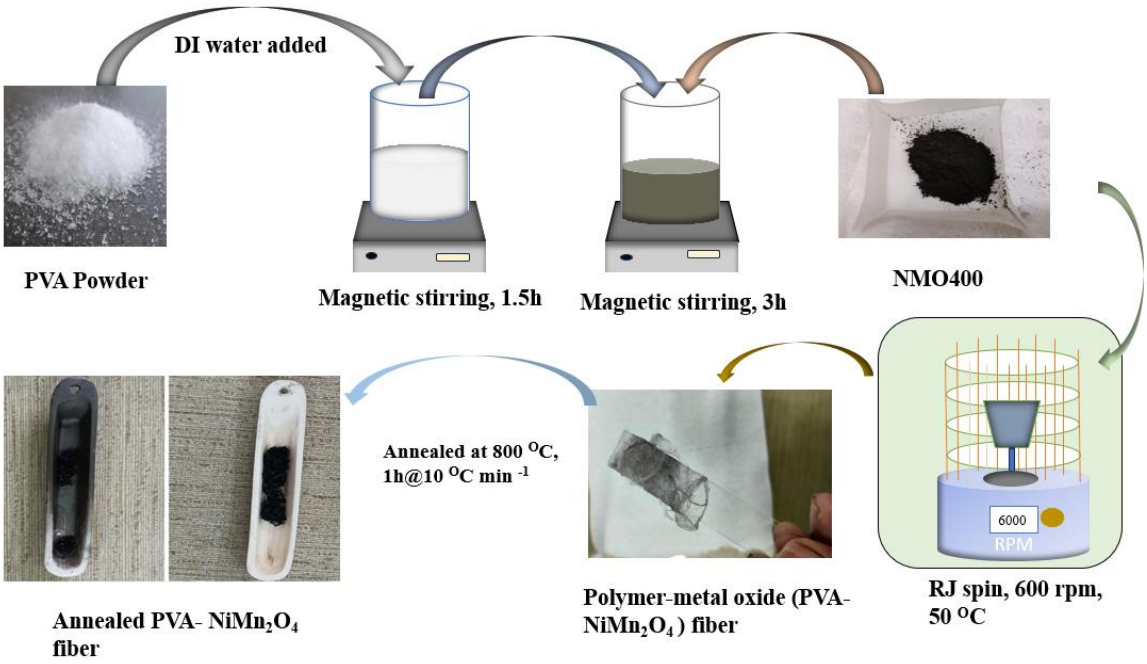
treatment the excess vapor was removed by using desiccator. As the obtained fiber was sublimated in N_2 or any air chamber during annealing, it was annealed 800 ^{O}C at vacuum with temperature increasing 10 ^{O}C per min rate. the collected fiber was collected and characterized further.

4.4 Synthesis of ordered microfiber of $NiMn_2O_4$ using RJ spin technique:

First an aqueous solution (15 wt %) prepared from PVA powder dissolved in DI water and stirred using magnetic stirrer at 700 rpm, for 1.5h kept at temperature 80 ^{O}C. Then the obtained $NiMn_2O_4$ powder (ball milled) mixed (1:4 wt ratio) with the aqueous PVA solution and further magnetic stirred at 900 rpm, for 3h at temperature 90 ^{O}C. Then this polymer-metal oxide solution was fed to the RJ spinner (Rotary Jet Spinner) using a micro-syringe. The RJ spin chamber was heated before (50 ^{O}C) and during the fiber collection it was dried using hot-air dryer to prevent further clotting. After completing the fiber was kept for 15 min for further drying and the collected. The $NiMn_2O_4$ embedded fiber was obtained. For better stability of

the polymer-metal oxide fibers were treated with Iodine vapor by keeping it in a close chamber with iodine vapor in it at 82 ^{O}C for 24h.

After iodine treatment the excess vapor was removed by using desiccator. This treatment prevents the fiber from breaking during the annealing process. Finally, the polymer-metal oxide



fiber annealed at 900 ^{O}C in Rotary vacuum chambers for 1h with temp increasing rate 10 ^{O}C per min. the collected fiber was collected and characterized further.

References

1. Cheetham, A. K.; Ferey, G.; Loiseau, T. Open-Framework Inorganic Materials.Angew. Chem., Int. Ed. Engl. 1999,38, 3268-3292.

2. Li, G.; Li, L.; Feng, S.; Wang, M.; Yao, X. An Effective Synthetic Route for a Novel Electrolyte: Nanocrystalline Solid Solutions of $(CeO_2)_{1-x}(BiO_{1.5})_x$. Adv. Mater. 1999, 11 (2), 146-149.

3. Mao, Y.; Li, G.; Xu, W.; Feng, S. Hydrothermal Synthesis and Characterization of Nanocrystalline Pyrochlore Oxides $M_2Sn_2O_7$M = La Bi, Gd or Y). J. Mater. Chem. 2000, 10 (2), 479-282.

4. Zhao, C.; Feng, S.; Chao, Z.; Xu, R.; Shi, C.; Ni, J. Hydrothermal Synthesis of the Complex Fluorides $LiBaF_3$ and $KMgF_3$ with Perovskite Structures under Mild Conditions. Chem Commun. 1996, 1641-1642.

5. Feng, S.; Wang, D.; Yu, R.; Na, L. Hydrothermal Synthesis Route to a Giant Magnetoresistance Material $La_{0.5}Ba_{0.5}MnO_3$, Proceedings of the International Symposium on Solvo-Hydro-Thermal Processes, Org. Comm. Solvothermal Tech. Res.: Takamatsu, Japan, 1997; p12.

CHAPTER 5

RESULTS AND DISCUSSIONS

5.1 $NiMn_2O_4$ nanoparticle via Hydrothermal route

This chapter discusses about the results from various characterization techniques.

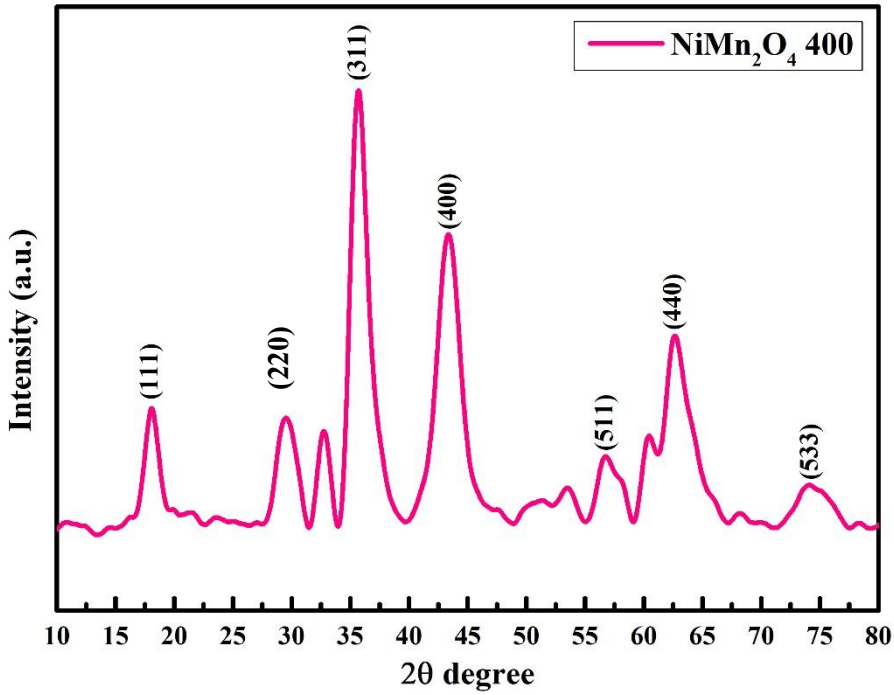


Fig 1: XRD pattern of synthesized NMO400

Fig.1 is the XRD pattern of the $NiMn_2O_4$ synthesized using Hydrothermal technique. The 2θ values of the peaks correspond to specific interplanar spacings (d-values). The XRD pattern displays distinct peaks at the following 2θ values; 18.28°, 30.06°, 35.45°, 43.25°, 57.16°, 62.72° and 72° corresponding to different crystallographic planes, labelled as (111), (220), (311), (400), (511), (440), and (533). These peaks are characteristic of the spinel structure of $NiMn_2O_4$. were matched perfectly with the JCPDS Card no. 71-0852 of the face-centric cubic structure of $NiMn_2O_4$. From the XRD plot the average size of the $NiMn_2O_4$ crystallite is found to be in the range of 3-5 nm.

Fig.2 represents FTIR (Fourier Transform Infrared Spectroscopy) data of the prepared $NiMn_2O_4$ sample annealed at 400 ^{O}C (NMO400). Within the range 400-600 cm^{-1} the main two characteristic bands observed. This region typically shows the metal-oxygen (M-O) stretching vibrations. For single spinel structures like $NiMn_2O_4$, these peaks indicate the presence of Mn-

O and Ni-O bonds in the lattice, spectrum correspond to the vibrational modes of octahedral $Ni^{2+} – O^{2-}$ and tetrahedral $Mn^{3+} – O^{2-}$ groups, respectively. The weak absorption

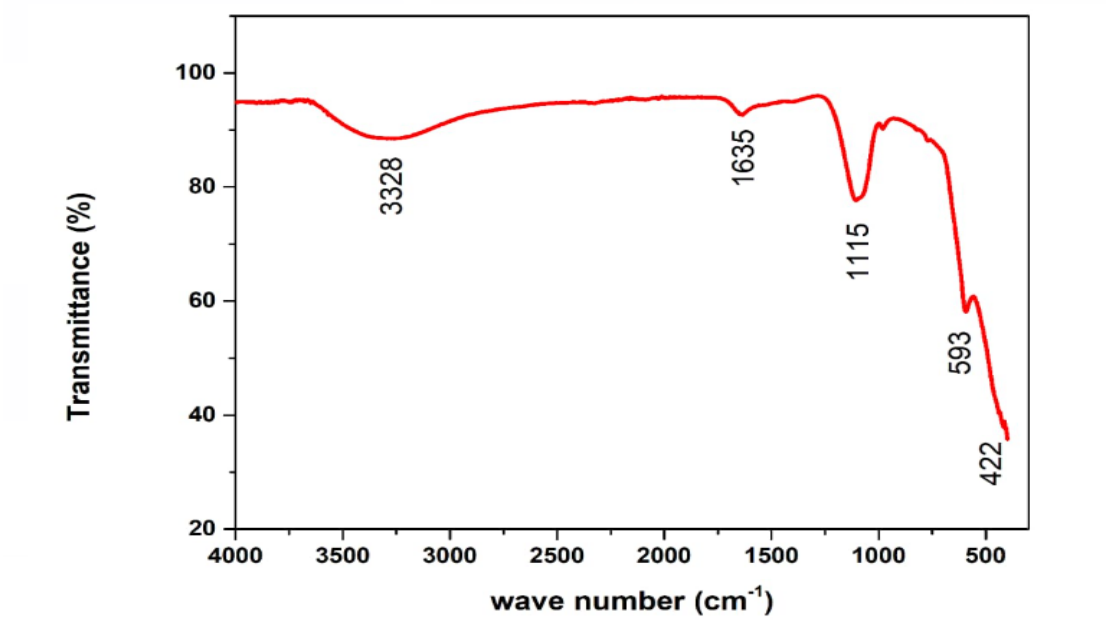


Fig.2: FTIR curve of NMO400

band appeared in between 2300 and 380 cm^{-1} at 1635 cm^{-1} corresponds to the C-O stretching vibration appearing either from the atmospheric CO_2 or residual ethylene glycol. The broad absorption band appeared in between 3328 cm^{-1} correspond to the stretching vibration of O-H group which is from H_2O molecules physio-adsorbed on the surface of the electrode material. The surface which adsorbed H_2O molecules further enhances the wettability of the electrode [1], which ultimately leads to improve the electrochemical performance of electrode material.

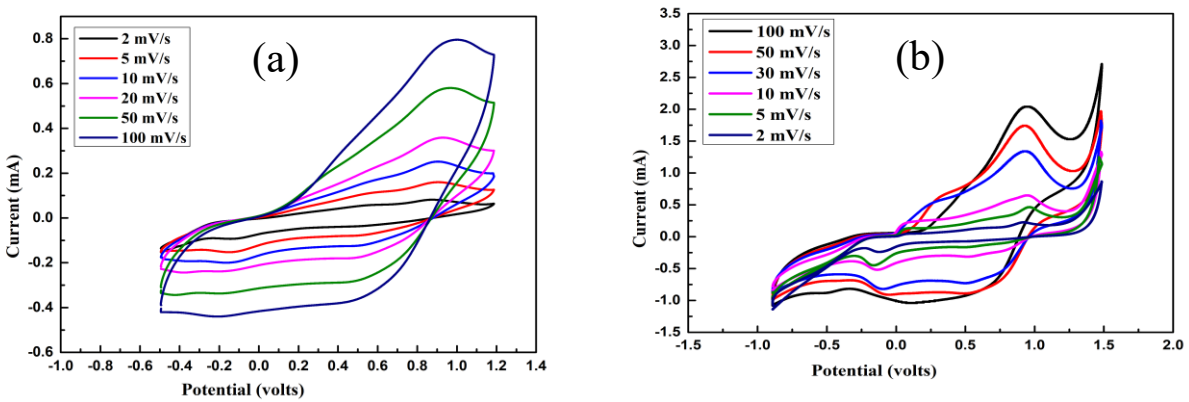


Fig 3. CV curve of NMO400, potential window (a) -0.5V to +1.2V, (b) -0.9V to +1.5V

Cyclic voltammetry (CV) has been performed in a three-electrode setup using aqueous 0.5M Na_2SO_4, solution as electrolyte within the potential range – 0.5V to +1.2V and – 0.9V to +1.5V. Results of obtained different specific capacitance for different scan-rate given below.

Table 5.1: *Calculation of specific capacitance of the material at various scan rate with the potential window -0.5V to +1.2V and the active mass loading was 0.04 mg (without Carbon black and without nefion) with electrolytic concentration 0.5M Na_2SO_4.*

Scan rate (k) in mV/s	Area under the CV curve	Specific capacitance (C) in F g^{-1}
100	0.001219	89.63
50	9.2808×10^{-4}	136.5
20	5.7×10^{-4}	209.6
10	4.2×10^{-4}	309.3
5	2.885×10^{-4}	424.3
2	1.704×10^{-4}	626.6

Table 5.2: *Calculation of specific capacitance of the material at various scan rate with the potential window –0.5V to +1.2V and the active mass loading was 0.04 mg (with 1% Nefion and without Carbon black) with electrolytic concentration 0.5M Na_2SO_4.*

Scan rate (k) in mV/s	Area under the CV curve	Specific capacitance (C) in F g^{-1}
100	2.093×10^{-3}	153.9
50	1.396×10^{-3}	205.3
20	5.55×10^{-4}	306.1
10	3.976×10^{-4}	438.5
5	4.3538×10^{-4}	640.1
2	3.0865×10^{-4}	1135.0

Table 5.3: *Calculation of specific capacitance of the material at various scan rate with the potential window –0.9V to +1.5V and the active mass loading was 0.04 mg (with 1% Nefion and without Carbon black) with electrolytic concentration 0.5M Na_2SO_4.*

Scan rate (k) in mV/s	Area under the CV curve	Specific capacitance (C) in F g^{-1}
100	2.605×10^{-3}	206.0
50	2.476×10^{-3}	347.0
30	2.099×10^{-3}	476.4
10	1.0892×10^{-3}	858.1
5	7.185×10^{-4}	1464.5
2	3.890×10^{-4}	3088.8

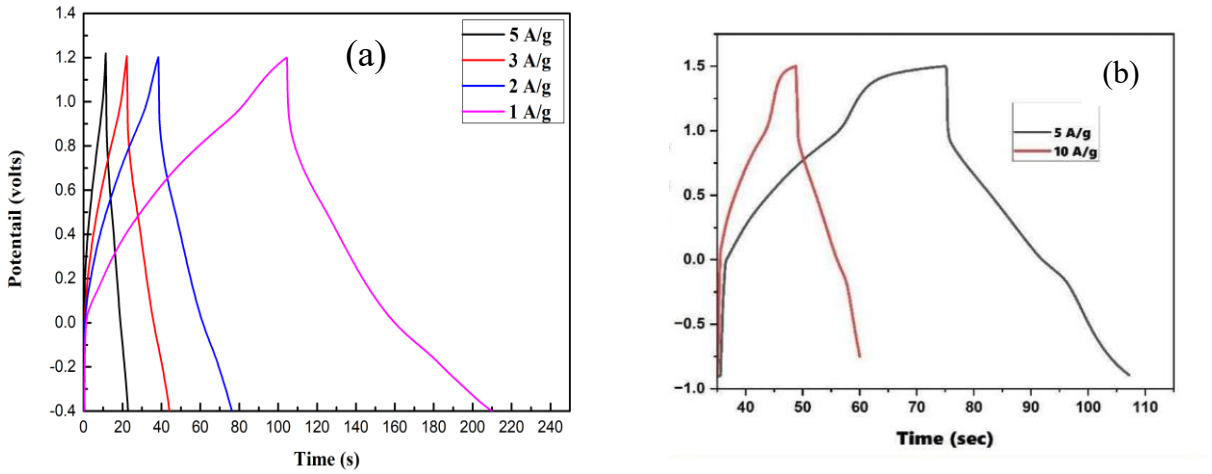


Fig 4: GCD curve of the synthesized NMO400 in the potential windows (a) -0.5V to +1.2V, (b) -0.9V to +1.5V

peaks ($Mn^{3+} \leftrightarrow Mn^{4+}$ and $Ni^{2+} \leftrightarrow Ni^{3+}$) in the CV curves, which can be clearly identified due to the faradaic redox processes related to Eq. (5.1) [2,3,4]

$$NiMn_2O_4 + Na^+ + e- \leftrightarrow NaNiMn_2O_4 \qquad (5.1)$$

From this equation (Eq. (5.1) it is obvious that Na^+ ions from electrolyte Na_2SO_4 diffuse into the $NiMn_2O_4$ electrode material and during the charging time it absorbs one electron with one ion. Subsequently, during discharging time Na^+ ions are released from electrode material into the electrolytic solution of Na_2SO_4 and one electron for an ion is released to the external circuit. Here Na^+ ions are working as charge compensator agent to enhance as a whole the capacitive performance of the $NiMn_2O_4$ electrode [5]. As can be observed in Fig. 3 CV curve, with the increase of potential scan rate, the potential peaks associated with oxidation and reduction potential shift towards positive and negative potential, respectively [6]. Upon increasing the

scan rate, the applied voltage with respect to the reference electrode increases faster. As a result, all the pores of the working electrode do not get enough time interact with the electrolyte and undergo oxidation and reduction reactions. The specific capacitance (C_m) of the electrode for each scan rate has been calculated from the CV curves by using Eqs. (3.1) and (3.2) and the maximum specific capacitance of 3088.8 F g^{-1} was obtained at a scan rate 2 mV s^{-1} within the potential window -0.9V to +1.5V.

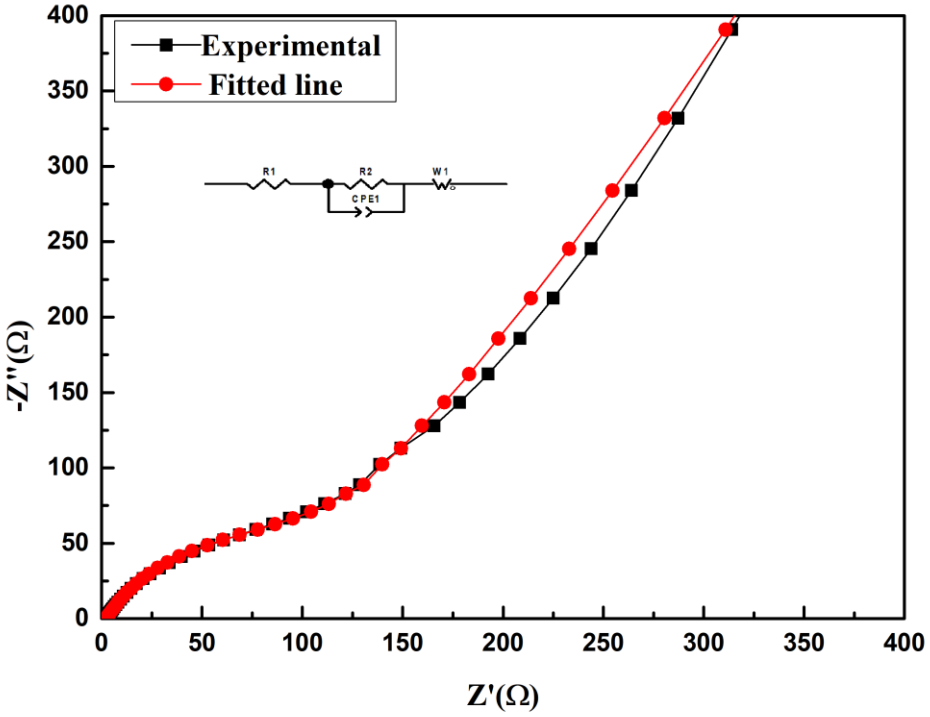


Fig 5. EIS result of NMO400 in the pot. window -0.5V to +1.2V

The change of electrode's specific capacitance with scan rate is shown in **Fig. 3** The specific capacitance initially decreases sharply with the increase of scan-rate, and then decreases very slowly at high scan rates. The variation of sp. capacitance value with scan rate can be explained on the basis of mobility of ions from electrolyte to electrode and electrode to electrolyte material. The charge storage capability of the electrode material is generally followed its oxidation and reduction. The oxidation of the working electrode occurs via the subtraction of electrons from the electrode material and diffusion of anions from the electrolyte solution to counter balance the developed positive charge, maintaining charge neutrality.

At lower scan rates, the ions from Na_2SO_4 electrolyte solution need longer time to access the outer and inner surface of the electrode, which leads to the accumulation of a large number of ions at the surface of active electrode, enhancing its charge storage capacity (enhanced capacitance). However, at higher scan rate, due to higher mobility of ions and slow diffusion of redox electrolyte, the ions from electrolyte can access only the outer surface of the electrode. Consequently, only a few numbers of ions can get accumulated at the outer surface of the electrode, thus reducing the specific capacitance value. Thus, the reduction of the rate performance of the capacitor at high scan rate is also related to the reduction of the electrolyte, not only related to the $NiMn_2O_4$ electrode material.

In the Fig 5 we have fitted the EIS data of the electrode material to obtain equivalent circuit using Z-view software. The constant phase elements (CPE) are modelled here as capacitor elements.

Table 5.1 Different parameters from the obtained fitting

Sample name	*Element*	*Value*
$NiMn_2O_4$	R1	2.356
	R2	118.40
	CPE1-T	0.00096417
	CPE1-P	0.72217
	W1-R	0.00016911
	W1-T	3.2834E-09
	W1-P	0.35775

5.2 Ordered $NiMn_2O_4$ microfiber

We have annealed PVA fiber at 800^{O}C the FTIR curve suggests it was reduced Graphene Oxide.

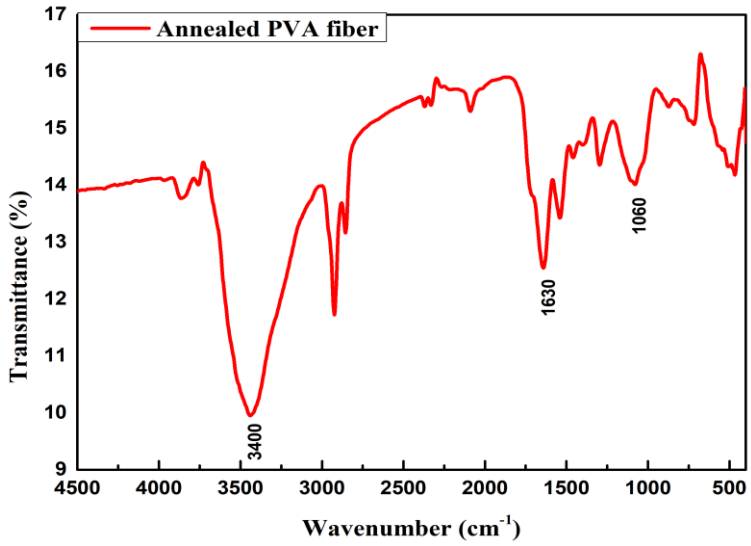


Fig 6. FTIR of annealed PVA fiber at 800 ^{O}C

A broad peak at 3400 cm^{-1} corresponds to O – H stretching vibration. In reduced Graphene oxide (rGO) it is typically less intense compared to Graphene oxide (GO) due to reduction of hydroxyl groups. A peak at 1630 cm^{-1} associated with C=C stretching vibration. Peak at 1060 cm^{-1} corresponds to C – O stretching vibration. Which suggests that the annealed sample contains rGO.

Now, we have compared the XRD results of annealed PVA fiber (800^{O}C), NMO400 (annealed $NiMn_2O_4$ at 400^{O}C), annealed PVA-NMO fiber (900^{O}C). At 18^{O}, 30^{O}, 35^{O}, 37^{O}, 43^{O}, 57^{O}, 62^{O} the peak of NMO (annealed $NiMn_2O_4$) which associated with the planes (111), (220), (311), (222), (400), (511), (440) and annealed PVA-NMO fiber matched, which suggests the presence of $NiMn_2O_4$ nanoparticle in the fiber.

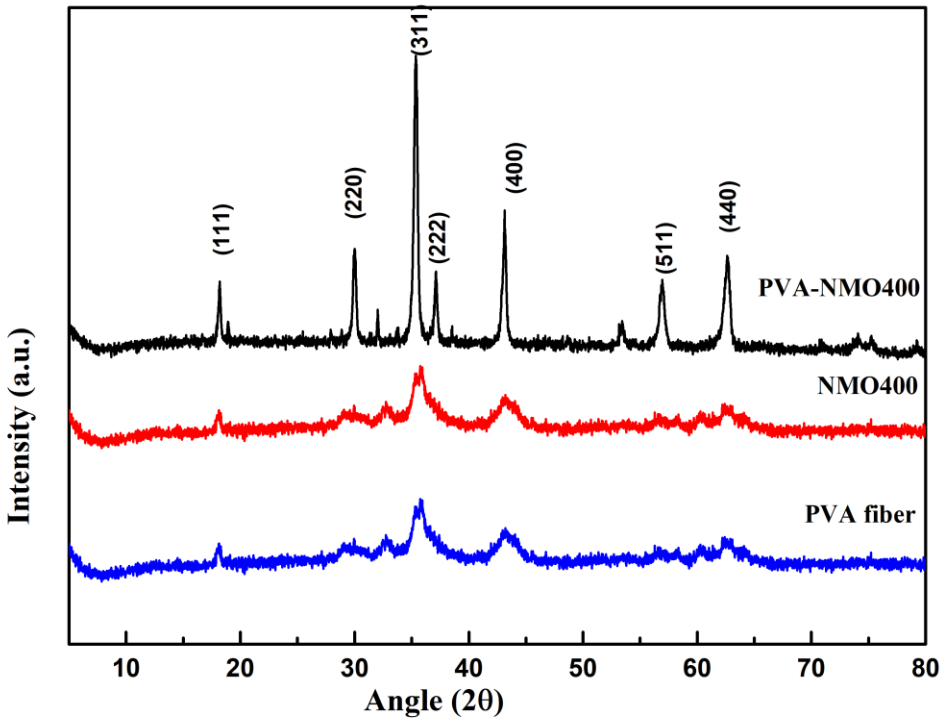


Fig 7. XRD patterns of annealed PVA fiber, NMO400, Annealed PVA-NMO fiber (900^{O} C)

SDS-assisted Hydrothermally synthesized $NiMn_2O_4$ shows a promising result for supercapacitor application as an electrode material. And the RJ-spin fabricate Metal oxide assisted microfiber could be a betterment for storing charge than the $NiMn_2O_4$. And RJ-spin is easier to use and ease to synthesize polymer assisted microfiber.

References

[1] Applied Surface Science 463 (2019) 513–525. https://doi.org/10.1016/j.apsusc.2018.08.259

[2] M.Y. Arsent'ev, N.Y. Koval'ko, A.V. Shmigel', P.A. Tikhonov, M.V. Kalinina, NiMn2O4 spinel as a material for supercapacitors with a pseudocapacity effect, Glas.Phys. Chem. 43 (2017) 376–379, https://doi.org/10.1134/S1087659617040022.

[3] S. Maiti, A. Pramanik, T. Dhawa, M. Sreemany, S. Mahanty, Bi-metal organic framework derived nickel manganese oxide spinel for lithium-ion battery anode, Mater. Sci. Eng. B Solid-State Mater. Adv. Technol. 229 (2018) 27–36, https://doi.org/10.1016/j.mseb.2017.12.018.

[4] W. Wang, N. Zhang, Z. Shi, Z. Ye, Q. Gao, M. Zhi, Z. Hong, Preparation of Ni-Al layered double hydroxide hollow microspheres for supercapacitor electrode, Chem.Eng. J. 338 (2018) 55–61, https://doi.org/10.1016/j.cej.2018.01.024.

[5] L. Mai, H. Li, Y. Zhao, L. Xu, X. Xu, Y. Luo, Z. Zhang, W. Ke, C. Niu, Q. Zhang, Fast ionic diffusion-enabled nanoflake electrode by spontaneous electrochemical pre-intercalation for high-performance supercapacitor, Sci. Rep. 3 (2013) 1–8, https://doi.org/10.1038/srep01718.

[6] Angew. Chem. Int. Ed. 10.1002/anie.202104167.https://doi.org/10.1002/anie.202104167.

CHAPTER 6

CONCLUSION AND FUTURE WORK

Conclusion:

In this work of thesis, we have synthesized and studied the morphological difference of metal-oxide based sample on their energy storage performance. We have so far optimized the polymer fiber synthesis using RJ-spin via increasing the yield as a whole. And synthesized polymer-assisted metal oxide fiber. We have seen via RJ-Spin in the weight ratio 4:1 polymer-assisted metal oxide which was PVA-$NiMn_2O_4$ fiber had the best yield. SDS-assisted $NiMn_2O_4$ gave the sp. Capacitance 3088.8 F g^{-1} at 2 mV s^{-1} scan rate in 0.5M Na_2SO_4 electrolyte. The overall study suggests its vast potential in the field of electrochemical energy storage, and promising future in the commercial usages.

Although the RJ-spin synthesized PVA assisted $NiMn_2O_4$ showed a very good yield of synthesis, and good binding with the $NiMn_2O_4$ nanoparticle, the stability of the fiber was not up to the standard as it has strong affinity to the moisture which ultimately led to breakage the fiber structure and was unstable at annealing with higher temperature.

Scope for future work

Transition metal oxide as electrode material offer high energy and power densities. However, because of the high internal resistance and short-term stability, they are not very popular as of now. For all that tuning the morphology of the material can solve many issues as we have seen. This thesis work explored such possibility so far, but was not up to the mark for ordered sample. There are few listed improvements which may address the problems we have faced for the transitional metal oxide electrodes.

1. Investigation of tri-metal oxides and beyond for the SC application.
2. Explore the other polymer assisted metal oxides and the morphologies on the electrochemical performances.
3. The exploration of two-dimensional (2D) materials, such as transition metal dichalcogenides (TMDs) and MXenes, holds great potential due to their high surface area, tunable electronic properties, and unique layered structures. Future research could focus on optimizing the synthesis, surface modification, and integration of these materials to enhance their electrochemical performance in supercapacitors.
4. More research on the enhancement of the Rotary-Jet Spin device is required as to fabricate fiber with better uniformity. As we know change in fiber dimensions also has an effect on available surface area so the specific capacitance.

THANK YOU